10
I29A
389
c.1

CIVIL ENGINEERING STUDIES
STRUCTURAL RESEARCH SERIES NO. 389

UILU-ENG-72-2011

A LAYERED FINITE ELEMENT NONLINEAR ANALYSIS OF REINFORCED CONCRETE PLATES AND SHELLS

Metz Reference Room
Civil Engineering Department
B106 C. E. Building
University of Illinois
Urbana, Illinois 61801

by
F. R. HAND
D. A. PECKNOLD
W. C. SCHNOBRICH

ISSUED AS A TECHNICAL
REPORT OF A RESEARCH
PROGRAM SPONSORED

by

The National Science Foundation
Grant No. GK 11190

UNIVERSITY OF ILLINOIS
URBANA, ILLINOIS
AUGUST 1972

A LAYERED FINITE ELEMENT NONLINEAR ANALYSIS OF REINFORCED CONCRETE PLATES AND SHELLS

by

F. R. Hand, Jr.

W. C. Schnobrich

and

D. A. W. Pecknold

Issued as a
Technical Report
of Research Supported by the
National Science Foundation
under
Grant GK-11190

Metz Reference Room
Civil Engineering Department
B106 C. E. Building
University of Illinois
Urbana, Illinois 61801

UNIVERSITY OF ILLINOIS

URBANA, ILLINOIS

AUGUST 1972

ACKNOWLEDGMENTS

This report is based on the dissertation of Dr. F. R. Hand, Jr. submitted to the Graduate College, University of Illinois at Urbana-Champaign, for the degree of Ph.D. in Civil Engineering. The study was conducted under the supervision of Dr. W. C. Schnobrich, Professor of Civil Engineering, as part of a research program supported by the National Science Foundation under research grant No. GK-11190.

The numerical calculations were performed on the IBM 360/75 system of the Computing Services Office of the University.

LIST OF TABLES

TABLE OF CONTENTS

Chapter Page

LIST OF FIGURES

Metz Reference Room
Civil Engineering Department
[illegible] C. E. Building
University of Illinois
Urbana, Illinois 61801

1. INTRODUCTION

1.1 General

Structural design of reinforced concrete plates and shells is usually based on linear elastic analysis or yield line theory. The effects of cracking and nonlinear material and geometric behavior are commonly neglected or grossly approximated. Under normal service loads, however, reinforced concrete plates and shells usually are too heavily loaded to remain totally in the range of validity of the linear elastic analysis but too lightly loaded to be in the range of the yield line theory. It is precisely this region after the elastic state but before the limit state in which knowledge of the load deflection characteristics is most beneficial.

Reinforced concrete plates and shells in this post-elastic range present a formidable stress analysis problem if the material behavior is idealized realistically. The basic prerequisite for the analysis is a suitable relation, usually in incremental form, between stress resultants and strain measures which adequately reflects yielding of the reinforcing steel and the cracking, biaxial yielding, and crushing of the concrete as loading progresses. In order to obtain such a relation, simplifying assumptions must be made. Thus, comparisons of calculations and experimental results are essential for establishing the adequacy of the mathematical model.

Two basically different approaches have been used to obtain idealized constitutive relations for use in finite element procedures. In the "modified EI" approach a macroscopic viewpoint is taken. An overall moment-curvature relation reflecting the various stages of material behavior

is assumed. This approach has been applied to reinforced concrete plates by Jofriet and McNeice[10] and to plates and shells by Bell.[2]

The second approach is based on idealized stress-strain relations for concrete and steel with some additional assumptions regarding deformation compatibility between the materials. Cervenka[6] used this technique in analyzing reinforced concrete panels under inplane loads. If flexural deformations are to be allowed, material variation through the thickness must be taken into account. This can be accomplished in a discretized fashion by a layering approach in which each layer is allowed to have different properties. However, the layering approach displays a coupling phenomenon between inplane extension and transverse bending not found in homogenous plates. If the cross section possesses vertical symmetry about its mid-depth, the coupling vanishes. Whang[27] used this concept to develop a rectangular shallow shell finite element composed of elastoplastic strain hardening material. These material properties are appropriate for some metals but not for reinforced concrete. Also, Franklin[8] applied this concept to a reinforced concrete frame element.

When applying a finite element approach, it is possible to model the cracking of concrete by allowing any node to split into two or more nodes each capable of displacing independent of its former common neighbors. This involves changes in topology as the solution proceeds, a major disadvantage. Other disadvantages of such a treatment are the cracks can only propagate along element boundaries and the occurrence of cracking is defined from nodal stresses. Such a procedure does have some merit provided there are several nodes throughout the depth. This approach can be applied to two- and three-dimensional structures when idealized as two- and three-dimensional structures, respectively. However, if one of the

dimensions is eliminated (constrained by some behavioral assumptions), this topology change approach should not be applied. For the cases considered herein, the real three-dimensional problem is reduced to a two-dimensional one by introducing the stress resultant concept. As a result, there is only one node (at the reference surface) throughout the depth. To release this single node due to cracking would then cause a rip or tear in the structure. Thus, the crack would instantly propagate through the entire depth of the structure. If, on the other hand, the problem is treated as a three-dimensional one, it is possible to propagate the crack gradually by releasing node after node through the depth. Since it is desired to stay away from the three-dimensional approach, the use of topology changes to account for cracking cannot be considered.

1.2 Object and Scope

The purpose of this investigation is to obtain analytically the load deflection history for any reinforced concrete plate or shell. The overall approach is to perform a nonlinear finite element analysis with a layered doubly curved rectangular shallow shell element. The analysis progresses through an iterative or step-by-step procedure while the nonlinearity is introduced through the material properties. The material properties permitted for the steel reinforcement are elastic or plastic while the concrete can be elastic, cracked, plastic or crushed.

The effect of bond between steel and concrete, the influence of creep and shrinkage of concrete, the effect of temperature, and the effect of long term or cyclic loading are not considered.

Finally, several numerical comparisons are made with experimental results for both plates and shells.

1.3 Nomenclature

Each symbol used in the text is explained when it first appears. However, a summary of frequently used symbols is also presented below for convenience. Several symbols have dual meaning. This was done in order to retain the previous authors' notation for those items which are taken from other references since it was felt that there would be no confusion when the symbol is considered in context.

a, b = half element dimensions in x and y directions, respectively or constants

A = matrix (20 x 20) relating nodal displacements and generalized unknowns

B = matrix (6 x 20) relating generalized unknowns and middle surface strains and curvatures

B_ε, B_χ = submatrices (3 x 20) of B, membrane and bending parts, respectively

C = material properties matrix (3 x 3)

C_j = j^{th} layer material properties matrix (3 x 3)

D, E, F = submatrices (3 x 3) of $\overline{D}$

D_j, E_j, F_j = submatrices (3 x 3) of $\overline{D}_j$

$\overline{D}$ = matrix (6 x 6) representing $[G]^T[C][G]$

$\overline{D}_j$ = $\overline{D}$ evaluated for j^{th} layer

E, E_c, E_d, E_s = moduli of elasticity

f_c = transition stress between first and second elastic regions for concrete

f'_c = concrete cylinder compressive strength

f_d = plastic stress level for concrete

f_t = tensile strength of concrete

f_y = yield stress for steel

F_{ex} = excess element nodal force vector (20 x 1)

$F_{j\ ex}$ = j^{th} layer excess element nodal force vector (20 x 1)

$\overline{F}$ = excess force vector

G = matrix (3 x 6) relating strain vector to middle surface strains and curvatures

h = element thickness

K = element stiffness matrix (20 x 20)

K^* = element stiffness matrix (20 x 20) in terms of generalized coordinates

L = element generalized load vector (20 x 1)

M = matrix (20 x 5) relating nodal displacements and generalized coordinates, or moment stress resultant vector (3 x 1): M_x, M_y, M_{xy}

M_j = j^{th} layer moment stress resultant vector (3 x 1)

M^{ex} = excess moment stress resultant vector (3 x 1)

M_j^{ex} = j^{th} layer excess moment stress resultant vector (3 x 1)

N = force stress resultant vector (3 x 1): N_x, N_y, N_{xy}

N_j = j^{th} layer force stress resultant vector (3 x 1)

N^{ex} = excess force stress resultant vector (3 x 1)

N_j^{ex} = j^{th} layer excess force stress resultant vector (3 x 1)

NL = number of layers

p = hydrostatic stress

p_ε = hydrostatic strain

r, s, t = curvatures of shell middle surface

t_j, t_{j+1} = distance from middle surface to bottom and top of j^{th} layer

T = transformation matrix (3 x 3)

u, v, w = displacements in the x, y and z directions, respectively

U = element displacement vector (20 x 1)

U_o = strain energy density

$\overline{U}$ = vector (5 x 1) of nodal displacements: u, v, w, w_x, w_y

W_{int} = internal work

w_x, w_y = slopes of w in the x and y directions, respectively

x, y, z = rectangular Cartesian coordinates

X = external distributed load vector (5 x 1)

α = vector (20 x 1) of generalized coordinates or experimental material constant

β = shear retention factor or experimental material constant

δW_{int} = internal virtual work

$\delta\varepsilon$ = incremental strain vector (3 x 1)

$\delta\sigma$ = incremental stress vector (3 x 1)

ε = strain vector (3 x 1): ε_x, ε_y, γ_{xy}

ε_o = middle surface strain vector (3 x 1): ε_{xo}, ε_{yo}, γ_{xyo}

ε_{oct} = octahedral shearing strain

ε_u = concrete crushing strain

$\overline{\varepsilon}$ = middle surface strains and curvatures vector (6 x 1)

ν = Poisson's ratio

σ = stress vector (3 x 1): σ_x, σ_y, τ_{xy}

σ_{ex} = excess layer stress vector (3 x 1)

τ_{oct} = octahedral shearing stress

ϕ = angle measured counter-clockwise from x-axis

χ = middle surface curvatures vector (3 x 1): χ_x, χ_y, $2\chi_{xy}$

∂ = matrix (6 x 5) of differential operators

2. MATERIAL BEHAVIOR CHARACTERISTICS

2.1 General

From the strength of materials viewpoint, reinforced concrete is far from an ideal material. The concrete is subject to creep, microcracking, and varying strength with age. The inclusion of reinforcement introduces the further problems of bond, anchorage, and bond slip. Nevertheless, the purpose of this chapter is to state explicitly what material properties are assumed for the plain concrete, the reinforcement, and the reinforced concrete composite. However, while putting forth these assumptions, it is understood that they are just that - assumptions, only approximations to reinforced concrete's real behavior.

The sign convention adopted for stress and strain is: tension and expansion are positive, compression and contraction are negative. Also, special values of stress or strain that are significant, such as the yield point of steel, f_y, or the concrete cylinder compressive strength, $-f'_c$, are such that the symbol represents the absolute value of the quantity denoted while any algebraic sign before the symbol reflects only the chosen sign convention.

2.2 Uniaxial Stress-Strain Curves

The assumed uniaxial stress-strain curves for steel and concrete are shown in Fig. 1. The steel is considered an elastic-plastic material with yield stress $\pm f_y$ and a modulus of elasticity E_s. The concrete is considered a bilinear elastic, perfectly plastic material in compression and elastic-brittle material in tension. The moduli of elasticity are

E_c and E_d for the first and second elastic regions respectively; the transition stress is $-f_c$. At stress level $-f_d$ the concrete becomes perfectly plastic until crushing occurs at a strain of $-\varepsilon_u$. The concrete is assumed to have a limited tensile strength of f_t.

2.3 Failure Criteria for Plain Concrete

The assumed failure criterion for plain concrete in a biaxial stress state was proposed by Kupfer, Hilsdorf, and Rüsch[13] and is shown in Fig. 2. This failure theory is based on an octahedral shearing stress criterion of the form

$$\tau_{oct} = a - bp \tag{2.1}$$

where τ_{oct} is the octahedral shearing stress

$$\tau_{oct} = \frac{1}{3}\left[(\sigma_{xx} - \sigma_{yy})^2 + (\sigma_{yy} - \sigma_{zz})^2 + (\sigma_{zz} - \sigma_{xx})^2 + 6\,(\tau_{xy} + \tau_{xz} + \tau_{yz})\right]^{1/2},$$

p is the hydrostatic stress

$$p = \frac{1}{3}(\sigma_{xx} + \sigma_{yy} + \sigma_{zz})$$

and a and b are material constants. In actual fact, Eq. 2.1 represents two equations, one for biaxial tension or tension-compression, and another for biaxial compression. These equations are respectively,

$$\tau_{oct} + \sqrt{2}\,\frac{1-\alpha}{1+\alpha}\,p - \frac{2\sqrt{2}}{3}\,\frac{\alpha}{1+\alpha}\,f_c' = 0 \qquad (\sigma_1 > 0) \tag{2.2}$$

$$\tau_{oct} + \sqrt{2}\,\frac{\beta-1}{2\beta-1}\,p - \frac{\sqrt{2}}{3}\,\frac{\beta}{2\beta-1}\,f_c' = 0 \qquad (\sigma_1 < 0) \tag{2.3}$$

where the values for α and β are in accordance with the experimental results given in Reference 13, and are

$$\alpha = f_t/f_c' \simeq 0.10 \qquad \beta \simeq 1.16$$

This failure criterion is modified to serve as the transition criterion to determine the boundaries of the different material property zones, Fig. 3. This is accomplished by simply scaling the yield surface of Kupfer, Hilsdorf, and Rüsch. To determine the boundary for the elastic and nonelastic (plastic and cracked) regions f_d replaces f_c' in Eqs. 2.2 and 2.3. To determine the boundary, in biaxial compression only, between the first and second elastic regions f_c replaces f_c' in Eq. 2.3. To determine the boundary, in biaxial compression only, between the noncrushed and crushed regions Eq. 2.3 is converted to strains. This conversion is accomplished by replacing f_c' with ε_u, τ_{oct} with the octahedral shearing strain ε_{oct}, and p with the hydrostatic strain p_ε, where

$$\varepsilon_{oct} = \frac{1}{3}\left[(\varepsilon_{xx} - \varepsilon_{yy})^2 + (\varepsilon_{yy} - \varepsilon_{zz})^2 + (\varepsilon_{zz} - \varepsilon_{xx})^2 + \right.$$

$$\left. + 3\,(\gamma_{xy} + \gamma_{yz} + \gamma_{xz})\right]^{1/2}$$

$$p_\varepsilon = \frac{1}{3}(\varepsilon_{xx} + \varepsilon_{yy} + \varepsilon_{zz})$$

The transition criterion are then, between elastic and nonelastic regions,

$$\tau_{oct} + \sqrt{2}\,\frac{1-\alpha}{1+\alpha}\,p - \frac{2\sqrt{2}}{3}\,\frac{\alpha}{1+\alpha}\,f_d = 0 \quad (\sigma_1 > 0) \qquad (2.4)$$

$$\tau_{oct} + \sqrt{2}\,\frac{\beta - 1}{2\beta - 1}\,p - \frac{\sqrt{2}}{3}\,\frac{\beta}{2\beta - 1}\,f_d = 0 \quad (\sigma_1 < 0) \qquad (2.5)$$

between the first and second elastic regions in biaxial compression,

$$\tau_{oct} + \sqrt{2}\,\frac{\beta}{2\beta - 1}\,p - \frac{\sqrt{2}}{3}\,\frac{\beta}{2\beta - 1}\,f_c = 0 \quad (\sigma_1 < 0) \qquad (2.6)$$

and between noncrushed and crushed regions in biaxial compression,

$$\varepsilon_{oct} + \sqrt{2}\,\frac{\beta}{2\beta - 1}\,p_\varepsilon - \frac{\sqrt{2}}{3}\,\frac{\beta}{2\beta - 1}\,\varepsilon_u = 0 \quad (\varepsilon_1 < 0) \qquad (2.7)$$

It should be noted that Eqs. 2.6 and 2.7 have points of discontinuity. Equation 2.6, the boundary between the first and second elastic regions, is valid only for states of biaxial compression. However, the region corresponding to the first elastic range is bounded by the curve connecting points $-f_c$, $-f_c$, $-f_d$, f_t, f_t, $-f_d$, and $-f_c$. That is, the boundary curve has discontinuities at $-f_c$ and $-f_d$ where the curve parallels the axis. This arises because of the differences in the stress-strain curve assumed here and that assumed by Kupfer, Hilsdorf, and Rüsch. The Kupfer, Hilsdorf, and Rüsch yield surface joins the tensile stress f_t to the maximum compressive stress $-f_c'$. Since the maximum compressive stress allowed in the uniaxial state corresponds to $-f_d$, then the boundary between elastic and nonelastic regions must connect f_t and $-f_d$. Since there is only one modulus allowed in tension, E_c, the discontinuity is unavoidable.

Equation 2.7, the boundary between crushed and noncrushed regions, is valid only for states of biaxial compression. If one or both of the principal strains is positive, no boundary is defined. Also, the boundary does not parallel the strain axes. If one or both of the principle strains

is positive it is assumed the concrete will crack long before the crushing strain is reached. Hence, it is not deemed necessary to define the boundary except in states of biaxial compression.

Through the use of these transition criterion it is possible to extend the assumed uniaxial stress-strain curve for concrete to cover biaxial stress states. It should be noted that these extrapolated relationships, the transition criterion, assume the failure criteria can predict things other than the elastic-plastic interface. Based on the experimental works of Kupfer, Hilsdorf, and Rüsch and Nilson[15] this is a reasonable assumption. These experimental works indicate the major difference in the stress-strain relations between uniaxial and biaxial states is that the biaxial states have a higher stress capacity. The shape of the stress-strain curve and the active modulus of elasticity show no major differences.

2.4 Concrete Properties

The purpose of this section is to define explicitly what biaxial stress-strain relations are applicable in the different regions of the uniaxial stress-strain curve. The transition from uniaxial to biaxial states was discussed in Section 2.3. The biaxial stress-strain relations presented are in accordance with the experimental results of Kupfer, Hilsdorf, and Rüsch and Nilson. In the following discussion it is implied that the material properties matrix, $[C]_{3x3}$, relates the stress vector, $\{\sigma\}_{3x1}$, to the strain vector, $\{\varepsilon\}_{3x1}$, as

$$\begin{Bmatrix} \sigma_x \\ \sigma_y \\ \tau_{xy} \end{Bmatrix} = [C] \begin{Bmatrix} \varepsilon_x \\ \varepsilon_y \\ \gamma_{xy} \end{Bmatrix}$$

2.4.1 Elastic Concrete

In spite of all its complicating characteristics, elastic concrete, in either range, is assumed an isotropic homogenous linear material. Thus, the stress-strain relations are

$$[C] = \frac{E}{1 - \nu^2} \begin{bmatrix} 1 & \nu & 0 \\ \nu & 1 & 0 \\ 0 & 0 & \frac{1 - \nu}{2} \end{bmatrix}$$

where ν is Poisson's ratio and E is E_c or E_d for the first and second elastic ranges respectively.

2.4.2 Concrete with One Crack

When elastic concrete cracks, which would be indicated by Eq. 2.4, the crack direction is assumed to be perpendicular to the principal tensile stress present in the concrete. This is in accordance with the experimental work of Nilson and Kupfer, Hilsdorf, and Rüsch. The assumed stress-strain relations for elastic concrete with a crack oriented at an angle ϕ counter-clockwise from the x-axis are

$$[C] = [T]^{-1} \begin{bmatrix} E & 0 & 0 \\ 0 & 0 & 0 \\ 0 & 0 & \frac{\beta E}{2(1 + \nu)} \end{bmatrix} [T]^{-1^T}$$

where

E is either E_c or E_d for concrete in the first or second elastic ranges respectively

β is a factor to account for aggregate interlock and any dowel action that may be present. It provides the shear strength capacity of cracked concrete.

T is the transformation matrix to go from the ϕ direction coordinate system to the x, y coordinate system. Its inverse is

$$[T]^{-1} = \begin{bmatrix} \cos^2 \phi & \sin^2 \phi & -2 \cos \phi \sin \phi \\ \sin^2 \phi & \cos^2 \phi & 2 \cos \phi \sin \phi \\ \cos \phi \sin \phi & -\cos \phi \sin \phi & \cos^2 \phi - \sin^2 \phi \end{bmatrix}$$

A few remarks are in order regarding the shear retention factor, β, used here. To omit this effect altogether would imply that elastic cracked concrete would behave as a bundle of uniaxial fibers capable of sustaining only a tensile or compressive load parallel to the direction of the crack. However, this is not a very realistic picture of the load-carrying capacity of cracked concrete. In reality, the cracks in the concrete are not smooth, parallel, frictionless slippage planes infinitesimally close together as mathematically implied. Rather they are irregular, rough planes at nonequal finite distances apart where all slippage is accompanied by a certain amount of expended energy. The shear retention factor accounts for this expenditure of energy plus any dowel action that may be present. By introducing it a shear force is induced on the cracked planes. It was realized that the shear strength along the crack is a function of the crack width, among other factors, and would have an upper and lower bound of one and zero, respectively, relative to the uncracked

shear strength capacity. In the present study, however, a constant value was assumed. The value selected was usually 40 percent (0.4).

The assumed incremental stress-strain relations for cracked and plastic concrete are

$$[C] = \begin{bmatrix} 0 & 0 & 0 \\ 0 & 0 & 0 \\ 0 & 0 & 0 \end{bmatrix}$$

It is conceivable that concrete which is cracked in one direction could be highly loaded in compression parallel to the cracks. Should such a situation develop, the concrete would be carrying the load principally as a two-force member, the shear retention factor notwithstanding. Since the concrete is assumed perfectly plastic beyond axial stress level $-f_d$, such a two-force member would be incapable of carrying further load. Hence, the incremental stiffness is zero.

2.4.3 Concrete with Two Cracks

Concrete is assumed to crack a second time when singly cracked concrete develops a tensile stress in excess of the tensile strength capacity. This second crack is assumed to form perpendicular to the direction of the principal tensile stress. This doubly cracked concrete is assumed to be unable to transfer any load in tension. Since unloading or cyclic loading of the concrete is not allowed, the tension forces which cracked the concrete should not reduce, much less become compressive. Thus, doubly cracked concrete is assumed to have zero stiffness. The stress-strain relations are

$$[C] = \begin{bmatrix} 0 & 0 & 0 \\ 0 & 0 & 0 \\ 0 & 0 & 0 \end{bmatrix}$$

2.4.4 Plastic Concrete

The plastic incremental stress-strain relations for plain concrete yielding in biaxial compression are taken from Mikkola[18] and are also re-developed in Appendix C. These relations assume concrete to yield if the yield criterion, Eq. 2.5,

$$\tau_{oct} + \sqrt{2}\,\frac{\beta - 1}{2\beta - 1}\,p - \frac{\sqrt{2}}{3}\,\frac{\beta}{2\beta - 1}\,f_d = 0$$

is satisfied. Also, the relations between the incremental stresses and strains obey the normality law and flow rule in the theory of plasticity. The incremental relations developed are in the form

$$\{\delta\sigma\} = [C]\,\{\delta\varepsilon\}$$

where [C] is a 3x3 matrix and is symmetric.

It should be noted that an elaborate scheme to handle plastic concrete may be completely unnecessary since true yielding in biaxial compression may be very rare in actual structures. Also, should yielding occur, assuming the concrete to behave as a perfectly plastic material during the early nonelastic deformations is a rather coarse assumption.

2.4.5 Crushed Concrete

Crushed concrete is assumed unable to support any load which would imply a stiffness of zero. Thus, the stress-strain relations are

$$[C] = \begin{bmatrix} 0 & 0 & 0 \\ 0 & 0 & 0 \\ 0 & 0 & 0 \end{bmatrix}$$

2.5 Reinforcement Properties

2.5.1 Elastic Reinforcement

The stress-strain relations for steel reinforcement at an angle ϕ counterclockwise from the x-axis are

$$[C] = [T]^{-1} \begin{bmatrix} E_s & 0 & 0 \\ 0 & 0 & 0 \\ 0 & 0 & 0 \end{bmatrix} [T]^{-1^T}$$

where E_s is the modulus of elasticity of steel.

2.5.2 Plastic Reinforcement

Steel reinforcement which has yielded is assumed to be unable to carry any increase in load. Thus, the incremental stress-strain relations are zero. That is

$$[C] = \begin{bmatrix} 0 & 0 & 0 \\ 0 & 0 & 0 \\ 0 & 0 & 0 \end{bmatrix}$$

2.6 Composite Material

In the previous sections the material properties were listed individually for each material. However, the need for the composite, steel and concrete, material properties exists.

The stress-strain relations for any composite material may be obtained through use of the strain energy density function, U_o,[3] Since strain energy is a scalar quantity, it is possible to compute the strain energy for the bars (steei reinforcement) and the matrix material (concrete) separately and add the energies to obtain the strain energy for the composite. The stress-strain relations for the composite, $[C_{com}]$, may then be found by differentiating the strain energy with respect to the strains. That is,

$$\sigma_{ij} = \frac{\partial U_o}{\partial \varepsilon_{ij}} = f \text{ (strains, material properties)} \quad i, j = 1, 2, 3$$

where

$$\frac{\partial U_o}{\partial \varepsilon_{ij}} \Rightarrow [C_{com}] \{\varepsilon\}$$

Since U_o can be expressed as the sum of the individual components of steel, U_s, and concrete, U_c, then

$$U_o = U_s + U_c$$

and

$$\sigma_{ij} = \frac{\partial U_o}{\partial \varepsilon_{ij}} = \frac{\partial U_s}{\partial \varepsilon_{ij}} + \frac{\partial U_c}{\partial \varepsilon_{ij}} \tag{2.8}$$

Here $\frac{\partial U_s}{\partial \varepsilon_{ij}}$ is the contribution due to the steel individually. These relations are known, say $[C_s]$. Likewise, let $[C_c]$ represent the concrete contribution. Thus Eq. 2.8 may be written as

$$\{\sigma\} = [C_{com}] \{\varepsilon\} = [C_s] \{\varepsilon\} + [C_c] \{\varepsilon\}$$

Therefore, since the materials will experience the same strains, the composite material relations are only the sum of the individual components. That is

$$[C_{com}] = [C_s] + [C_c]$$

3. FINITE ELEMENT APPROACH

3.1 Review of Element Derivation

It is not the purpose of this section to theoretically justify the finite element approach, nor to rigorously derive the element stiffness matrix. The purpose of this section is, however, to logically and systematically review the steps in the element derivation while introducing the notation to be used later. The particular finite element approach taken is the displacement formulation.

The coordinate system selected is a right handed orthogonal set, xyz, with the positive z axis directed upward from the curved shell surface, Fig. 4.

The mathematical sign convention for curvature is adopted.[25] Geometrically the convention is, for the types of shells to be considered here,

1. Curvature is positive if the concave side of the curve is "up", and
2. Curvature is negative if the concave side of the curve is "down".

This may be more evident later when the approximations for the curvatures are introduced, namely

$$\chi_{xx} = z_{,xx}$$

where $z = f(x,y)$ defines the surface of the shell. For example, if $f(x,y) = x^2$ then z is positive for all x and $\chi_{xx} = z_{,xx}$ is positive.

The shape of equation $z = x^2$ is a parabola in the x-z plane opening upwards, which is concave "up".

The element nodal numbering system and local element coordinate system are shown in Fig. 5.

3.1.1 Displacement Function

In the displacement formulation the critical stage is the selection of the assumed approximating displacement functions. The displacement functions for Pecknold's[20] doubly curved shallow shell element, including the twelve-parameter polynomial expression for w used by Melosh,[17] Zienkiewicz[34] and others, are

$$
\begin{aligned}
u &= \alpha_1 + \alpha_2 x + \alpha_3 y + \alpha_4 xy + \alpha_9 (rx + sy) + \\
&+ \alpha_{10}(\tfrac{1}{2} rx^2 - \tfrac{1}{2} ty^2) + \alpha_{11}(rxy + sy^2) \\
v &= \alpha_5 + \alpha_6 x + \alpha_7 y + \alpha_8 xy + \alpha_9 (sx + ty) + \\
&+ \alpha_{10}(sx^2 + txy) + \alpha_{11}(\tfrac{1}{2} ty^2 - \tfrac{1}{2} rx^2) \\
w &= \alpha_9 + \alpha_{10} x + \alpha_{11} y + \alpha_{12} xy + \alpha_{13} x^2 + \alpha_{14} y^2 + \alpha_{15} x^3 + \\
&+ \alpha_{16} x^2 y + \alpha_{17} xy^2 + \alpha_{18} y^3 + \alpha_{19} x^3 y + \alpha_{20} xy^3
\end{aligned}
\tag{3.1}
$$

where

$$
\begin{aligned}
r &= z_{,xx} \\
s &= z_{,xy} \\
t &= z_{,yy} \\
z &= f(x,y)
\end{aligned}
$$

where r, s, and t approximate the curvatures in the x, xy, and y directions respectively and z defines the equation of the surface of the shell.

3.1.2 Strain Displacement Relations

The strain displacement relations used are,

$$\begin{aligned} \varepsilon_{xo} &= u,_x - rw \\ \varepsilon_{yo} &= v,_y - tw \\ \gamma_{xyo} &= u,_y + v,_x - 2sw \\ \chi_x &= w,_{xx} \\ \chi_y &= w,_{yy} \\ 2\chi_{xy} &= 2w,_{xy} \end{aligned} \tag{3.2}$$

These relations include the following assumptions.

1. Normals to the undeformed surface remain straight and normal to the deformed surface.
2. Normals will undergo no extension when the shell is deformed.
3. The strains and deformations of the shell are small compared to the thickness of the shell.
4. The shell is of constant thickness.

Assumption one implies that there is no deformation due to transverse shear. This was first introduced by Love[16] to the theory of shells. Its counterpart in the theory of plates is the Kirchoff assumption and in the theory of beams is - plane sections remain plane. The error involved in this assumption is small provided the shell is "thin", that is,

the ratio of shell thickness to the radius of curvature is small compared to unity. This assumption enables the strains a positive distance z from the middle surface to be expressed as

$$\begin{aligned} \varepsilon_x &= \varepsilon_{xo} - z\chi_x \\ \varepsilon_y &= \varepsilon_{yo} - z\chi_y \\ \gamma_{xy} &= \gamma_{xyo} - 2z\chi_{xy} \end{aligned} \tag{3.3}$$

Assumption three is invoked to reduce the problem from a nonlinear problem to a linear one. This assumption, again, has its counterpart in the theory of beams and theory of plates, namely "small deflection theory".

3.1.3 Doubly Curved Rectangular Shallow Shell Element

For the particular doubly curved rectangular shallow shell element considered the nodal degrees of freedom defined at the middle or reference surface are u, v, w, w_x, and w_y. Here u, v, and w are the tangential and normal displacements at a node in the x, y, and z directions respectively. Also, w_x and w_y are the slopes of w in the x and y directions respectively. These are shown in their positive directions in Fig. 6. Thus, the nodal degrees of freedom can be represented as

$$\{\overline{U}\}_{5\times 1} = \begin{Bmatrix} u \\ v \\ w \\ w_x \\ w_y \end{Bmatrix} = \begin{Bmatrix} u \\ v \\ w \\ \partial w/\partial x \\ \partial w/\partial x \end{Bmatrix}$$

The displacements at one node expressed in terms of the coefficients α are

$$\{\overline{U}\}_{5x1} = [M]_{5x20} \{\alpha\}_{20x1} \tag{3.4}$$

where [M], listed in Table 1, is a function of x, y, r, s, and t only. Using the element nodal numbering system, Fig. 5, a vector of element nodal displacements may be expressed as

$$\{U\}_{20x1} = \begin{Bmatrix} \overline{U}_I \\ \overline{U}_{II} \\ \overline{U}_{III} \\ \overline{U}_{IV} \end{Bmatrix} = \begin{Bmatrix} M_I \\ M_{II} \\ M_{III} \\ M_{IV} \end{Bmatrix}_{20x20} \begin{Bmatrix} \alpha \end{Bmatrix}_{20x1}$$

or as

$$\{U\} = [A]\{\alpha\}$$

where the I, II, III, and IV imply "evaluated at node number". The inverse of this relationship, which will be desired later, is

$$\{\alpha\} = [A]^{-1}\{U\} \tag{3.5}$$

Matrices [A] and $[A]^{-1}$ are given in Tables 2 and 3.

The strain displacement relations, Eq. 3.2, may be written as

$$\{\overline{\varepsilon}\}_{6x1} = \begin{Bmatrix} \varepsilon_o \\ \chi \end{Bmatrix} = [\partial]_{6x5} \{\overline{U}\}_{5x1} \tag{3.6}$$

where

ε_o = vector of middle surface strains,

χ = vector of middle surface curvatures, and

∂ = matrix of differential operators.

Substitution of Eq. 3.4 into Eq. 3.6 yields,

$$\{\bar{\varepsilon}\}_{6x1} = [\partial]\,[M]\,\{\alpha\} = [B]_{6x20}\,\{\alpha\}_{20x1} \tag{3.7}$$

which relates the middle surface strains and curvatures to the unknown coefficients. Matrix [B], listed in Table 4, is a function of x, y, r, s, and t only.

Expressing Love's assumption, Eq. 3.3, regarding strains at any depth to the middle surface quantities, in matrix form, yields

$$\{\varepsilon\}_{3x1} = [G]_{3x6} \begin{Bmatrix} \varepsilon_o \\ \chi \end{Bmatrix}_{6x1} \tag{3.8}$$

where

$$[G] = \begin{bmatrix} 1 & 0 & 0 & -z & 0 & 0 \\ 0 & 0 & 0 & 0 & -z & 0 \\ 0 & 0 & 1 & 0 & 0 & -z \end{bmatrix}$$

The last expression required is to relate stress to strain, namely

$$\{\sigma\}_{3x1} = [C]_{3x3}\,\{\varepsilon\}_{3x1} \tag{3.9}$$

Form the internal work expression

$$W_{int} = \int_V \frac{1}{2}\{\varepsilon\}^T\{\sigma\}\,dv$$

which is integrated over the volume of the element, then substitute Eqs. 3.9, 3.8, 3.7, and 3.5 in turn to obtain,

$$W_{int} = \int_V \frac{1}{2}\{U\}^T\,[A^{-1}]^T\,[B]^T\,[G]^T\,[C]\,[G]\,[B]\,[A^{-1}]\,\{U\}\,dv$$

From the internal work expression, form the internal virtual work by preforming a variation on $\{U\}$. Thus

$$\delta W_{int} = \int_v \{\delta U\}^T [A^{-1}]^T [B]^T [G]^T [C] [G] [B] [A^{-1}] \{U\} \, dv$$

But, since $[A]^{-1}$ and $\{U\}$ are independent of x, y, and z and $[B]$ is independent of z,

$$\delta W_{int} = \{\delta U\}^T [A^{-1}]^T \int_A [B]^T \int_z [G]^T [C] [G] \, dz \, [B] \, dA \, [A^{-1}] \{U\}$$

where

$$[K]_{20x20} = [A^{-1}]^T \int_A [B]^T \int_z [G]^T [C] [G] \, dz \, [B] \, dA \, [A^{-1}] \qquad (3.10)$$

is the desired element stiffness matrix.

Preforming the matrix multiplication for $[G]^T [C] [G]$ and calling the product $[\overline{D}]$ yields,

$$[\overline{D}]_{6x6} = \left[\begin{array}{c|c} [C]_{3x3} & -z[C]_{3x3} \\ \hline -z[C]_{3x3} & z^2[C]_{3x3} \end{array}\right] \qquad (3.11)$$

Substitution of $[\overline{D}]$ into Eq. 3.10 yields

$$[K]_{20x20} = [A^{-1}]^T \int_A [B]^T \int_z [\overline{D}] \, dz \, [B] \, da \, [A^{-1}] \qquad (3.12)$$

a more generally recognized form of the element stiffness matrix.

At this point it is necessary to pause before evaluating the element stiffness matrix. Up until now the development has followed the normal procedure in the finite element approach based on the displacement

formulation. However, if a layered finite element is to be developed it is necessary to introduce the layering concept prior to actually evaluating Eq. 3.12. There are two possible alternatives here. The first is to introduce the concept as directly related to the finite element approach. This will be done here with only the mechanics of the concept being introduced. The second alternative is to introduce the concept independent of the finite element method. This will be done in the next section while discussing the implications of the layering approach.

In evaluating the element stiffness matrix, the mechanics of the layering concept only require that the intermost integral of Eq. 3.12 be integrated for each layer individually rather than as one integration over the total thickness. If the element thickness is divided into layers as in Fig. 7, then this requirement is only that

$$\int_z [\bar{D}]dz = \int_{t_1}^{t_2} [\bar{D}]dz + \int_{t_2}^{t_3} [\bar{D}]dz + \ldots + \int_{t_j}^{t_{j+1}} [\bar{D}_j]dz + \ldots + \int_{t_{NL}}^{t_{NL+1}} [\bar{D}_{NL}]dx \tag{3.13}$$

where

t_j and t_{j+1} = the distance from the middle surface to the bottom and top of the j^{th} layer respectively,

$\bar{D}_j$ = Expression 3.11 with the material properties for the j^{th} layer incorporated, and

NL = the number of layers.

This is simply a step-wise evaluation of a total integral.

The integrated form of one of the right hand side integrals in Eq. 3.13 is

$$\int_{t_j}^{t_{j+1}} [\overline{D}_j]dz = \left[\begin{array}{c|c} (t_{j+1} - t_j)\ [C_j] & -\frac{1}{2}(t_{j+1}^2 - t_j^2)\ [C_j] \\ \hline -\frac{1}{2}(t_{j+1}^2 - t_j^2)\ [C_j] & \frac{1}{3}(t_{j+1}^3 - t_j^2)\ [C_j] \end{array}\right] \tag{3.14}$$

This equation together with Eq. 3.13 is the very heart of the layering concept.

To begin the actual element evaluation, let the three submatrices in Eq. 3.14 be denoted as D_j, E_j, and F_j where

$$\int_{t_j}^{t_{j+1}} [\overline{D}_j]dz = \left[\begin{array}{c|c} [D_j] & [E_j] \\ \hline [E_j] & [F_j] \end{array}\right]$$

and let

$$\int_z [\overline{D}]dz = \left[\begin{array}{c|c} [D] & [E] \\ \hline [E] & [F] \end{array}\right] \tag{3.15}$$

where the j subscript implies the j^{th} layer only and no subscript implies the sum of all the layers. When Eq. 3.14 is evaluated for each layer and summed the result is Eq. 3.15. Equation 3.15 may then be substituted in Eq. 3.12.

If [B] is partitioned to separate the membrane effects, B_ε, from the bending effects, B_χ, then Eq. 3.12 may be expressed as

$$[K] = [A^{-1}]^T \int_x \int_y \left[\begin{array}{c} B_\varepsilon \\ \hline B_\chi \end{array}\right]^T \left[\begin{array}{c|c} D & E \\ \hline E & F \end{array}\right] \left[\begin{array}{c} B_\varepsilon \\ \hline B_\chi \end{array}\right] dxdy\ [A^{-1}] \tag{3.16}$$

It is then possible to express the integral portion of Eq. 3.16 as

$$[K^*]_{20x20} = \int_{-a}^{a} \int_{-b}^{b} \Big([B_\varepsilon]^T [D] [B_\varepsilon] + [B_\varepsilon]^T [E] [B_\chi] + [B_\chi]^T [E] [B_\varepsilon] + [B_\chi]^T [F] [B_\chi] \Big) \, dxdy$$

These matrix products have been evaluated and are presented in Tables 5, 6, 7, and 8. The actual triple matrix product $[A^{-1}]^T [K^*] [A^{-1}]$ is not performed. It is evaluated in the computer.

In order to simplify the tables, the notation

$$[D] = \begin{bmatrix} D_1 & D_4 & D_5 \\ D_4 & D_2 & D_6 \\ D_5 & D_6 & D_3 \end{bmatrix}$$

is introduced for matrices D, E, and F.

3.2 Layering Concept

The layering concept can be considered simply as a discretized application of the stress resultant concept. Unlike the previous approach, this viewpoint is independent of the finite element method. Thus, it is more desirable to present the implications of the method here rather than before. The discussion presented below contrasts the layered with the nonlayered stress resultant concepts.

By introducing the layering system, it is possible to have an out-of-plane variation in material properties while not suffering the consequences of going to a complete three-dimensional finite element analysis.

By layering a two-dimensional element, it is possible to retain the limited degree of freedom from the two-dimensional approach, while securing the material variation with depth advantage of the three-dimensional approach. Also, since each layer is assumed, as in the nonlayered approach, to be in a state of plane stress, it is only necessary to have the two-dimensional constitutive relations.

In the general theory of plates and shells the three-dimensional problem is reduced to a two-dimensional one by introducing the idea of stress resultants. In the nonlayered approach the stress resultants are integrated, in one step, over the total thickness and represent an average of the stress state and material properties present. In this approach there is usually only one set of material properties allowed throughout the depth even though inplane variations may be allowed. In the layered approach, the total thickness is divided into layers, Fig. 8. The stress resultants are then defined for each layer separately by integrating over the layer thickness only. The stress resultants for the total thickness are then obtained by summing the layer resultants.

Within a first order theory the nonlayered stress resultants are defined as, Fig. 9,

$$N_x = \int_{-\frac{h}{2}}^{\frac{h}{2}} \sigma_x dz \qquad M_x = -\int_{-\frac{h}{2}}^{\frac{h}{2}} z\sigma_x dz$$

$$N_y = \int_{-\frac{h}{2}}^{\frac{h}{2}} \sigma_y dz \qquad M_y = -\int_{-\frac{h}{2}}^{\frac{h}{2}} z\sigma_y dz \qquad (3.17)$$

$$N_{xy} = \int_{-\frac{h}{2}}^{\frac{h}{2}} \tau_{xy} dz \qquad M_{xy} = -\int_{-\frac{h}{2}}^{\frac{h}{2}} z\tau_{xy} dz$$

Using the assumption of Love and Kirchoff, the strains a distance z from the middle surface are

$$\begin{aligned} \varepsilon_x &= \varepsilon_{xo} - z\chi_x \\ \varepsilon_y &= \varepsilon_{yo} - z\chi_y \\ \gamma_{xy} &= \gamma_{xyo} - 2z\chi_{xy} \end{aligned} \tag{3.18}$$

Some general stress-strain relations are

$$\{\sigma\} = [C]\{\varepsilon\} \tag{3.19}$$

Using Eqs. 3.18 and 3.19, Eq. 3.17 may be expressed in matrix form as,

$$\begin{Bmatrix} N_x \\ N_y \\ N_{xy} \\ \hdashline M_x \\ M_y \\ M_{xy} \end{Bmatrix} = \left[\begin{array}{c:c} h[C] & 0 \\ \hdashline 0 & \frac{h^3}{12}[C] \end{array}\right] \begin{Bmatrix} \varepsilon_{xo} \\ \varepsilon_{yo} \\ \gamma_{xyo} \\ \hdashline \chi_x \\ \chi_y \\ 2\chi_{xy} \end{Bmatrix}$$

It is important to note that:

1. The equations uncouple, that is, the membrane forces depend only on the middle surface strains and the moments only on the curvatures. With the more refined shell theories, a coupling would be present. However, theories containing a Donnell order of approximation are considered adequate and these as shown above are uncoupled.

2. The 6 x 6 matrix is a function of the limits of integration defining the stress resultants and the material properties matrix only.
3. The equations refer to the total thickness.

The individual layer stress resultants are defined as in Eq. 3.17 except the limits of integration are t_j and t_{j+1} instead of -h/2 and h/2. Here again t_j and t_{j+1}, Fig. 8, represent the distance from the middle surface to the bottom and top of the j^{th} layer, respectively. Using Eqs. 3.18 and 3.19 the j^{th} layer resultants may be expressed as,

$$\left\{\begin{array}{c} N_x \\ N_y \\ N_{xy} \\ \hline M_x \\ M_y \\ M_{xy} \end{array}\right\}_j = \left[\begin{array}{c|c} (t_{j+1} - t_j)\,[C_j] & -\frac{1}{2}(t_{j+1}^2 - t_j^2)\,[C_j] \\ \hline -\frac{1}{2}(t_{j+1}^2 - t_j^2)\,[C_j] & \frac{1}{3}(t_{j+1}^3 - t_j^3)\,[C_j] \end{array}\right] \left\{\begin{array}{c} \varepsilon_{xo} \\ \varepsilon_{yo} \\ \gamma_{xyo} \\ \hline \chi_x \\ \chi_y \\ 2\chi_{xy} \end{array}\right\} \tag{3.20}$$

Study of this system of equations reveals that

1. The equations now do not uncouple.
2. The 6 x 6 matrix is a function of the limits of integration and the layer material properties matrix only.
3. The equations refer only to the j^{th} layer.
4. The 6 x 6 matrix is the same as the matrix in Eq. 3.14.

Civil Engineering Department
Bliss C. E. Building
University of Illinois
Urbana, Illinois 61801

Thus, Eq. 3.20 could be expressed as

$$\left\{\begin{matrix} N \\ M \end{matrix}\right\}_j = \int_{t_j}^{t_{j+1}} [\bar{D}_j] dz \left\{\begin{matrix} \varepsilon_o \\ \chi \end{matrix}\right\}$$

which implies $[\bar{D}_j]$ relates the j^{th} layer stress resultants to the middle surface strains and curvatures.

In order to obtain the total thickness stress resultant relations, it is only necessary in the layering approach to obtain each layers' contribution and add them, as was previously indicated in Eq. 3.13. In contrast to the nonlayered approach, even the total stress resultants relations do not uncouple unless the section has vertical symmetry.

For each layer the method is independent of the specific type of material properties present; and, as a whole, the sum does not require all layers to have the same material properties. Thus, it is conceivable that a particular finite element employing this approach could contain as many different layer material properties as it has layers. This, then allows for any material property variation through the thickness of the structure.

To demonstrate the desirability of this out-of-plane variation, consider a real reinforced concrete slab loaded to failure. Presumably before, but most definitely at failure, a vertical section cut through the slab would reveal that the compression region contained elastic, plastic, and possibly crushed concrete. Also, the tensile region would contain elastic, singly cracked, and possibly doubly cracked concrete. There is also the possibility of the reinforcing being at yielding or even in the strain hardening region. The influence of such variations can only be simulated through modifications in the flexural stiffness of the slab,

modified EI, or can be achieved through the layered system. Both schemes are readily adapted to account for any plan-wise variation. However, the modified EI concept does experience difficulty in accounting for the coupling effects, as discussed in the following paragraphs.

Classical laminate plate theory,[22,24,31] along with the layering approach described here, displays a coupling phenomenon between inplane extension and transverse bending not found in homogeneous plates. For laminates which are symmetric with respect to the middle plane of the plate, the coupling vanishes. The severity of the coupling effect depends on the number of plies in the composite and on the degree of anisotropy of the individual layers. Since the orthotropic solution is the limiting case, the effects of the coupling can be ascertained. Also, only a few layers are necessary to make the orthotropic solution a reasonable estimate of the response of coupled plates,[28] Fig. 10.

For the highly anisotropic composites recent work[28,29,31,32] has shown that coupling can severely effect laminate behavior. In particular, bending deflections are increased while buckling loads and vibration frequencies are reduced compared to results obtained by neglecting coupling.[30] Thus the real effect of coupling is to reduce the effective stiffness of the plate.[28]

Using the idea of the reduced effective stiffness, Ashton[1] considered an approximate method of solution to reduce the problem to an equivalent anisotropic bending problem. His "reduced stiffness matrix" uncouples the potential energy expression, that is the inplane extension and transverse bending, at the expense of coupling the compatibility conditions. He states this new coupling should have a smaller effect than the

extension-bending coupling. Thus, he concludes the "reduced stiffness matrix" appears likely to yield a more accurate solution than when extension-bending coupling is neglected.

Kicher[12] analyzed unbalanced cross-plied laminated plates of elliptic planform under uniform pressure. He obtained closed form solutions for two cases of membrane boundary conditions, either free (zero normal and shear boundary forces) or clamped (zero normal and tangential displacements). Bending displacements were always considered clamped. When the coupling effect is neglected at the outset, there is no need to select membrane boundary conditions and the displacement results indicated that the plate is too stiff. For the class of composites considered the selection of membrane boundary conditions played a minor role in the displacement predictions provided coupling is considered. Ashton's approximate method was considered and agreement was very close for the free membrane boundary conditions. However, when the boundary conditions were considered clamped, the approximate solution yielded the same results as when coupling is neglected.

Whitney[30] using a Fourier series method also investigated some boundary condition effects. He concluded that the effect of bending-extensional coupling on laminate response is essentially independent of boundary conditions and is primarily a function of the anisotropy of the individual plies and the number of layers in the laminate. However, for certain orientations of antisymmetric angle-ply plates, membrane boundary conditions can significantly influence plate response. As a result, the reduced bending stiffness approximation does not give acceptable agreement with coupled laminate solutions for these orientations. Pryor and Barker,[21] using a finite element analysis, substantiated the conclusions of Whitney.

Since the severity of the coupling effect depends on the number of plies, among other factors, the coupling should have a dominate effect in a finite element analysis when cracking of concrete is considered. For unlike the ideal regular lamina in a manufactured composite, cracked concrete could at best be modeled as a two unequal laminate composite, one cracked, one uncracked. Thus, the worst case in laminate theory, the two-ply case, is of interest here. Also, in all of the cases cited here, some assumptions are usually made concerning the terms in the coupling matrix E in order to obtain closed form or Fourier series solutions. None of these assumptions are as general as the coupling matrix used here. This could invalidate most or all of the results just reported, particularly any correlation between approximate and more exact solutions. Also, it would probably aggravate all influences on the plate response. Presumably it would be safe to assume that if the membrane boundary conditions can significantly influence plate response as indicated by Whitney, then these boundary conditions must be considered. For the finite element method, in particular, the membrane boundary conditions correspond to the inplane degree of freedom. The actual importance of these degrees of freedom is shown in the McNeice reinforced concrete plate example, Section 5.3.3.

The modified EI approach of Bell[2] and Jofriet and McNeice[10] or the anisotropic stiffness approach of Cervenka[6] and Franklin[8] are similar to the approximate method of Ashton where the problem is reduced to an equivalent anisotropic bending problem. In essence all three of these methods presuppose the relationship of inplane and out-of-plane quantities. However, Kicher and Whitney indicate that for certain types of composites and membrane boundary conditions the approximation does not give acceptable

results. The layering, on the other hand, does not attempt to predefine inplane - out-of-plane relationships nor does it require any simplifying assumptions regarding the coupling matrix in order to obtain a solution.

3.3 Generalized Load Vector

The generalized load vector is given by the expression.

$$\{L\}_{20x1} = [A^{-1}]^T_{20x20} \int_x \int_y [M]^T_{20x5} \int_z dz \{X\}_{5x1} \, dxdy$$

where $\{X\}$ is the vector of external distributed loads. For the case of uniform pressure load, of interest later, $\{X\}$ reduces to

$$\{X\} = \begin{Bmatrix} 0 \\ 0 \\ x_o \\ 0 \\ 0 \end{Bmatrix}$$

and the load vector is,

$$\{L\}^T_{20x1} = \{0,\ 0,\ 1,\ \frac{a}{3},\ \frac{b}{3},\ 0,\ 0,\ 1,\ \frac{a}{3},\ -\frac{b}{3},\ 0,\ 0,\ 1,\ -\frac{a}{3},\ \frac{b}{3},$$

$$0,\ 0,\ 1,\ -\frac{a}{3},\ -\frac{b}{3}\}abx_o$$

If statically equivalent loads were used instead, the moments $\pm\frac{a}{3}$ and $\pm\frac{b}{3}$ would not appear.

3.4 Displacement Compatibility

The compatibility of displacements across element boundaries depends only on the assumed displacement functions and the nodal degrees

of freedom. To see if an element is conforming, equality must exist for the deflections of the two elements A and B shown in Fig. 11 along their common edge.

First, the inplane displacement, u, from Eq. 3.1, is quadratic in y. Thus, three boundary conditions are required for compatibility. However, only two are available, the u displacements at each end of the common edge. Thus, the inplane displacements are not compatible. If r, s, and t were zero, however, the displacements would be compatible. A similar situation exists for the v displacements.

Second, the w displacement, from Eq. 3.1, is cubic in y. Thus, four boundary conditions are required; four are available, w and w_y at each end. Thus, the w displacements and the slope along the edge w_y are compatible.

Third, the slope across the common edge, w_x is cubic in y. Again four boundary conditions are required; only two exist, $w_{,x}$ at each end. Thus, the transverse slope is not compatible.

Since the other edges could be treated likewise, the element only conforms with respect to the out-of-plane displacement w and the slope w_y along the edge.

3.5 Boundary Conditions

Boundary conditions are only of the displacement class and are either fixed or free. All nodal degrees of freedom are considered at the reference surface, which is usually the midsurface, used in defining the element stiffness matrix. They are either normal or tangential to the shell surface at the node. Thus, when an inplane displacement is specified

to be zero, only the reference surface is constrained in that direction. It does not constrain any other inplane displacements through the depth. If the inplane displacement is considered free, there is no constraint on the movement of the "neutral surface". Likewise, when one of the slopes is specified to be zero, this requires that there is no variation in the corresponding inplane displacement through the depth but does not in any way constrain the reference surface displacement.

4. INCREMENTAL ANALYSIS

4.1 General Steps

The overall approach of the investigation is the performance of a nonlinear finite element analysis of reinforced concrete surface structures using the displacement finite element formulation. The method progresses through the use of an iterative or step-by-step procedure with the nonlinearity being introduced through the material properties. Since reinforced concrete structures are the prime interest, geometric nonlinearities are not considered in this initial study. The numerical procedure used in this step-by-step approach is referred to by Zienkiewicz[35] as the "incremental-variable elasticity" procedure. Although the nonlinearity is introduced only through the material properties, it should be noted, at least in this investigation, that any given layer of an element is composed of material in only one property state.

The incremental analysis incorporates the layering concept, the allowable material properties, and the transition between material property zones. As programmed the incremental procedure must analyze the structure, generate the layer stress states, check these against the transition criteria, make any necessary material property modifications, obtain any necessary correction forces, and then reanalyze the structure.

This analysis and reanalysis of the structure falls into two main categories. The first category is analyzing the structure with an applied load increment; called increments. The second is analyzing the structure with the correction forces; called iterations. In the course of the incremental analysis it becomes necessary to apply a load increment

and then iterate about this loading until the structure reaches an equilibrium state, Fig. 12. Once equilibrium is obtained, then another load increment is applied. This is analogous to loading a real specimen in the laboratory and allowing it to come to an equilibrium balance before increasing the load. The steplike or plateau shape of the analytical curve, Fig. 12, is due to this search for an equilibrium configuration before increasing the external load.

The structural stiffness matrix is updated at the beginning of each load increment. The updating procedure is carried out simultaneously with layer stress generation and various checking routines. In addition to this one mandatory update, other updates occur at random whenever it is possible to completely absorb a material property change and the accompanying displacements in only one update. Examples of this type of behavior are cracking or crushing of the concrete and yielding of the reinforcement. Plastic behavior of the concrete does not fall in this category. The reason for the random update is two-fold. First, it makes for much easier book-keeping in the computer program. Second, it is an attempt to reduce the number of iterations about a particular load increment by improving the next guess to the correction displacements, since a more recent structural stiffness matrix would be available. The iterations about a load increment are assumed to have converged when all the interation displacements due to the correction forces are small compared to all corresponding incremental displacements caused by the last load increment. The system is assumed to have converged when no more than a ±5 percent change occurs in any quantity.

The essential steps in the solution process for a typical load increment are as follows.

1. Apply a load increment and analyze the structure to obtain the nodal displacements.

Do the following for each element i:

2. Convert the nodal displacements to middle surface strains and curvatures.

Do the following for each layer j of element i:

3. Convert the middle surface strains and curvatures to layer strains.
4. Using the old material properties (the ones incorporated in the system of equations) for the layer determine the layer stresses.
5. Check this stress state against the applicable transition criteria. If none are exceeded, go to step 8.
6. Calculate the excess amount of stress present in layer j and convert to excess layer stress resultants, $\begin{Bmatrix} N \\ M \end{Bmatrix}_j^{ex}$, and add these to the element sum, $\begin{Bmatrix} N \\ M \end{Bmatrix}^{ex}$.
7. If the structural stiffness matrix is to be updated, compute the difference between the old and new material properties. Use this difference to obtain the change in the layer stress resultant - middle surface strain and curvature relations and add to the element sum.
8. If more unprocessed layers of element i exist, repeat steps 3 through 7. If not, go to step 9.
9. If no transition criteria were exceeded for the i^{th} element, go to step 11. Otherwise, convert the excess stress resultants into excess element nodal forces as

$$\{F\}_{ex} = [A^{-1}]^T \int_{-a}^{a} \int_{-b}^{b} [B]^T \, dx \, dy \begin{Bmatrix} N \\ M \end{Bmatrix}^{ex}$$

and put these forces in the excess force vector, $\{\overline{F}\}$.

10. If the structural stiffness matrix is to be changed, use the change in the stress resultant relations to generate the difference in the element stiffness matrix and substract this from the system stiffness matrix. This substraction of the difference in effect yields a new system stiffness matrix with the new material properties, but does not require all the effort of reassembling it.
11. If all elements have not been checked repeat steps 2 through 10. Otherwise, reanalyze the structure using the excess force vector, $\{\overline{F}\}$.
12. Check the displacements from step 11 for convergence. If they have converged, repeat steps 1 through 12. If they have not converged, repeat steps 2 through 12 until convergence is obtained or until the maximum number of allowed iterations about a load increment has been completed. The program then stops.

4.2 Middle Surface Strains

From the equations in the previous chapter, it is possible to express the middle surface strains and curvatures in terms of the nodal displacement as

$$\left\{\begin{matrix}\varepsilon_o \\ \chi\end{matrix}\right\}_{6x1} = [\partial]\,[M]\,\{\alpha\} = [B]\,\{\alpha\} = [B]_{6x20}\,[A^{-1}]_{20x20}\,\{U\}_{20x1}$$

This expression defines the distribution of strains and curvatures throughout the element based on the nodal displacements. If [B] is evaluated by integrating over the area of the element and averaged, then

$$\left\{\begin{matrix}\varepsilon_o \\ \chi\end{matrix}\right\} = \frac{1}{4ab} \int_{-a}^{a} \int_{-b}^{b} [B(x,y)]\,[A^{-1}]\,\{U\}\,dx\,dy$$

Since $[A^{-1}]$ and $\{U\}$ are independent of x and y, this reduces to

$$\left\{\begin{matrix}\varepsilon_o \\ \chi\end{matrix}\right\} = \frac{1}{4ab} \int_{-a}^{a} \int_{-b}^{b} [B(x,y)]\,dx\,dy\,[A^{-1}]\,\{U\} \qquad (4.1)$$

which gives the "integrated average" middle surface strains and curvatures in the element. However, the "horizontal" location of the quantities on the middle surface is unknown. Furthermore, none of the six quantities are required to be at the same location on the middle surface. Equation 4.1 has been evaluated and the results are listed in Table 9.

In spite of their unknown location, the "integrated average" values are much preferred to some of the other possibilities. These possibilities include, among others, evaluating the middle surface quantities at the element center or at the nodes. If evaluated at the nodes it is necessary to average the values in some fashion to obtain one set of values to represent the element. However, both of these schemes are susceptible to some error if the element distribution is quadratic, cubic, or has some sharp peaks. If such distributions occur, it is felt the "integrated

average" will better represent the actual distribution present, since it has no particular bias toward a linear, quadratic, cubic, or other distribution. Also, this approach has the elegance of continuity since the same matrices are used here as in the element formulation.

4.3 Layer Stresses

In order to determine the layer stresses it is necessary to first determine the layer strains. Based on Love's assumption of normals remaining normal, the j^{th} layer strains at the mid-depth of the layer are

$$\varepsilon_x = \varepsilon_{xo} - \frac{1}{2}(t_{j+1} + t_j)\chi_x$$

$$\varepsilon_y = \varepsilon_{yo} - \frac{1}{2}(t_{j+1} + t_j)\chi_y$$

$$\gamma_{xy} = \gamma_{xyo} - \frac{1}{2}(t_{j+1} + t_j)\ (2\chi_{xy})$$

where $\frac{1}{2}(t_{j+1} + t_j)$ is the distance from the middle surface to the mid-depth of the j^{th} layer. These mid-depth layer strains are assumed to be representative of the strains in the layer. Again the "horizontal" location of the strains is not known since the "horizontal" location of the middle surface quantities is not known.

Based on the representative layer strains, some representative component layer stresses are obtained through the use of the component material properties, as

$$\begin{Bmatrix} \sigma_x \\ \sigma_y \\ \tau_{xy} \end{Bmatrix} = [C]_{3x3} \begin{Bmatrix} \varepsilon_x \\ \varepsilon_y \\ \gamma_{xy} \end{Bmatrix}$$

It should be noted that in order to determine the stresses in the concrete or steel only the stress-strain relations for that individual material should be used. Also, the stress-strain relations used should be those incorporated in the system stiffness matrix, for it is this stiffness that is reflected in the layer strains via the middle surface quantities and the nodal displacements. These representative component layer stresses are then checked, through the use of the transition criterion, to determine if any material properties have been exceeded or if any excess stresses need to be accounted for.

4.4 Excess Nodal Forces

Excess layer stresses are converted to excess element nodal forces by the following logic. Considering the individual terms in the basic equation,

$$\{F\}_{20\times 1} = [A^{-1}]^T \int_x \int_y [B]^T \int_z [\bar{D}]\, dz\, [B]\, dx\, dy\, [A^{-1}]\, \{U\} \qquad (4.2)$$

and using Eq. 3.7

$$\begin{Bmatrix} \varepsilon_o \\ \chi \end{Bmatrix} = [B]\, [A^{-1}]\, \{U\}$$

the layer stress resultants may be expressed as

$$\begin{Bmatrix} N \\ M \end{Bmatrix}_j = \int_z [\bar{D}_j]\, dz \begin{Bmatrix} \varepsilon_o \\ \chi \end{Bmatrix} = \int_z [\bar{D}_j]\, dz\, [B]\, [A^{-1}]\, \{U\} \qquad (4.3)$$

Substitution of Eq. 4.3 in Eq. 4.2 yields

$$\{F\}_{20\times 1} = [A^{-1}]^T \int_x \int_y [B]^T\, dx\, dy \begin{Bmatrix} N \\ M \end{Bmatrix}_j$$

If $\left\{\begin{matrix} N \\ M \end{matrix}\right\}_j^{ex}$ are the excess stress resultants where

$$\int_{t_j}^{t_{j+1}} [G]^T \{\sigma\}_{ex} \, dz = \left\{\begin{matrix} N \\ M \end{matrix}\right\}_j^{ex}$$

and $\{\sigma\}_{ex}$ is the excess layer stress, then

$$\{F_j\}_{ex} = [A^{-1}]^T \int_x \int_y [B]^T \, dx \, dy \left\{\begin{matrix} N \\ M \end{matrix}\right\}_j^{ex} \tag{4.4}$$

are the excess nodal forces that result from layer j due to the excess stresses for that layer. Equation 4.4 is listed in Table 10.

4.5 Changing Material Properties

When the transition criterion indicates the need to change some material properties and the computer program allows the changes to be made, the changes are made in accordance with the following logic. In general, the present and the desired new material types are known. Thus, the material properties can be generated as in Chapter 2. Therefore, the difference between the two material states can be obtained. If the difference is used to create an element stiffness matrix, by evaluating Eq. 3.12, this matrix would represent the difference between the present element stiffness matrix incorporated in the system stiffness matrix and the new desired element stiffness matrix. It is only necessary then to subtract the matrix based on the difference from the system stiffness matrix in order to obtain a new system matrix with the desired new material properties. The net effect of this manuevering is to obtain a new system matrix without having to reassemble all of it.

When changing material properties some excess stresses usually exist. These excess stresses are only the difference between the stress states caused by the same strain state on the different material properties. Mathematically this is,

$$\{\sigma\}_{ex} = \{\sigma_{old}\} - \{\sigma_{new}\}$$

where

$\{\sigma\}_{ex}$ = the excess stress vector,

$\{\sigma_{old}\}$ = the stress state the old material properties indicate to be present, and

$\{\sigma_{new}\}$ = the stress state the new material properties can tolerate.

The only complications arise when plastic behavior of concrete is involved. Here two cases exist:

1. When the concrete was elastic and is to go plastic, and
2. When the concrete is plastic and continues to be plastic.

In the first case, the procedure is diagrammatically shown in Fig. 13. Here the old elastic state is designated as $\{\sigma_{old}\}$ and the new indicated state, beyond the yield surface, is $\{\sigma_{xy}\}$. This change in stress was caused by the strain increment $\{\delta\varepsilon\}$; the plastic strain increment is $\{\delta\varepsilon^p\}$. Stress level $\{\sigma_{xy}\}$ is scaled to the yield surface along a radial; the scaled value is $\{\sigma_{yd}\}$. Using stress state $\{\sigma_{yd}\}$ and the plastic stress-strain relations of Mikkola some incremental stress-strain relations, [C], are obtained. Using the incremental stress-strain relations, [C], and the plastic strain increment $\{\delta\varepsilon^p\}$ the incremental plastic stresses, $\{\sigma^p\}$, are found. Adding $\{\sigma^p\}$ to $\{\sigma_{yd}\}$ the total plastic stress state is found, $\{\sigma^*\}$.

However, this stress state is not on the yield surface. Thus, $\{\sigma^*\}$ is scaled to the yield surface to form the final plastic stress state, $\{\sigma^*_{yd}\}$. The excess stress is then

$$\{\sigma\}_{ex} = \{\sigma_{xy}\} - \{\sigma^*_{yd}\}$$

and the new material properties are $[C^*]$.

In the second case, the procedure is shown diagrammatically in Fig. 14. Here the old stress state and material properties are $\{\sigma_{yd}\}$ and $[C]$. The incremental strains, $\{\delta\varepsilon\}$, equal the plastic incremental strains, $\{\delta\varepsilon^p\}$. The indicated stress state is $\{\sigma^*\}$, where

$$\{\sigma^*\} = \{\sigma_{yd}\} + \{\sigma^p\} = \{\sigma_{yd}\} + [C]\ \{\delta\varepsilon\}$$

Like before, this stress state is not on the yield surface so it is scaled to form stress state $\{\sigma^*_{yd}\}$ with incremental stress-strain relations $[C^*]$. The excess stress is then

$$\{\sigma\}_{ex} = \{\sigma^*\} - \{\sigma^*_{yd}\}$$

and the new material properties are $[C^*]$.

5. NUMERICAL EXAMPLES

5.1 General

To demonstrate the applicability and flexibility of the proposed incremental analysis a series of numerical examples are presented. The examples are presented in a logical sequence of increasing complexity; beams then plates then shells.

The beam examples considered are of two types, theoretical and experimental. The theoretical beams are for comparison of the theoretical and computational procedures. The first experimental beam shows the effect of the loading increment size, while the second the effects of inplane forces.

The plate examples are also of two types. First some ideal uniform stress-state comparisons are made with the experimental results of Houbolt[9] and Cardenas and Sozen.[5] Second, the experimental slab of McNeice[10] is analyzed.

The shell example is experimental. Comparisons are made with the experimental funicular shell of Odello and Allgood.[19]

5.2 Beams

For the purpose of distinguishing what the element and the incremental analysis characteristics and idiocrasies are, a series of determinate beams are investigated. To remove all experimental uncertainties and complications the first beams considered are completely theoretical. These simply supported beams are loaded with either end moments or concentrated mid-span loads. These beams are primarily to check out the

cracking behavior. The third beam is to compare the analytical load deflection curve with an experimental one and to determine the influence of the load increment size. The fourth beam is similar to the third except for the inclusion of an axial load. The primary intent of these two experimental checks is to provide a basic feel for and confidence in the analysis technique.

5.2.1 Simply Supported Theoretical Beams

In order to determine the accuracy of the cracking procedure, including the application of excess nodal loads, two simply supported theoretical beams are considered. The beam configuration is shown in Fig. 15. Two loading conditions, equal end moments and concentrated mid-span load, both extreme cases, are investigated. A theoretical analysis, using simple beam theory, and the incremental analysis as described in this study are performed. The load deflection curves, as computed from these two methods, are presented in Figs. 16 and 17.

It is the inconsistence in the agreement for the two sets of curves that is of interest. This inconsistence arises because the excess nodal forces (correction forces) depend only on the total energy to be dissipated, not on the distribution of the energy. This in itself may not be startling; however, it does have a visible effect on the load-deflection curves. The scheme used to generate excess nodal forces from excess stresses has a tendency to create large nodal moments and small vertical shears irregardless of the type of external loading. It is precisely this tendency that has an effect on the load-deflection curves, for moments do not create the same deflection shape as vertical loads.

Consider the two loading cases here. The first, equal end moments, causes a uniform energy (stress) distribution. The correction forces, principally moments, yield correction displacements based on a uniform energy distribution. Thus, the external and the correction displacements are of the same type - both based on end moments. Hence, the agreement is excellent.

The second loading, concentrated mid-span load, causes a linear energy distribution. The correction forces, again principally moments, yield correction displacements based on a uniform energy distribution. Thus, the external and the correction displacement shapes are of different types. Hence, there is a disagreement in the deflection computed by the two schemes.

Admittedly these are two extreme cases of stress distribution; however, it should be realized that this basic behavior is incorporated in the analysis technique. Also, it should be realized that the bias extends only to external manifestations, like deflections and rotations, not to internal quantities such as stresses and strains.

5.2.2 Burns and Siess

The effect of the load increment size and the ability of the incremental finite element analysis to accurately predict the ultimate load are shown by comparison with the beam tested by Burns and Siess.[4] The beam with its physical properties and the element grid with the layering and properties noted are shown in Figs. 18 and 19. The experimental and analytical load-deflection curves are shown in Fig. 20. One analytical curve is obtained by five equal load increments of 4000 pounds. The other curve is obtained by four equal load increments of 4000 pounds.

and then eight 500 pound increments. In the case of the larger increments the analysis overshoots the ultimate load and then makes tremendous corrections to try to attain an equilibrium configuration. Such a configuration is finally reached at a displacement of 1.85 inches with a load of 20,000 pounds. As should be expected the smaller increments do not overshoot the ultimate load as greatly. Equilibrium is reached with a load of 20,000 pounds at a displacement of 1.49 inches.

The final equilibrium displacements attained from the two alternative load increment schemes are different. This is because the final cracked configurations are slightly different for the two cases, Fig. 21. The larger increment size causes slightly more cracking and steel reinforcement yielding to penetrate further. Admittedly, a large number of corrections are made at the load level of 20,000 pounds since this is the practical ultimate load. Nevertheless, the excellent agreement of the curves is encouraging.

5.2.3 Wight

The effect of the inplane loads is shown in the beam tested by Wight.[33] The beam with its physical properties and the finite element grid arrangement are shown in Figs. 22 and 23. In the test axial load is held constant while the vertical shear is increased from zero to the maximum. The experimental and analytical load-deflection curves are shown in Fig. 24. Although the beam is very similar to that of Burns there is a rather pronounced disagreement between the computed results and the experimental values. This may be due in part to the tendency of the test beam to rotate with the loading condition. Also, the secondary P-δ effects of the axial load are

not incorporated in the analytical analysis. Finally, the ability of the program to handle inplane loads is not as refined as for out-of-plane loads, since the only quadratic term in the assumed inplane displacement functions is the cross product term. Nevertheless, the program is capable of estimating the ultimate load, even though the deflections just prior to ultimate are about one-half the experimental in this case. Thus, it appears the analysis technique is rather sensitive to inplane loads. The beam material properties at equilibrium for a load of 21.64 kips are shown in Fig. 25.

5.3 Plates

To indicate the accuracy of the analysis technique and the behavior of the layered element system in biaxial stress states, a series of comparisons are made with the experimental results of Houbolt[9] and Cardenas and Sozen.[5] These are ideal specimens in the sense that they have a constant stress field. Also, the two-way slab of McNeice is analyzed since it has a more realistic stress distribution.

5.3.1 Houbolt

In the test performed by Houbolt[9] only rectangular specimens were considered, Fig. 26. The specimens were used in conjunction with third point line loads creating a constant moment region in uniaxial bending. A total of fifteen specimens were tested; six isotropically reinforced, nine nonisotropically reinforced. The purpose of the tests was to determine the effectiveness of reinforcing steel placed in two layers when the two layers make different angles with each other and with the directions of principal

moments. The test results were presented as load versus steel strain, longitudinal concrete strain, and transverse concrete strain plots.

A layered element analysis was performed on selected specimens. Comparisons between the experimental and the computed results are presented in Figs. 28, 29, 30, and 31. The discontinuity in the experimental curve is due to unloading and then reloading the test specimen. The properties of the specimens considered are summarized in Table 11. The main conclusion from this series of tests is that the analysis technique is capable of handling steel reinforcing placed in any direction.

5.3.2 Cardenas and Sozen

In the tests performed by Cardenas,[5] both circular and rectangular specimens were involved. Only the rectangular specimens are of interest here, Fig. 32. The rectangular specimens were subjected to three different loading conditions to create a constant moment region: uniaxial bending, pure torsion, and combined bending and torsion. A total of thirty-five specimens were tested; twenty-three were isotropically reinforced and twelve were nonisotropically reinforced. The main variables investigated were: the amount of reinforcement and the orientation of the reinforcement with respect to the principal moment axes. The results of the tests were presented as moment to curvature, moment to steel strain, and moment to concrete strain plots.

A layered element analysis was performed on selected specimens from each group. The load increments and layer scheme used in the analysis with a one element idealization of the constant moment region are given in Table 12 and Fig. 32 respectively. The properties of the specimens considered and the important parameters in the analysis procedure are summarized in

Table 12. The experimental and computed results are presented in Figs. 33 to 38.

It should be emphasized that not only do the moment-curvature plots but also the moment-strain, concrete and steel, plots show excellent agreement. These comparisons then establish how accurately the analytical model can describe what is occurring at a point or on a small region of the plate. Thus, the comparisons establish the validity or at least the credibility of the models' assumed material properties.

The need for the shear retention factor β became evident while checking the pure torsion specimen, B15. Without the shear retention term the computer program indicated an unstable crack configuration was attained when the load was approximately one-fourth of the experimental ultimate. The cracked configuration at this instant indicated a series of cracks at $-45°$ with respect to the x-axis had just reached the middle surface from the top, while a similar series of cracks at $45°$ had approached from the bottom. Physically such a concrete slab would still be stable; however, due to the mathematical assumptions regarding the behavior of cracked concrete the system was mathematically unstable. The problem is that the cracked concrete was assumed to have no torsional or shear stiffness whatsoever. It is precisely these stiffnesses which physically can be attributed to aggregate interlock and dowel action that the shear retention factor retains in cracked concrete. When this factor was included, the curves in Figs. 33 to 38 were obtained.

There appears to be little sensitivity of the solution to the particular numerical value of β used, provided it is above some minimum.

Main Reference Room
Civil Engineering Department
B106 C. E. Building
University of Illinois
Urbana, Illinois 61801

This same torsion specimen was analyzed with β values of 0.2 and 0.4 and very little difference was noted in the solution. In the case of pure torsion as in the other cases considered, the inclusion of the shear retention factor only causes the mathematical model to remain stable so the equations remain solvable and has little direct influence on the numerical values generated. In all, values of β ranged from 0.2 to 1.0 in addition to the unacceptable value of 0.0. In view of the negligible numerical effect, the value of β was arbitrarily selected as 0.4

If the β factor is looked upon as resulting from aggregate interlock its magnitude should vary with the size of the crack opening. However, since the results of these slab models indicated little sensitivity to the numerical value chosen, the use of a constant rather than a variable value seems justified.

5.3.3 McNeice

The corner supported two-way slab of McNeice[10] was also analyzed. The principal reasons for using the slab are that there is a variation of moments thru the slab plan and that others have made comparisons with it. The disadvantages of the slab are the lack of detailed test results and the possibility that it may be a micro-concrete model. This belief is supported simply by the size of the specimen. If it is a micro-concrete model then the material properties assumed in Chapter 2 are not as adequate as they are for regular concrete. McNeice's slab was 36 inches square by 1.75 inches thick with an isotropic mesh of 0.85 percent reinforcing steel.

The slab was subjected to a central concentrated load. Since the yield point of the steel reinforcement was not given two possible values are assumed, 40 ksi and 50 ksi, to determine the effect of the steel yield point. Scanlon[23] and Lin[14] have also analytically investigated this slab. Scanlon used a layered rectangular plate bending element with four degrees of freedom at each corner node. Lin extended Scanlon's approach to include elasto-plastic behavior for steel and concrete. Figure 39 shows the finite element grid used; Fig. 40 shows the load deflection curves for experimental and analytical results.

McNeice's slab was also analyzed with the corner support considered pinned (the first solution considered the corners as roller supports). These results are also presented in Fig. 40. As is very evident from the figure, the inplane support conditions greatly influence the stiffness of the system. The particular membrane boundary conditions here do not affect the plate response before any cracking occurs. This is probably because the coupling present in the original elastic state is small since its only contribution is from the steel reinforcing. However, once cracking occurs and the amount of coupling increases due to the increase in the anti-symmetric composition, the membrane boundary conditions become very important. The plate deflections are not as great in the clamped case as in the free. Part of the difference is due directly to the boundary conditions and the rest is due to the different structural configurations caused by a different rate of cracking in the two cases. This reduction in cracking is shown in Figs. 41 and 42 where the cracked configuration for both boundary conditions are given at equilibrium with a load of 2800 pounds. In the free case 231

layers are cracked compared to 148 cracked layers in the clamped. In all there are 360 layers in the analytical model.

5.4 Shells

To indicate the accuracy of the analysis technique and the behavior of the layered element system in a structural shell configuration, comparison is made with the reinforced concrete shell of Odello and Allgood.[19] This experimental shell was selected because the load is carried primarily by membrane action and the sensitivity of the analysis technique to inplane loads, as shown in the comparison with Wight's beam, required further investigation. The ability of the analysis procedure to handle bending is not under question due to the excellent agreement with the experimental results of Cardenas and Sozen.

The concrete funicular shell, Fig. 43, 35 x 40 feet in plan with a 2 inch thickness and a 30 inch rise, tested by Odello and Allgood[19] was analyzed. The shell was loaded to failure, 135 psf, under uniform load. The shell had edge beams 13-1/2" deep by 14" on all four edges; but, since the experimental data indicated that the edge beam thrust and moment were low even at loads near ultimate, the edges are considered fixed for the analysis. Figure 44 shows the element grid and layering schemes, while Fig. 45 shows the load deflection curves for the center of the shell.

Also shown in Fig. 45 are two elastic analyses. The curve referred to as LINSHEB[7] was generated by a computer program utilizing a modified finite difference technique wherein the shell is idealized as a framework of rigid bars connected by elastic hinges. GENSHL[11] refers to a

program developed at the University of California at Berkeley for the linear elastic analysis of thin shells of arbitrary shape using the finite element method.

Although the ultimate load of the shell was reported as 135 psf, it was lower than anticipated. Odello and Allgood stated at this load a pop through or buckling failure occurred near node 10 where the deflection increased to 3.9 inches compared to the center value of 1.4 inches. They also state this was unexpected since the buckling equation used in the design of the shell is very conservative. In view of these remarks, the continuing ascent of the analytical curve is much more acceptable.

Also, the agreement of the experimental and calculated curves implies the analysis technique does not have an adverse sensitivity to inplane loads when considered in the context of a structural shell system.

6. SUMMARY AND CONCLUSIONS

6.1 Summary

A layered nonlinear finite element procedure for determining the load-deflection history up to failure of reinforced concrete plates and shells of constant thickness is presented. A twenty degree-of-freedom shallow shell layered finite element is used. The nonlinear structural behavior is introduced only through the material properties. Geometric nonlinearities are not considered.

The reinforcing steel is assumed to be elastic-plastic. The concrete is assumed to be tension-limited and to yield in biaxial compression in accordance with a yield criterion proposed by Kupfer, Hilsdorf, and Rüsch. A shear retention factor is introduced to provide the torsional and shear stiffnesses for cracked concrete. These stiffnesses can physically be attributed to aggregate interlock and dowel action. The effect of bond between steel and concrete, the influence of creep and shrinkage of concrete, the effects of temperature, and the effect of long term or cyclic loading are not considered.

The layering of a finite element, which allows the idealized constitutive relations to be defined in a discretized fashion, permits the material properties to vary through the element depth. However, the depth-wise variation in material properties displays a coupling phenomenon between inplane extension and transverse bending which is not found in homogeneous plates or shells. This coupling phenomenon causes the inplane boundary conditions to become important, particularly for the incremental analysis here.

The nonlinear finite element analysis progresses through the use of an iterative or step-by-step procedure with the nonlinearity being introduced only through the material properties. This numerical procedure is often referred to as the "incremental-variable elasticity" procedure. Even though a nonlinear analysis is being performed, each iteration is treated as a linear problem.

Several numerical examples are presented to confirm the adequacy of the mathematical model and establish the validity of the assumed material properties. Additional numerical examples, both plates and shells, are presented to demonstrate the applicability and flexibility of the proposed incremental analysis.

6.2 Conclusions

The general class of problems capable of being considered using this particular analysis procedure are "medium thick" reinforced concrete plates and "thin" shells whose dominant load-carrying mechanisms are either bending or membrane action or a combination of the two. Problems in which transverse shear is the important load-carrying mechanism and prime contributor to the failure mode cannot be considered because of the assumption regarding normals remaining normal and inextensible. Thus, punching shear failure near concentrated loads or supports cannot be considered. However, the method is applicable for most such problems up until the shear failure mode develops.

The material properties assumed for the mathematical model are adequate for balanced or under-reinforced concrete surface structures.

Highly over-reinforced structures were not investigated and the adequacy of the assumed material properties in this range is not known.

The layering of a finite element to allow a material variation through the element depth yields numerical results as good or better than a modified EI approach. Also, the idealized constitutive relations are obtained much more easily if the layering, instead of the modified EI, approach is used. Further, the layering is a more economical approach than a true three-dimensional approach.

Considering the class of problems investigated, it appears that this analysis technique is capable of determining the load-deflection history of a reinforced concrete plate or shell accurately and economically. This suggests it would be a valuable tool in determining structural behavior in the intermediate region between the elastic and limit state.

The incremental analysis presented herein is not intended as an every day design tool, but rather is intended to help understand the structural behavior in this intermediate range. Once this behavior is understood it may be possible to determine whether bending action is a significant load-carrying mechanism (1) after some inelastic behavior (cracking, plasticity, etc.) has occurred and (2) when the shell is approaching the limit state. Further, once this behavior of the shell is understood the effects the shell has on the edge beams should be more clearly defined.

6.3 Recommendations for Further Study

Some possible extensions for the analysis technique are:

1. Extend the analysis technique to cover nonshallow and varying thickness shells.

2. Incorporate an edge beam element in the analysis to include plates and shells with edge beams.
3. Extend the analyses procedure to include nonlinear geometric effects.
4. It may be advantageous to allow a layer to be composed of more than one material type in the "horizontal" plane to permit a reduction in the grid size.
5. It may be possible to allow a more gradual vertical material change by allowing a crack, for example, to gradually propagate through a layer thickness rather than being either cracked or uncracked. If so, it may permit fewer layers with no loss of accuracy.

Some possible areas of further study are:

1. Determine, in a more precise nature, the actual mathematical effect of the shear retention factor β.
2. Determine if it is necessary to further modify the cracked material properties to account for the finite spacing of the cracks rather than the infinitesimal spacing that is now assumed.
3. Determine the actual importance of the membrane boundary conditions as related to the coupling phenomenon for both elastic and incremental analyses.
4. Make any necessary changes or additions to the assumed material models to accomodate highly over-reinforced concrete surface structures.

5. Revise the basic assumption regarding normals remaining normal and inextensible to include transverse shear as a load-carrying mechanism and possible failure mode.

LIST OF REFERENCES

1. Ashton, J. E., "Approximate Solutions for Unsymmetrically Laminated Plates," Journal of Composite Material, Vol. 3, January 1969, pp. 189-191.

2. Bell, J. C., "A Complete Analysis for Reinforced Concrete Slabs and Shells," Ph.D. Thesis, University of Canterbury, Christchurch, New Zealand, 1970.

3. Boresi, A. P., Elasticity in Engineering Mechanics, N. M. Newmark and W. J. Hall, ed., Prentice-Hall, 1965.

4. Burns, N. H. and Siess, C. P., "Load-Deformation Characteristics of Beam-Column Connections in Reinforced Concrete," Civil Engineering Studies, SRS No. 234, University of Illinois, Urbana, Illinois, January 1962.

5. Cardenas, A. and Sozen, M. A., "Strength and Behavior of Isotropically and Nonisotropically Reinforced Concrete Slabs Subjected to Combinations of Flexural and Torsional Moments," Civil Engineering Studies, SRS No. 336, University of Illinois, Urbana, Illinois, May 1968.

6. Cervenka, V., "Inelastic Finite Element Analysis of Reinforced Concrete Panels under In-Plane Loads," Ph.D. Thesis, University of Colorado, Boulder, Colorado, 1970.

7. Chelapati, C. V., "Analysis of Rectangular Shallow Shells," Contract Report CR-69.002, Naval Civil Engineering Laboratory, Port Hueneme, California, July 1968 (Contract N62399-67-C-0040) (AD 854939L).

8. Franklin, H. A., "Nonlinear Analysis of Reinforced Concrete Frames and Panels," Ph.D. Thesis, University of California, Berkeley, California, 1970.

9. Houbolt, J. C., "The Effectiveness of Various Arrangements of Reinforcement in Concrete Slabs," M.S. Thesis, University of Illinois, Urbana, Illinois, 1942.

10. Jofreit, J. C. and McNeice, G. M., "Finite Element Analysis of Reinforced Concrete Slabs," Journal, Structural Division, ASCE, Vol. 97, No. ST3, March 1971, pp. 785-806.

11. Johnson, C. P. and Smith, P. G., "A Computer Program for the Analysis of Thin Shells," Contract Report CR-70.012, Structural Engineering Laboratory, University of California, Berkeley, California, January 1969 (Contract N62399-68-C-0035).

12. Kicher, T. P., "The Analysis of Unbalanced Cross-Plied Elliptic Plates under Uniform Pressure," Journal of Composite Material, Vol. 3, July 1969, pp. 424-432.

13. Kupfer, H., Hilsdorf, H. K. and Rüsch, H., "Behavior of Concrete under Biaxial Stresses," Journal, American Concrete Institute, Vol. 66, No. 8, August 1969, pp. 656-666.

14. Lin, C. S., "Nonlinear Analysis of Reinforced Concrete Slabs and Shells," Ph.D. Thesis, University of California, Berkeley, California, September 1972.

15. Liu, T. C. Y., Nilson, A. H. and Slate, F. O., "Stress-Strain Response and Fracture of Concrete in Uniaxial and Biaxial Compression," Journal, American Concrete Institute, Vol. 69, No. 5, May 1972, pp. 291-295.

16. Love, A. E. H., A Treatise on the Mathematical Theory of Elasticity, Cambridge University Press, 4th Ed., 1927.

17. Melosh, R. J., "Basis for Derivation of Matrices for the Direct Stiffness Method," Journal, AIAA, July 1963.

18. Mikkola, M. J. and Schnobrich, W. C., "Material Behavior Characteristics for Reinforced Concrete Shells Stressed Beyond the Elastic Range," Civil Engineering Studies, SRS No. 367, University of Illinois, Urbana, Illinois, August 1970.

19. Odello, R. J. and Allgood, J. R., "Concrete Funicular Shells for Floors and Roofs," Technical Report R-693, Naval Civil Engineering Laboratory, Port Hueneme, California, September 1970 (YF 38.534.001.01.003).

20. Pecknold, D. A. W. and Schnobrich, W. C., "Finite Element Analysis of Skewed Shallow Shells," Civil Engineering Studies, SRS No. 336, University of Illinois, Urbana, Illinois, January 1968.

21. Pryor, C. W., Jr. and Barker, R. M., "Finite Element Analysis of Bending-Extensional Coupling in Laminated Composites," Journal of Composite Materials, Vol. 4, October 1970, pp. 549-552.

22. Reissner, E. and Stavsky, Y., "Bending and Stretching of Certain Types of Heterogeneous Aeolotropic Elastic Plates," Journal of Applied Mechanics, Vol. 28, September 1961, pp. 402-408.

23. Scanlon, A., "Time Dependent Deflections of Reinforced Concrete Slabs," Ph.D. Thesis, University of Alberta, Edmonton, Canada, 1971.

24. Stavsky, Y., "Bending and Stretching of Laminated Aeolotropic Plates," Journal, Engineering Mechanics Division, ASCE, Vol. 87, No. EM6, 1961, p. 31.

25. Thomas, G. B., Jr., Calculus and Analytic Geometry, E. Reissner, ed., Addison-Wesley, 1962, pp. 585-591.

26. Valliappan, S. and Doolan, T. F., "Nonlinear Stress Analysis of Reinforced Concrete," Journal, Structural Division, ASCE, Vol. 98, No. ST4, April 1972, pp. 885-898.

27. Whang, B., "Elastic-Plastic Orthotropic Plates and Shells," Application of Finite Element Methods in Civil Engineering, Vanderbilt University, November 1969, pp. 481-515.

28. Whitney, J. M., "Bending-Extensional Coupling in Laminated Plates under Transverse Loading," Journal of Composite Materials, Vol. 3, January 1969, pp. 20-28.

29. Whitney, J. M., "Shear Buckling of Unsymmetrical Cross-Ply Plates," Journal of Composite Materials, Vol. 3, April 1969, pp. 359-363.

30. Whitney, J. M., "The Effect of Boundary Conditions on the Response of Laminated Composites," Journal of Composite Materials, Vol. 4, April 1970, pp. 192-203.

31. Whitney, J. M. and Leissa, A. W., "Analysis of Heterogeneous Anisotropic Plates," Journal of Applied Mechanics, Vol. 36, 1969, p. 261.

32. Whitney, J. M. and Leissa, A. W., "Analysis of a Simply-Supported Laminated Anisotropic Rectangular Plate," Journal, AIAA, Vol. 8, 1970, p. 28.

33. Wight, J. K. and Sozen, M. A., present research at the University of Illinois, Urbana, Illinois, sponsored by the National Science Foundation (GI 30760X).

34. Zienkiewicz, O. C. and Cheung, Y. K., "The Finite Element Method for Analysis of Elastic Isotropic and Orthotropic Slabs," Proceedings, Institute of Civil Engineers, August 1964.

35. Zienkiewicz, O. C. and Cheung, Y. K., The Finite Element Method in Structural and Continuum Mechanics, P. C. Colman, ed., McGraw-Hill, London, 1967, pp. 198-201.

APPENDIX A

TABLES

1	x	y	xy	.	.	.	.	$rx + sy - \frac{1}{2}ty^2$	$\frac{1}{2}rx^2 + sy^2$	rxy	.	.	.	.	.	.	.	.	.
.	.	.	.	1	x	y	xy	$sx + ty$	$sx^2+txy - \frac{1}{2}rx^2$	$\frac{1}{2}ty^2$	.	.	.	.	.	.	.	.	.
.	.	.	.	.	.	.	.	1	x	y	xy	x^2	y^2	x^3	x^2y	xy^2	y^3	x^3y	xy^3
.	.	.	.	.	.	.	.	.	1	.	y	2x	.	$3x^2$	2xy	y^2	.	$3x^2y$	y^3
.	.	.	.	.	.	.	.	.	.	1	x	.	2y	.	x^2	2xy	$3y^2$	x^3	$3xy^2$

TABLE 1 M MATRIX

1	-a	-b	ab	.	.	.	.	$-ra$ $-sb$	$\frac{ra^2}{2}$ $-\frac{tb^2}{2}$	rab $+sb^2$	.	.	.	.	.	.	.	.	.
.	.	.	.	1	-a	-b	ab	$-sa$ $-tb$	sa^2 $-tab$	$t\frac{b^2}{2}$ $-\frac{ra^2}{2}$	.	.	.	.	.	.	.	.	.
.	.	.	.	.	.	.	.	1	-a	-b	ab	a^2	b^2	$-a^3$	$-a^2b$	$-ab^2$	$-b^3$	a^3b	ab^3
.	.	.	.	.	.	.	.	.	1	.	-b	-2a	.	$3a^2$	2ab	b^2	.	$-3a^2b$	$-b^3$
.	.	.	.	.	.	.	.	.	.	1	-a	.	-2b	.	a^2	2ab	$3b^2$	$-a^3$	$-3ab^2$
1	-a	b	-ab	.	.	.	.	$-ra$ $+sb$	$\frac{ra^2}{2}$ $-\frac{tb^2}{2}$	$-rab$ $+sb^2$	.	.	.	.	.	.	.	.	.
.	.	.	.	1	-a	b	-ab	$-sa$ $+tb$	sa^2 $+tab$	$t\frac{b^2}{2}$ $-\frac{ra^2}{2}$	.	.	.	.	.	.	.	.	.
.	.	.	.	.	.	.	.	1	-a	b	-ab	a^2	b^2	$-a^3$	a^2b	$-ab^2$	b^3	$-a^3b$	$-ab^3$
.	.	.	.	.	.	.	.	.	1	.	b	-2a	.	$3a^2$	-2ab	b^2	.	$3a^2b$	b^3
.	.	.	.	.	.	.	.	.	.	1	a	.	2b	.	a^2	-2ab	$3b^2$	$-a^3$	$-3ab^2$
1	a	-b	-ab	.	.	.	.	$+ra$ $-sb$	$\frac{ra^2}{2}$ $-\frac{tb^2}{2}$	$-rab$ $+sb^2$	.	.	.	.	.	.	.	.	.
.	.	.	.	1	a	-b	-ab	sa $-tb$	sa^2 $+tab$	$t\frac{b^2}{2}$ $-\frac{ra^2}{2}$	.	.	.	.	.	.	.	.	.
.	.	.	.	.	.	.	.	1	a	-b	-ab	a^2	b^2	a^3	$-a^2b$	ab^2	$-b^3$	$-a^3b$	$-ab^3$
.	.	.	.	.	.	.	.	.	1	.	-b	2a	.	$3a^2$	-2ab	b^2	.	$-3a^2b$	$-b^3$
.	.	.	.	.	.	.	.	.	.	1	a	.	-2b	.	a^2	-2ab	$3b^2$	a^3	$3ab^2$
1	a	b	ab	.	.	.	.	ra $+sb$	$\frac{ra^2}{2}$ $-\frac{tb^2}{2}$	rab $+sb^2$	.	.	.	.	.	.	.	.	.
.	.	.	.	1	a	b	ab	sa $+tb$	sa^2 $-tab$	$t\frac{b^2}{2}$ $-\frac{ra^2}{2}$	.	.	.	.	.	.	.	.	.
.	.	.	.	.	.	.	.	1	a	b	ab	a^2	b^2	a^3	a^2b	ab^2	b^3	a^3b	ab^3
.	.	.	.	.	.	.	.	.	1	.	b	2a	.	$3a^2$	2ab	b^2	.	$3a^2b$	b^3
.	.	.	.	.	.	.	.	.	.	1	a	.	2b	.	a^2	2ab	$3b^2$	a^3	$3ab^2$

TABLE 2 A MATRIX

$$
\begin{bmatrix}
1 & . & \frac{3h_1}{a} & h_1 & \frac{b}{a}h_1 & 1 & . & \frac{3h_2}{a} & h_2 & -\frac{b}{a}h_2 & 1 & . & -\frac{3h_2}{a} & h_2 & -\frac{b}{a}h_2 & 1 & . & -\frac{3}{a}h_1 & h_1 & \frac{b}{a}h_1 \\
\frac{1}{r} & . & -r & -\frac{ra}{2} & -\frac{rb}{2} & -\frac{1}{a} & . & -r & -\frac{ra}{2} & \frac{rb}{2} & \frac{1}{a} & . & -r & \frac{ra}{2} & -\frac{rb}{2} & \frac{1}{a} & . & -r & \frac{ra}{2} & \frac{rb}{2} \\
-\frac{1}{s} & . & -s & -\frac{sa}{2} & -\frac{sb}{2} & \frac{1}{b} & . & -s & -\frac{sa}{2} & \frac{sb}{2} & -\frac{1}{b} & . & -s & \frac{sa}{2} & -\frac{sb}{2} & \frac{1}{b} & . & -s & \frac{sa}{2} & \frac{sb}{2} \\
\frac{1}{2r} & . & \frac{3r}{2b} & \frac{ra}{2b} & \frac{r}{2} & -\frac{1}{ab} & . & -\frac{3r}{2b} & -\frac{ra}{2b} & \frac{r}{2} & -\frac{1}{ab} & . & \frac{3r}{2b} & -\frac{ra}{2b} & \frac{r}{2} & \frac{1}{ab} & . & -\frac{3r}{2b} & \frac{ra}{2b} & \frac{r}{2} \\
. & 1 & -\frac{3}{b}h_2 & -\frac{a}{b}h_2 & -h_2 & . & 1 & \frac{3}{b}h_1 & \frac{a}{b}h_1 & -h_1 & . & 1 & -\frac{3}{b}h_1 & \frac{a}{b}h_1 & -h_1 & . & 1 & \frac{3}{b}h_2 & -\frac{a}{b}h_2 & -h_2 \\
. & -\frac{1}{a} & -s & -\frac{sa}{2} & -\frac{sb}{2} & . & -\frac{1}{a} & -s & -\frac{sa}{2} & \frac{sb}{2} & . & \frac{1}{a} & -s & \frac{sa}{2} & -\frac{sb}{2} & . & \frac{1}{a} & -s & \frac{sa}{2} & \frac{sb}{2} \\
. & -\frac{1}{b} & -t & -\frac{ta}{2} & -\frac{tb}{2} & . & \frac{1}{b} & -t & -\frac{ta}{2} & \frac{tb}{2} & . & -\frac{1}{b} & -t & \frac{ta}{2} & -\frac{tb}{2} & . & \frac{1}{b} & -t & \frac{ta}{2} & \frac{tb}{2} \\
. & \frac{1}{ab} & +\frac{3t}{2a} & +\frac{t}{2} & +\frac{tb}{2a} & . & -\frac{1}{ab} & +\frac{3t}{2a} & +\frac{t}{2} & -\frac{tb}{2a} & . & -\frac{1}{ab} & -\frac{3t}{2a} & +\frac{t}{2} & -\frac{tb}{2a} & . & \frac{1}{ab} & -\frac{3t}{2a} & +\frac{t}{2} & +\frac{tb}{2a} \\
. & . & 1 & \frac{a}{2} & \frac{b}{2} & . & . & 1 & \frac{a}{2} & -\frac{b}{2} & . & . & 1 & -\frac{a}{2} & \frac{b}{2} & . & . & 1 & -\frac{a}{2} & -\frac{b}{2} \\
. & . & -\frac{3}{2a} & -\frac{1}{2} & -\frac{b}{2a} & . & . & -\frac{3}{2a} & -\frac{1}{2} & \frac{b}{2a} & . & . & \frac{3}{2a} & -\frac{1}{2} & \frac{b}{2a} & . & . & \frac{3}{2a} & -\frac{1}{2} & -\frac{b}{2a} \\
. & . & -\frac{3}{2b} & -\frac{a}{2b} & -\frac{1}{2} & . & . & \frac{3}{2b} & \frac{a}{2b} & -\frac{1}{2} & . & . & -\frac{3}{2b} & \frac{a}{2b} & -\frac{1}{2} & . & . & \frac{3}{2b} & -\frac{a}{2b} & -\frac{1}{2} \\
. & . & \frac{2}{ab} & \frac{1}{2b} & \frac{1}{2a} & . & . & -\frac{2}{ab} & -\frac{1}{2b} & \frac{1}{2a} & . & . & -\frac{2}{ab} & \frac{1}{2b} & -\frac{1}{2a} & . & . & \frac{2}{ab} & -\frac{1}{2b} & -\frac{1}{2a} \\
. & . & . & -\frac{1}{2a} & . & . & . & . & -\frac{1}{2a} & . & . & . & . & \frac{1}{2a} & . & . & . & . & \frac{1}{2a} & . \\
. & . & . & . & -\frac{1}{2b} & . & . & . & . & \frac{1}{2b} & . & . & . & . & -\frac{1}{2b} & . & . & . & . & \frac{1}{2b} \\
. & . & \frac{1}{2a^3} & \frac{1}{2a^2} & . & . & . & \frac{1}{2a^3} & \frac{1}{2a^2} & . & . & . & -\frac{1}{2a^3} & \frac{1}{2a^2} & . & . & . & -\frac{1}{2a^3} & \frac{1}{2a^2} & . \\
. & . & . & \frac{1}{2ab} & . & . & . & . & -\frac{1}{2ab} & . & . & . & . & -\frac{1}{2ab} & . & . & . & . & \frac{1}{2ab} & . \\
. & . & . & . & \frac{1}{2ab} & . & . & . & . & -\frac{1}{2ab} & . & . & . & . & -\frac{1}{2ab} & . & . & . & . & \frac{1}{2ab} \\
. & . & \frac{1}{2b^3} & . & \frac{1}{2b^2} & . & . & -\frac{1}{2b^3} & . & \frac{1}{2b^2} & . & . & \frac{1}{2b^3} & . & \frac{1}{2b^2} & . & . & -\frac{1}{2b^3} & . & \frac{1}{2b^2} \\
. & . & -\frac{1}{2a^3b} & -\frac{1}{2a^2b} & . & . & . & \frac{1}{2a^3b} & \frac{1}{2a^2b} & . & . & . & \frac{1}{2a^3b} & -\frac{1}{2a^2b} & . & . & . & -\frac{1}{2a^3b} & \frac{1}{2a^2b} & . \\
. & . & -\frac{1}{2ab^3} & . & -\frac{1}{2ab^2} & . & . & \frac{1}{2ab^3} & . & \frac{1}{2ab^2} & . & . & \frac{1}{2ab^3} & . & \frac{1}{2ab^2} & . & . & -\frac{1}{2ab^3} & . & \frac{1}{2ab^2}
\end{bmatrix}
$$

$$h_1 = \frac{1}{4}(a^2r - b^2t + 2sab)$$

$$h_2 = \frac{1}{4}(a^2r - b^2t - 2sab)$$

TABLE 3 A^{-1} MATRIX

.	1	.	y	.	.	.	.	.	.	.	$-rxy$	$-rx^2$	$-ry^2$	$-rx^3$	$-rx^2y$	$-rxy^2$	$-ry^3$	$-rx^3y$	$-rxy^3$
.	.	.	.	.	.	1	x	.	.	.	$-txy$	$-tx^2$	$-ty^2$	$-tx^3$	$-tx^2y$	$-txy^2$	$-ty^3$	$-tx^3y$	$-txy^3$
.	.	1	x	.	1	.	y	.	.	.	$-2sxy$	$-2sx^2$	$-2sy^2$	$-2sx^3$	$-2sx^2y$	$-2sxy^2$	$-2sy^3$	$-2sx^3y$	$-2sxy^3$
.	.	.	.	.	.	.	.	.	.	.	.	-2	.	-6x	-2y	.	.	-6xy	.
.	.	.	.	.	.	.	.	.	.	.	.	.	-2	.	.	-2x	-6y	.	-6xy
.	.	.	.	.	.	.	.	.	.	.	-2	.	.	.	-4x	-4y	.	$-6x^2$	$-6y^2$

TABLE 4 B MATRIX

$$
\begin{bmatrix}
D_1 & D_5 & & & D_5 & D_4 & & & & & -\frac{1}{3}f_1a^2-\frac{1}{3}f_1b^2 & & & & & & \\
 & D_3 & & & D_3 & D_6 & & & & & -\frac{1}{3}f_3a^2-\frac{1}{3}f_3b^2 & & & & & & \\
 & & \frac{1}{3}D_3a^2+\frac{1}{3}D_1b^2 & & & \frac{1}{3}D_6a^2+\frac{1}{3}D_5b^2 & & & & & & -\frac{1}{5}f_3a^4-\frac{1}{9}f_1a^2b^2-\frac{1}{9}f_3a^2b^2-\frac{1}{5}f_1b^4 & & \\
 & & & & D_3 & D_6 & & & & & -\frac{1}{3}f_3a^2-\frac{1}{3}f_3b^2 & & & & & & \\
 & & & & & D_2 & & & & & -\frac{1}{3}f_2a^2-\frac{1}{3}f_2b^2 & & & & & & \\
 & & & & & & \frac{1}{3}D_2a^2+\frac{1}{3}D_3b^2 & & & & & -\frac{1}{5}f_2a^4-\frac{1}{9}f_3a^2b^2-\frac{1}{9}f_2a^2b^2-\frac{1}{5}f_3b^4 & & \\
 & & & & & & & & & & & & & & & & \\
 & & & & & & & & & & & & & & & & \\
 & & & & & & & & & & & & & & & & \\
 & & & & & & & & & & \frac{9}{9}a^2b^2 & & & & & \frac{9}{15}a^4b^2 & \frac{9}{15}a^2b^4 \\
 & & & & & & & & & & \frac{9}{5}a^4 & \frac{9}{9}a^2b^2 & & & & & \\
 & & & & & & & & & & & \frac{9}{5}b^4 & & & & & \\
 & & & & & & & & & & & & \frac{9}{7}a^6 & & \frac{9}{15}a^4b^2 & & \\
 & & & & & & & & & & & & & \frac{9}{15}a^4b^2 & & \frac{9}{15}a^2b^4 & \\
 & & & & & & & & & & & & & & \frac{9}{15}a^2b^4 & & \\
 & & & & & & & & & & & & & & & \frac{9}{7}b^6 & \\
 & & & & & & & & & & & & & & & \frac{9}{21}a^6b^2 & \frac{9}{25}a^4b^4 \\
 & & & & & & & & & & & & & & & \frac{9}{21}a^2b^6 &
\end{bmatrix}
$$

symmetric

$$f_1 = rD_1+tD_4+2sD_5$$
$$f_2 = rD_4+tD_2+2sD_6$$
$$f_3 = rD_5+tD_6+2sD_3$$
$$g = rf_1+tf_2+2sf_3$$

TABLE 5 $\iint B_\varepsilon^T D B_\varepsilon \, dxdy$ MATRIX

$8ab$

.	.	.	.	.	.	.	.	.	.	.	.	.	.	.	.	.	.	.	.
.	.	.	.	.	.	.	.	.	.	.	$-E_5$	$-E_1$	$-E_4$	.	.	.	.	$-E_5a^2$	$-E_5b^2$
.	.	.	.	.	.	.	.	.	.	.	$-E_3$	$-E_5$	$-E_6$	.	.	.	.	$-E_3a^2$	$-E_3b^2$
.	.	.	.	.	.	.	.	.	.	.	.	.	.	$-E_5a^2$	$-\frac{2}{3}E_3a^2$ $-\frac{1}{3}E_1b^2$	$-\frac{1}{3}E_6a^2$ $-\frac{2}{3}E_5b^2$	$-E_4b^2$	.	.
.	.	.	.	.	.	.	.	.	.	.	.	.	.	.	.	.	.	.	.
.	.	.	.	.	.	.	.	.	.	.	$-E_3$	$-E_5$	$-E_6$	.	.	.	.	$-E_3a^2$	$-E_3b^2$
.	.	.	.	.	.	.	.	.	.	.	$-E_6$	$-E_4$	$-E_2$	.	.	.	.	$-E_6a^2$	$-E_6b^2$
.	.	.	.	.	.	.	.	.	.	.	.	.	.	$-E_4a^2$	$-\frac{2}{3}E_6a^2$ $-\frac{1}{3}E_5b^2$	$-\frac{1}{3}E_2a^2$ $-\frac{2}{3}E_3b^2$	$-E_6b^2$	.	.
.	.	.	.	.	.	.	.	.	.	.	.	.	.	.	.	.	.	.	.
.	.	.	.	.	.	.	.	.	.	.	.	.	.	.	.	.	.	.	.
.	.	.	.	.	.	.	.	.	.	.	.	.	.	.	.	.	.	.	.
.	.	.	.	.	.	.	.	.	.	.	.	.	.	.	.	.	.	$\frac{1}{3}f_1a^2b^2$	$\frac{1}{3}f_2a^2b^2$
.	.	.	.	.	.	.	.	.	.	.	$\frac{1}{3}f_3a^2$	$\frac{1}{3}f_1a^2$	$\frac{1}{3}f_2a^2$	.	.	.	.	$\frac{3}{5}f_3a^4$	$\frac{1}{3}f_3a^2b^2$
.	.	.	.	.	.	.	.	.	.	.	$\frac{1}{3}f_3b^2$	$\frac{1}{3}f_1b^2$	$\frac{1}{3}f_2b^2$	.	.	.	.	$\frac{1}{3}f_3a^2b^2$	$\frac{3}{5}f_3b^4$
.	.	.	.	.	.	.	.	.	.	.	.	.	.	$\frac{3}{5}f_1a^4$	$\frac{2}{5}f_3a^4$	$\frac{1}{5}f_2a^4$	.	.	.
.	.	.	.	.	.	.	.	.	.	.	.	.	.	.	$\frac{1}{9}f_1a^2b^2$	$\frac{2}{9}f_3a^2b^2$	$\frac{1}{3}f_2a^2b^2$	.	.
.	.	.	.	.	.	.	.	.	.	.	.	.	.	$\frac{1}{3}f_1a^2b^2$	$\frac{2}{9}f_3a^2b^2$	$\frac{1}{9}f_2a^2b^2$	.	.	.
.	.	.	.	.	.	.	.	.	.	.	.	.	.	.	$\frac{1}{5}f_1b^4$	$\frac{2}{5}f_3b^4$	$\frac{3}{5}f_2b^4$	.	.
.	.	.	.	.	.	.	.	.	.	.	.	.	.	.	.	.	.	$\frac{1}{5}f_1a^4b^2$	$\frac{1}{5}f_2a^4b^2$
.	.	.	.	.	.	.	.	.	.	.	.	.	.	.	.	.	.	$\frac{1}{5}f_1a^2b^4$	$\frac{1}{5}f_2a^2b^4$

$f_1 = rE_1+tE_4+2sE_5$

$f_2 = rE_4+tE_2+2sE_6$

$f_3 = rE_5+tE_6+2sE_3$

TABLE 6 $\iint B_\varepsilon^T E B_\chi \, dxdy$ MATRIX

8ab

.	.	.	.	.	.	.	.	.	.	.	.	.	.	.	.	.	.	.	.
.	.	.	.	.	.	.	.	.	.	.	.	.	.	.	.	.	.	.	.
.	.	.	.	.	.	.	.	.	.	.	.	.	.	.	.	.	.	.	.
.	.	.	.	.	.	.	.	.	.	.	.	.	.	.	.	.	.	.	.
.	.	.	.	.	.	.	.	.	.	.	.	.	.	.	.	.	.	.	.
.	.	.	.	.	.	.	.	.	.	.	.	.	.	.	.	.	.	.	.
.	.	.	.	.	.	.	.	.	.	.	.	.	.	.	.	.	.	.	.
.	.	.	.	.	.	.	.	.	.	.	.	.	.	.	.	.	.	.	.
.	.	.	.	.	.	.	.	.	.	.	.	.	.	.	.	.	.	.	.
.	.	.	.	.	.	.	.	.	.	.	.	.	.	.	.	.	.	.	.
.	.	.	.	.	.	.	.	.	.	.	.	.	.	.	.	.	.	.	.
.	$-E_5$	$-E_3$	.	.	$-E_3$	$-E_6$	.	.	.	.	.	$\frac{1}{3}f_3a^2$	$\frac{1}{3}f_3b^2$	.	.	.	.	.	.
.	$-E_1$	$-E_5$	.	.	$-E_5$	$-E_4$	.	.	.	.	.	$\frac{1}{3}f_1a^2$	$\frac{1}{3}f_1b^2$	.	.	.	.	.	.
.	$-E_4$	$-E_6$	.	.	$-E_6$	$-E_2$	.	.	.	.	.	$\frac{1}{3}f_2a^2$	$\frac{1}{3}f_2b^2$	.	.	.	.	.	.
.	.	.	$-E_5a^2$	.	.	.	$-E_4a^2$	.	.	.	.	.	.	$\frac{3}{5}f_1a^4$	.	$\frac{1}{3}f_1a^2b^2$	.	.	.
.	.	.	$-\frac{2}{3}E_3a^2$ $-\frac{1}{3}E_1b^2$	.	.	.	$-\frac{2}{3}E_6a^2$ $-\frac{1}{3}E_5b^2$	.	.	.	.	.	.	$\frac{2}{5}f_3a^4$	$\frac{1}{9}f_1a^2b^2$	$\frac{2}{9}f_3a^2b^2$	$\frac{1}{5}f_1b^4$	.	.
.	.	.	$-\frac{1}{3}E_6a^2$ $-\frac{2}{3}E_5b^2$	.	.	.	$-\frac{1}{3}E_2a^2$ $-\frac{2}{3}E_3b^2$	.	.	.	.	.	.	$\frac{1}{5}f_2a^4$	$\frac{2}{9}f_3a^2b^2$	$\frac{1}{9}f_2a^2b^2$	$\frac{2}{5}f_3b^4$	.	.
.	.	.	$-E_4b^2$	.	.	.	$-E_6b^2$	.	.	.	.	.	.	.	$\frac{1}{3}f_2a^2b^2$	.	$\frac{3}{5}f_2b^4$	.	.
.	$-E_5a^2$	$-E_3a^2$	.	.	$-E_3a^2$	$-E_6a^2$	.	.	.	.	$\frac{1}{3}f_1a^2b^2$	$\frac{3}{5}f_3a^4$	$\frac{1}{3}f_3a^2b^2$	.	.	.	.	$\frac{1}{5}f_1a^4b^2$	$\frac{1}{5}f_1a^2b^4$
.	$-E_5b^2$	$-E_3b^2$	.	.	$-E_3b^2$	$-E_6b^2$	.	.	.	.	$\frac{1}{3}f_2a^2b^2$	$\frac{1}{3}f_3a^2b^2$	$\frac{3}{5}f_3b_4$	.	.	.	.	$\frac{1}{5}f_2a^4b^2$	$\frac{1}{5}f_2a^2b^4$

$f_1 = rE_1+tE_4+2sE_5$

$f_2 = rE_4+tE_2+2sE_6$

$f_3 = rE_5+tE_6+2sE_3$

TABLE 7 $\iint B_\chi^T E B_\varepsilon \, dxdy$ MATRIX

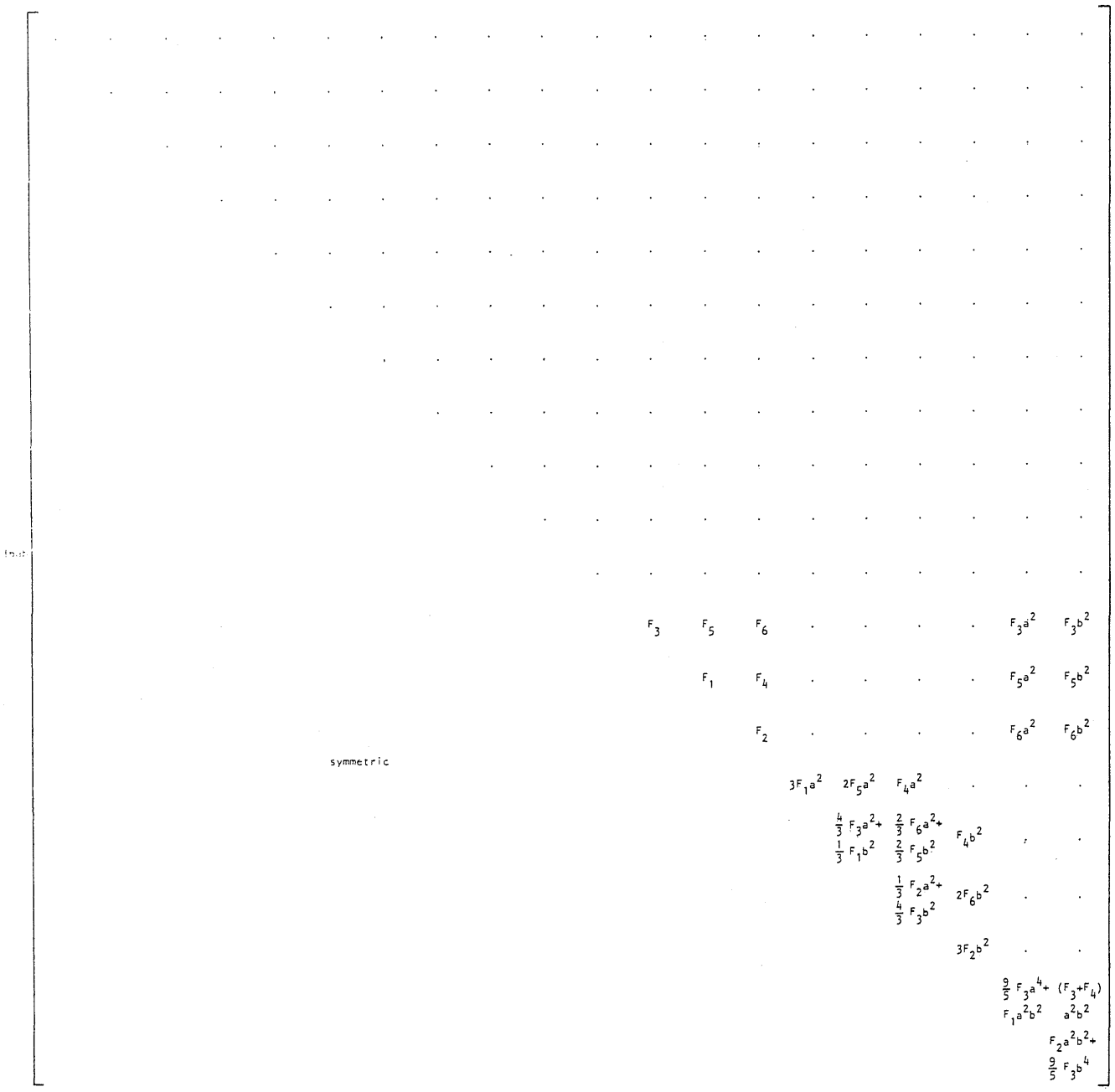

TABLE 8 $\iint B_X^T F B_X \, dxdy$ MATRIX

Metz Reference Room
Civil Engineering Department
B106 C. E. Building
University of Illinois
Urbana, Illinois 61801

$$\{\bar{\varepsilon}\}=\left\{\frac{\varepsilon_o}{\chi}\right\}=\left\{\begin{array}{l}\varepsilon_{xo}\\ \varepsilon_{yo}\\ \gamma_{xyo}\\ \chi_x\\ \chi_y\\ 2\chi_{xy}\end{array}\right\}=\left\{\begin{array}{l}\frac{1}{4a}(-U_1-U_6+U_{11}+U_{16})+\frac{r}{4}(-U_3-U_8-U_{13}-U_{18})+\frac{ra}{12}(-U_4-U_9+U_{14}+U_{19})+\frac{rb}{12}(-U_5+U_{10}-U_{15}+U_{20})\\ \frac{1}{4b}(-U_2+U_7-U_{12}+U_{17})+\frac{t}{4}(-U_3-U_8-U_{13}-U_{18})+\frac{ta}{12}(-U_4-U_9+U_{14}+U_{19})+\frac{tb}{12}(-U_5+U_{10}-U_{15}+U_{20})\\ \frac{1}{4b}(-U_1+U_6-U_{11}+U_{16})+\frac{1}{4a}(-U_2-U_7+U_{12}+U_{17})+\frac{s}{2}(-U_3-U_8-U_{13}-U_{18})+\frac{sa}{6}(-U_4-U_9+U_{14}+U_{19})+\frac{sb}{6}(-U_5+U_{10}-U_{15}+U_{20})\\ -\frac{1}{4a}(U_4+U_9-U_{14}-U_{19})\\ -\frac{1}{4b}(U_5-U_{10}+U_{15}-U_{20})\\ \frac{1}{ab}(U_3-U_8-U_{13}+U_{18})+\frac{1}{4b}(U_4-U_9+U_{14}-U_{19})+\frac{1}{4a}(U_5+U_{10}-U_{15}-U_{20})\end{array}\right\}$$

TABLE 9 MIDDLE SURFACE STRAIN AND CURVATURE VECTOR, $\{\bar{\varepsilon}\}$

$$\{F\} = \begin{Bmatrix} F_1 \\ F_2 \\ F_3 \\ F_4 \\ F_5 \\ F_6 \\ F_7 \\ F_8 \\ F_9 \\ F_{10} \\ F_{11} \\ F_{12} \\ F_{13} \\ F_{14} \\ F_{15} \\ F_{16} \\ F_{17} \\ F_{18} \\ F_{19} \\ F_{20} \end{Bmatrix} = \begin{Bmatrix} - b N_x - a N_{xy} \\ - b N_{xy} - a N_y \\ - h_5 + 2 M_{xy} \\ - \frac{1}{2} a h_5 - \frac{1}{2} b h_3 \\ - \frac{1}{2} b h_5 - \frac{1}{2} a h_4 \\ - b N_x + a N_{xy} \\ - b N_{xy} + a N_y \\ - h_5 - 2 M_{xy} \\ - \frac{1}{2} a h_5 - \frac{1}{2} b h_3 \\ \frac{1}{2} b h_5 + \frac{1}{2} a h_4 \\ b N_x - a N_{xy} \\ b N_{xy} - a N_y \\ - h_5 - 2 M_{xy} \\ \frac{1}{2} a h_5 + \frac{1}{2} b h_3 \\ \frac{1}{2} b h_5 - \frac{1}{2} a h_4 \\ b N_x + a N_{xy} \\ b N_{xy} + a N_y \\ - h_5 + 2 M_{xy} \\ \frac{1}{2} a h_5 + \frac{1}{2} b h_3 \\ \frac{1}{2} b h_5 + \frac{1}{2} a h_4 \end{Bmatrix}$$

$$h_3 = - \frac{1}{3} a^2 (r N_x + t N_y + 2s N_{xy}) + 2 M_x$$

$$h_4 = - \frac{1}{3} b^2 (r N_x + t N_y + 2s N_{xy}) + 2 M_y$$

$$h_5 = ab(r N_x + t N_y + 2s N_{xy})$$

TABLE 10 NODAL FORCE VECTOR, $\{F\}$

Mark	Thickness in inches	Material Properties, psi										
		Given					Assumed					
		f_t	f'_c	f_y	E_c	E_s	f_c	f_d	f_t	E_c	E_d
03-906	5.17	665	5130	50200	4.00×10^6	28.6×10^6	4350	4350	430	4.00×10^6	1.0
453-453	5.17	680	4910	50200	4.47×10^6	28.6×10^6	4200	4200	420	4.47×10^6	1.0
303-303	5.17	600	3800	50200	3.50×10^6	28.6×10^6	3250	3250	370	3.50×10^6	1.0
603-603	5.17	610	3980	50200	3.65×10^6	28.6×10^6	3380	3380	380	3.65×10^6	1.0

Mark	Load Increments kips	Reinforcement				Loads, kips		
		Amount in^2/ft	Angle degrees	Amount in^2/ft	Angle degrees	Calculated		Experimental
						cracking	first yield	ultimate
03-906	5.0	.44	0	.22	90	14.65	50.00	55.06
453-453	5.0	.44	45	.44	-45	13.12	48.00	50.76
303-303	5.0	.44	30	.44	-30	12.67	67.73	71.76
603-603	5.0	.44	60	.44	-60	11.37	25.00	26.96

TABLE II MATERIAL PROPERTIES FOR HOUBOLT'S SPECIMENS

Mark	Applied Moment, K-in/in			Reinforcement					Comments
	Ratio of	Increment Size		Layers	Amount	Angle*	Amount	Angle*	
	Torque/Moment	Moment	Torque		in^2/ft	degrees	in^2/ft	degrees	
B7	0	1.0	.0	2, 9	.40	45	.40	-45	Uniaxial Moment
B10	0	1.0	.0	2, 9	.40	0	.40	90	Uniaxial Moment
B15	∞	.0	1.0	2, 9	.40	45	.40	-45	Pure Torque
B17	∞	.0	1.0	2, 9	.40	67.5	.40	-22.5	Pure Torque
B27A	.435	.860	.374	2, 9	.40	45	.40	-45	Combined Bending and Torque
B39	1.22	.550	.670	2, 9	.40	90	.10	0	Combined Bending and Torque

*measured counter-clockwise from x-axis

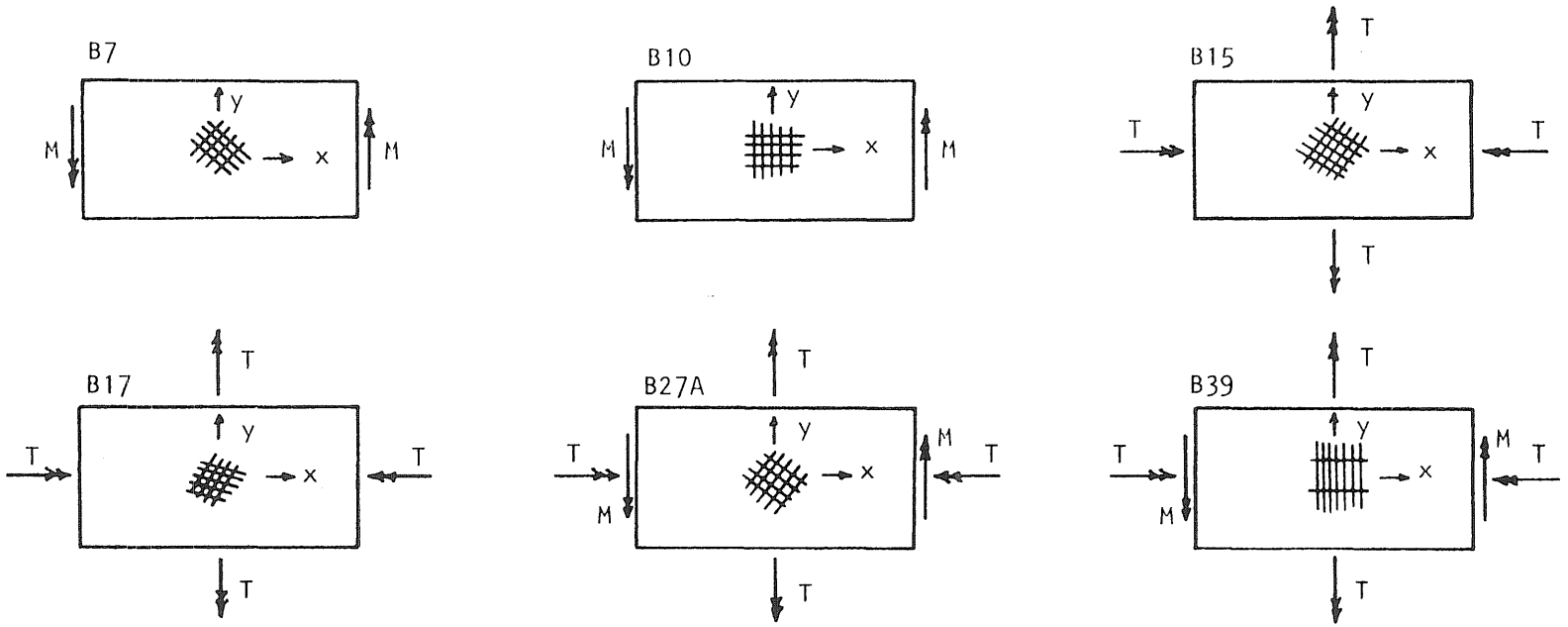

TABLE 12 MATERIAL PROPERTIES FOR CARDENAS' SPECIMENS

Mark	Material Properties, psi								Thickness		Moments, K-in/in			
	Given			Assumed					inches		Calculated		Experimental	
	f'_c	f_t	f_y	f_c	f_d	E_c	E_d	E_s	Total	Delta	Cracking	Yield	Cracking	Yield
B7	5150	430	50000	3000	5150	3.00×10^6	1.43×10^6	30.0×10^6	4.14	.14	1.50	5.52	1.67	5.60
B10	4920	360	50000	3000	4920	3.00×10^6	1.28×10^6	30.0×10^6	4.14	.14	1.43	5.43	1.36	5.55
B15	5260	380	47900	3000	5260	3.00×10^6	1.51×10^6	30.0×10^6	4.09	.09	1.57	5.11	1.80	5.20
B17	5530	380	50800	3000	5530	3.00×10^6	1.69×10^6	30.0×10^6	4.03	.03	1.32	4.51	1.46	5.50
B27A	5230	380	49900	3000	5230	3.00×10^6	1.49×10^6	30.0×10^6	4.04	.04	1.33	4.42	1.77	5.08
B39	5340	430	51300	3000	5340	3.00×10^6	1.56×10^6	30.0×10^6	4.07	.07	1.34	1.77	1.51	2.35

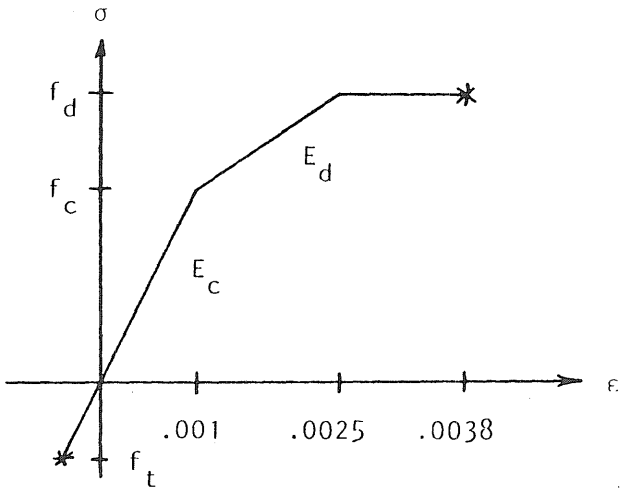

Concrete Stress-Strain Curve

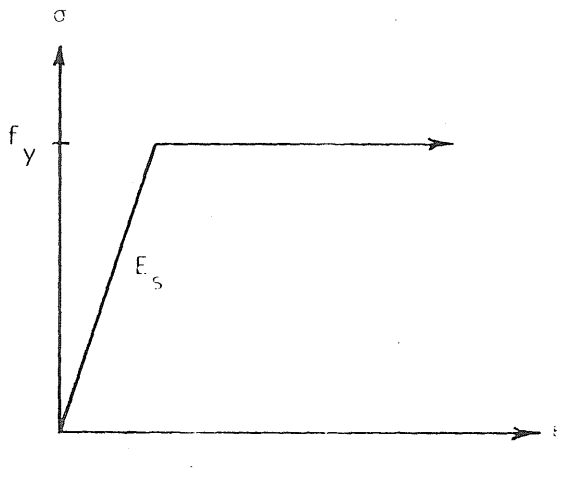

Steel Stress-Strain Curve

TABLE 12 (CON'T) MATERIAL PROPERTIES FOR CARDENAS' SPECIMENS

APPENDIX B

FIGURES

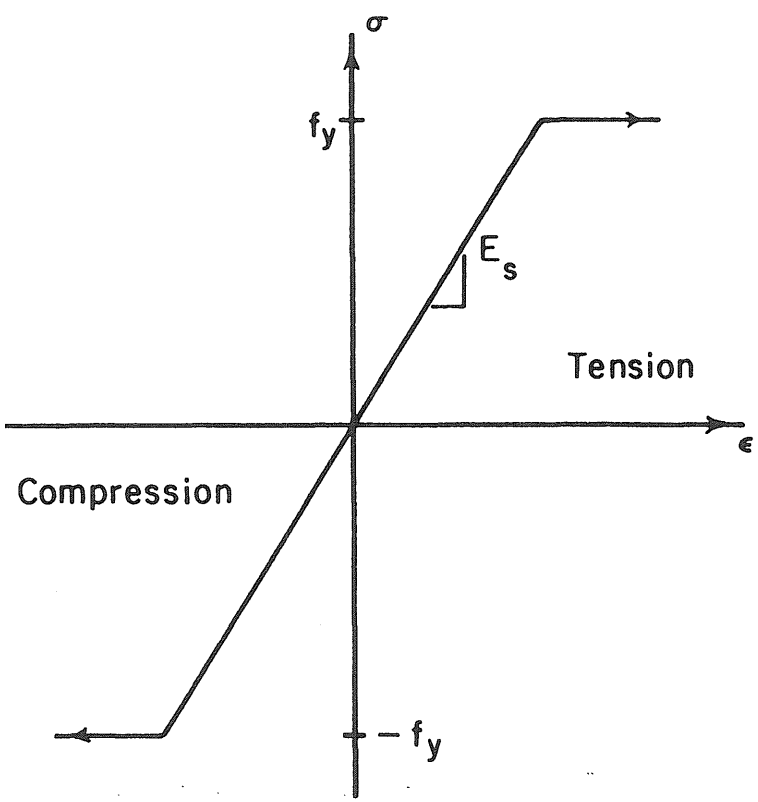

(a) Steel

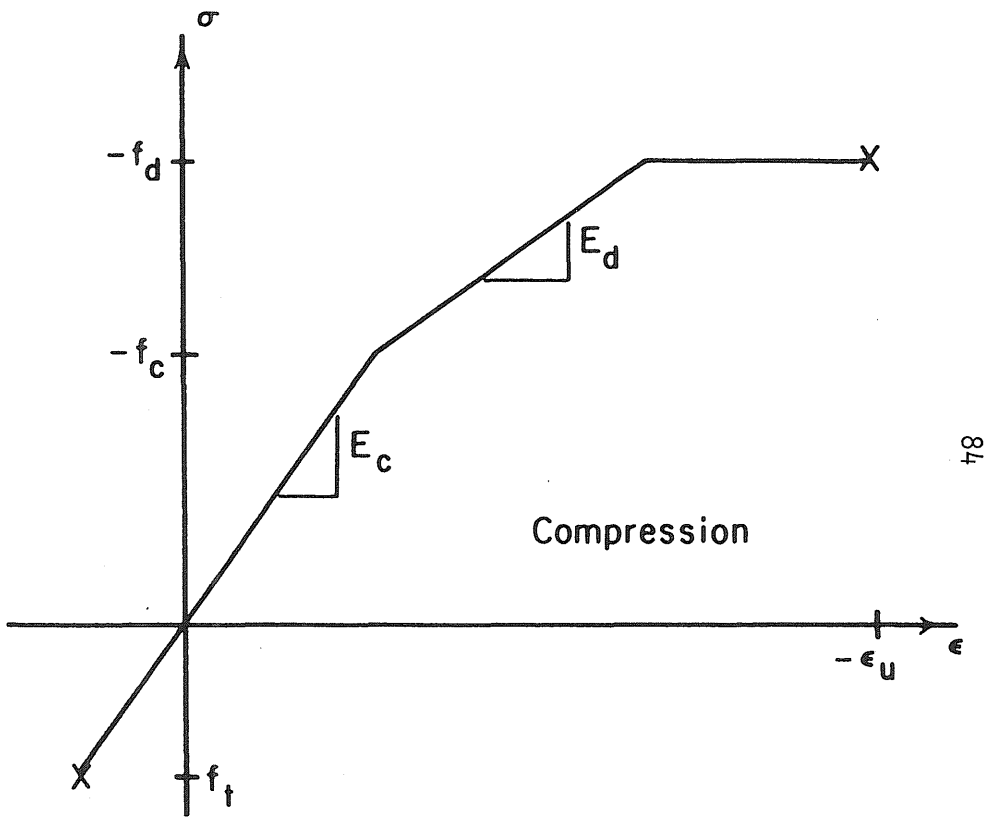

(b) Concrete

FIG. 1 ASSUMED UNIAXIAL STRESS-STRAIN CURVES FOR STEEL AND CONCRETE

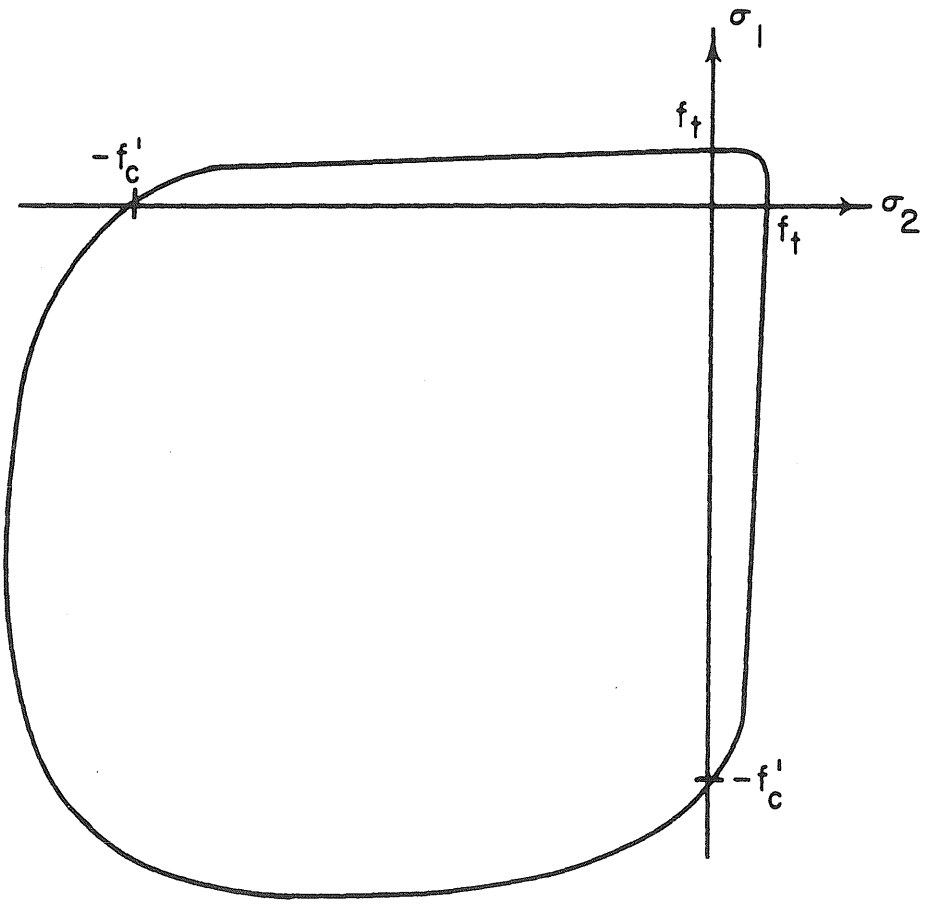

FIG. 2 BIAXIAL STRENGTH OF CONCRETE PROPOSED BY KUPFER, HILSDORF, AND RÜSCH

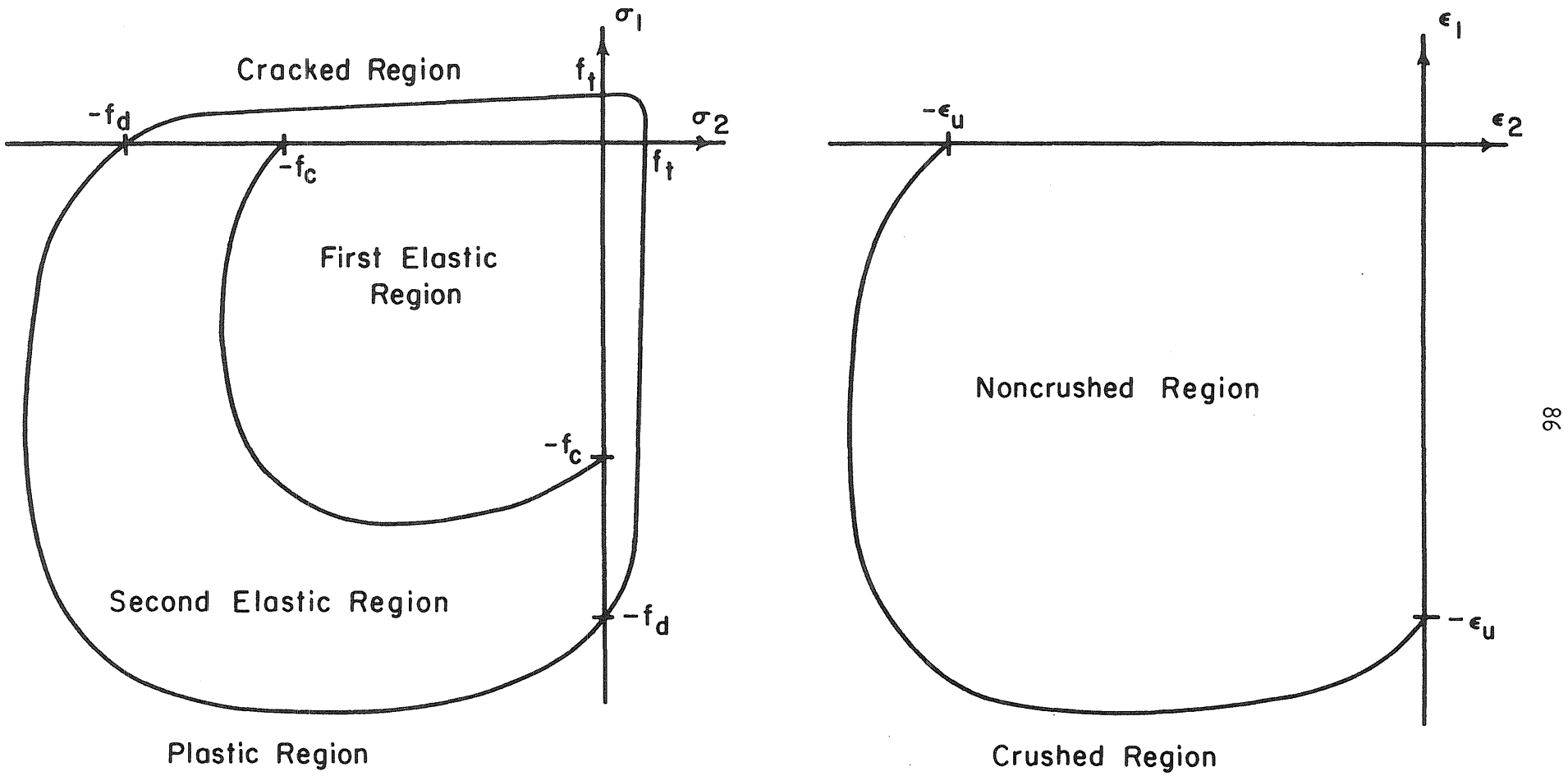

FIG. 3 BOUNDARIES BETWEEN THE DIFFERENT MATERIAL BEHAVIOR REGIONS

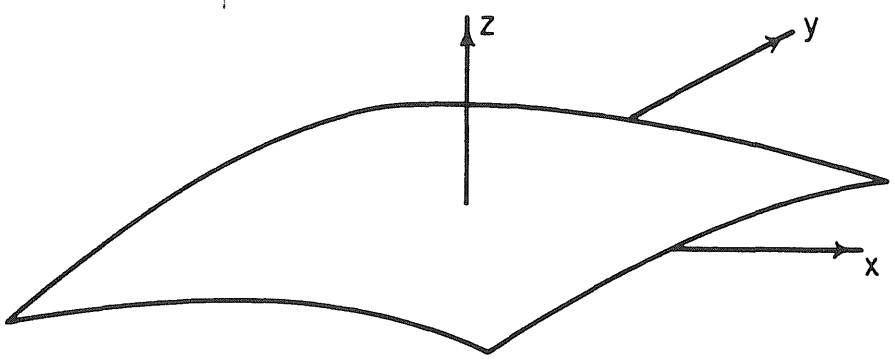

FIG. 4 POSITIVE COORDINATE SYSTEM

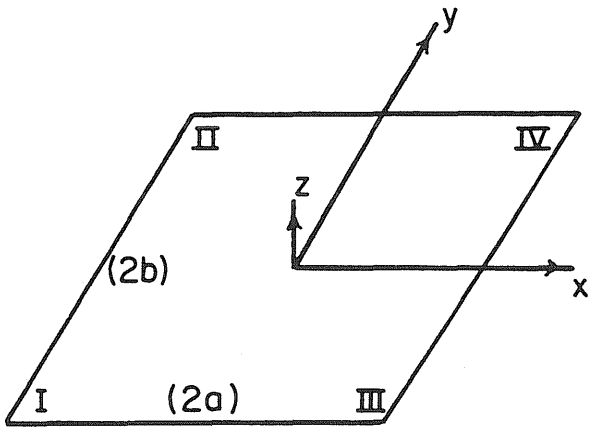

FIG. 5 ELEMENT NODAL NUMBERING SYSTEM AND LOCAL ELEMENT COORDINATE SYSTEM

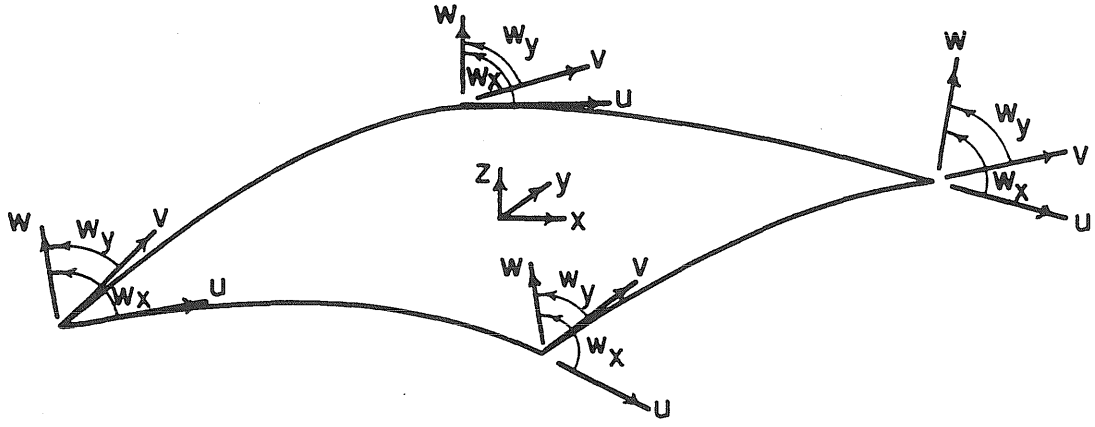

FIG. 6 POSITIVE ORIENTATION OF THE NODAL DEGREES OF FREEDOM

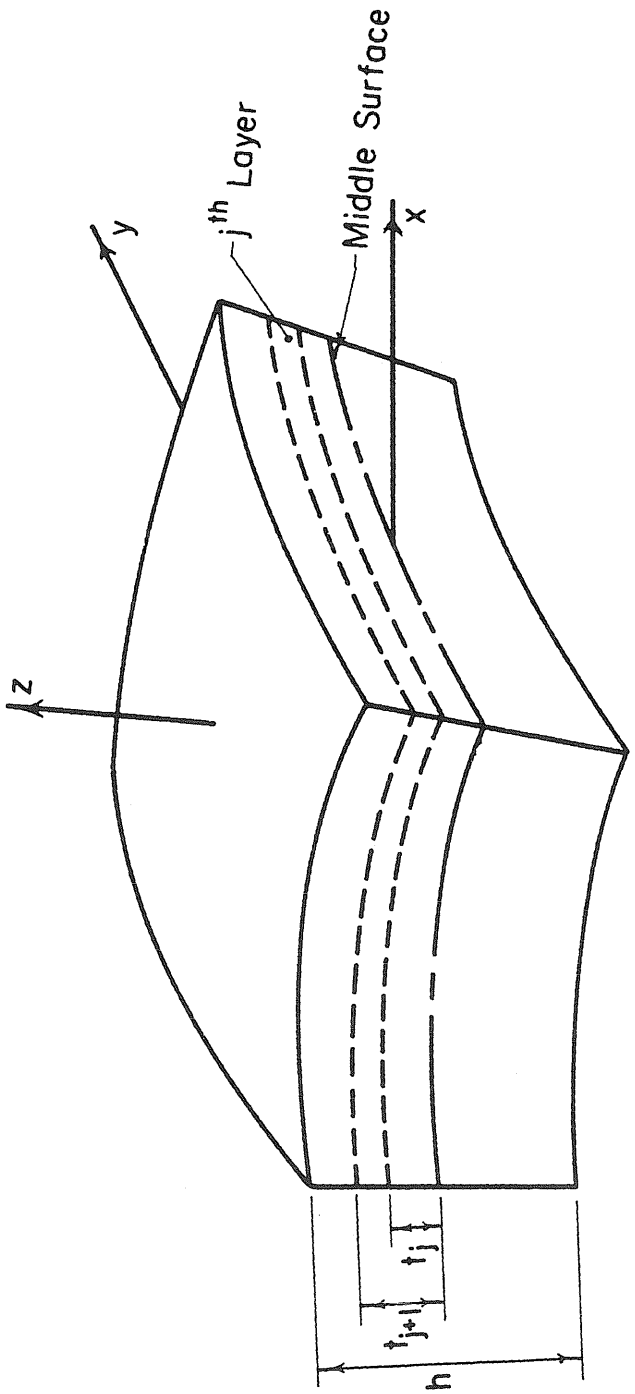

FIG. 7 POSITION OF THE j-th LAYER

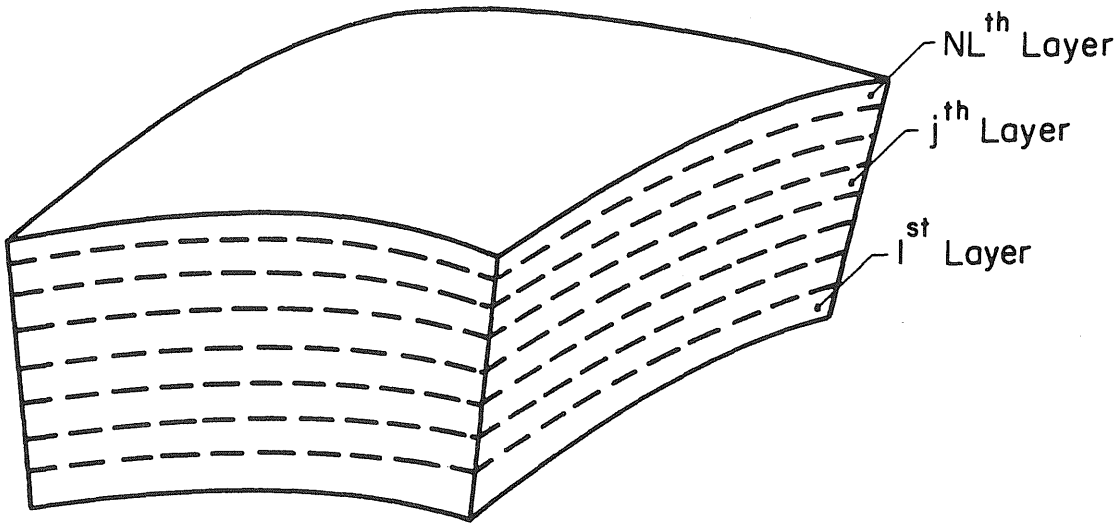

FIG. 8 LAYERED ELEMENT

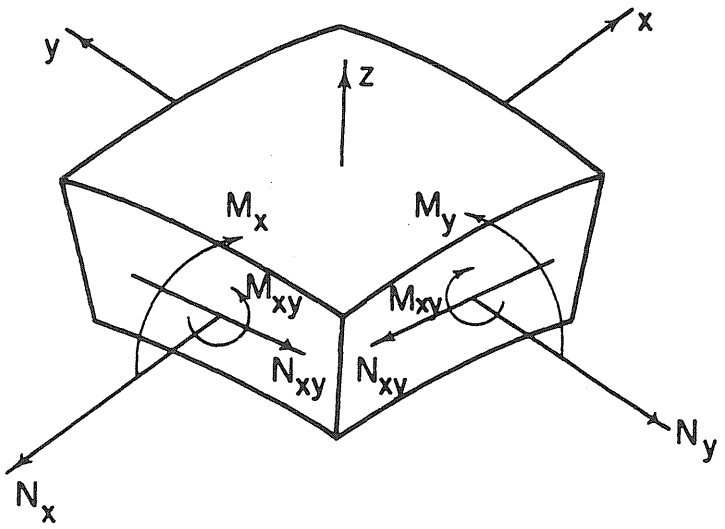

FIG. 9 POSITIVE ORIENTATION OF THE STRESS RESULTANTS

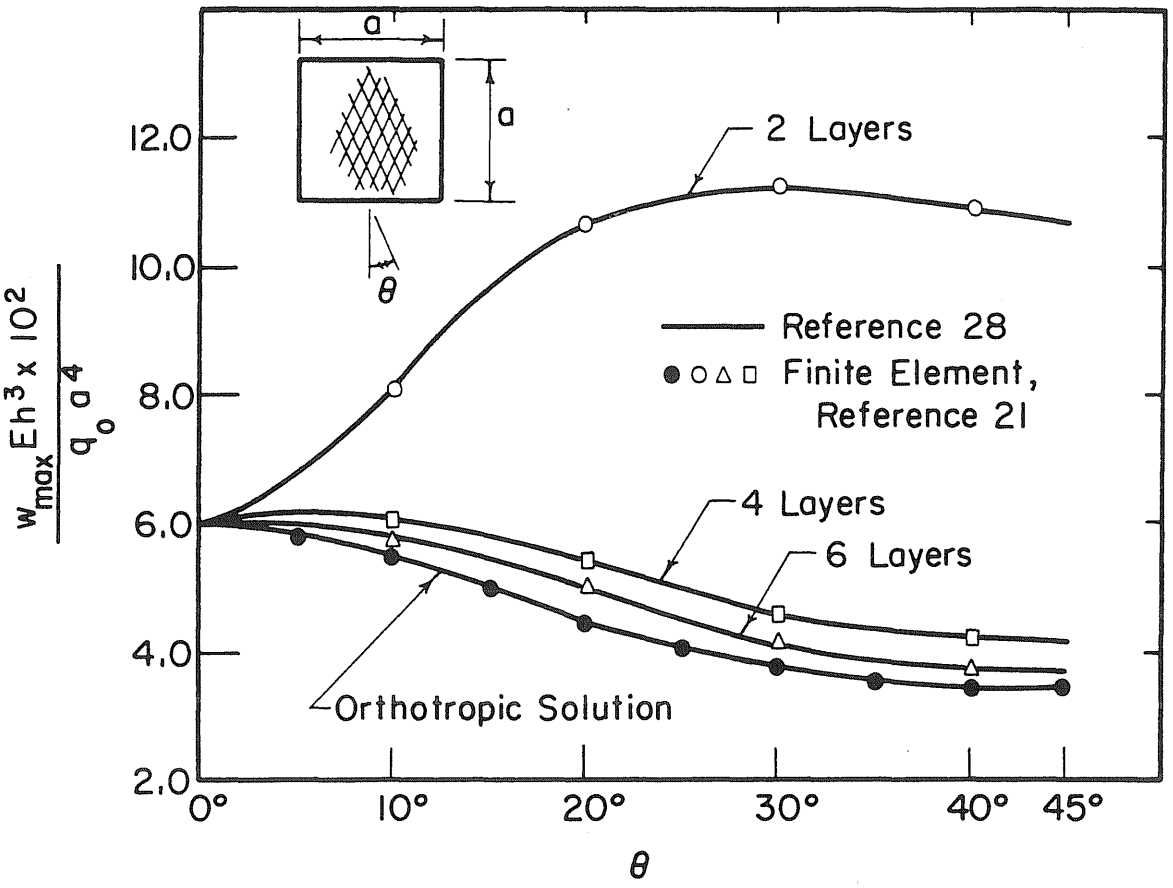

FIG. 10 MAXIMUM DEFLECTION AS A FUNCTION OF ANGLE-PLY ORIENTATION FOR GRAPHITE-EPOXY SQUARE PLATE UNDER UNIFORM TRANSVERSE LOAD (FROM REFERENCE 21)

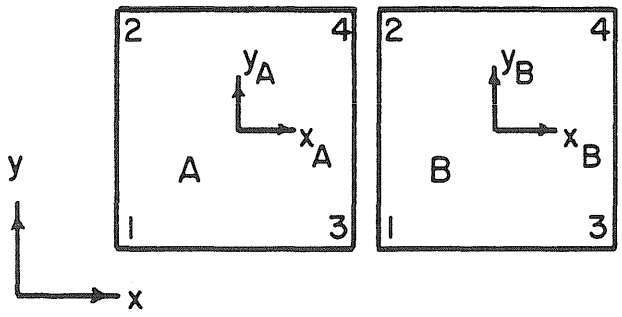

FIG. 11 ELEMENT DISPLACEMENT COMPATIBILITY

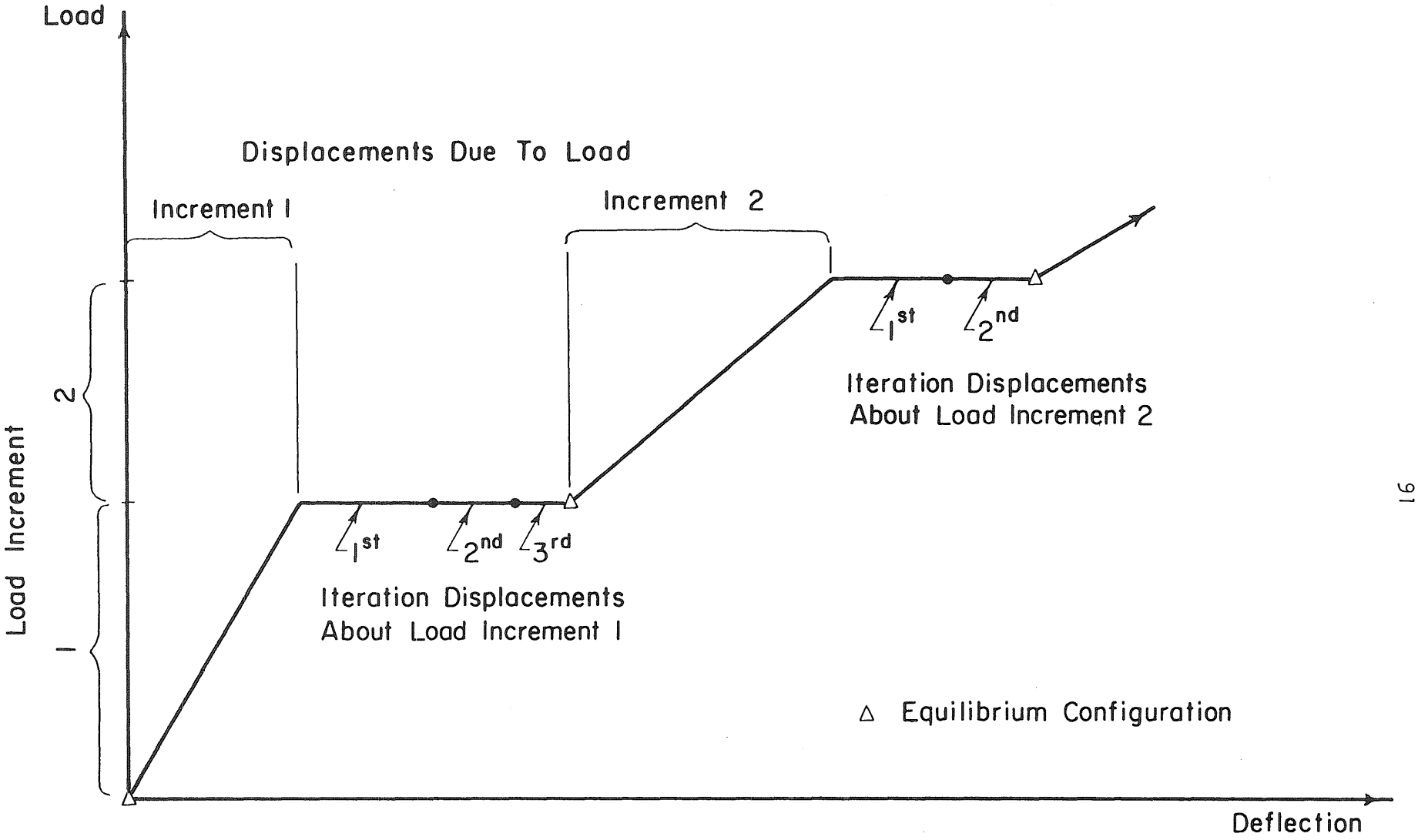

FIG. 12 RELATIVE RELATIONSHIP BETWEEN LOADING INCREMENTS AND ITERATIONS ABOUT A LOAD LEVEL

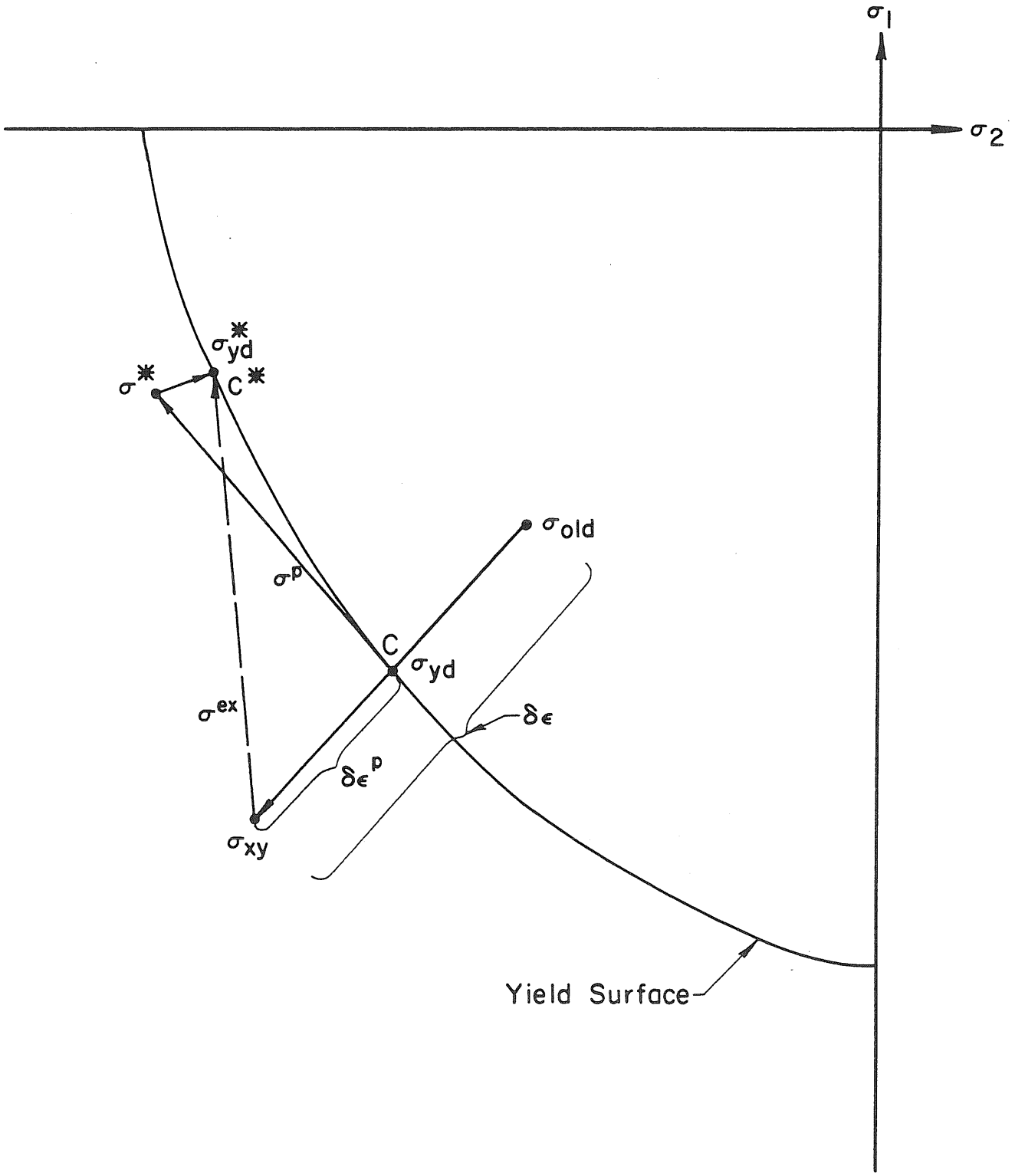

FIG. 13 DIAGRAMMATIC REPRESENTATION OF ELASTIC CONCRETE GOING PLASTIC

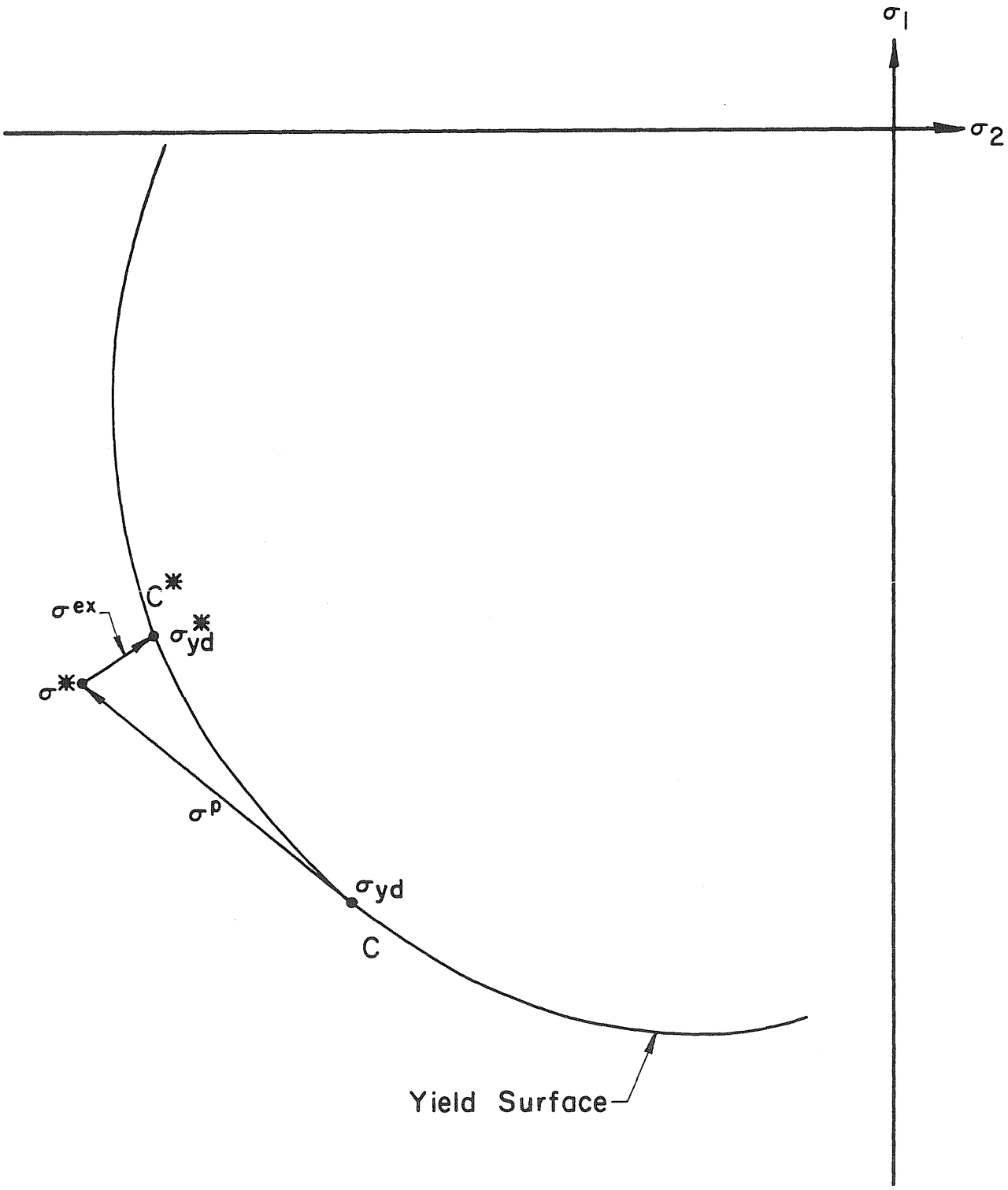

FIG. 14 DIAGRAMMATIC REPRESENTATION OF PLASTIC CONCRETE DEFORMING PLASTICLY

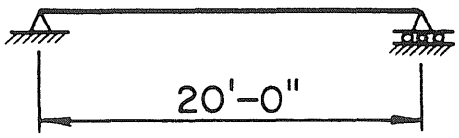

(a) Beam

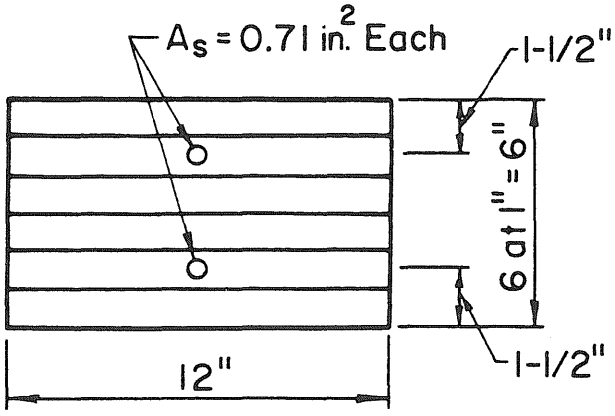

(b) Cross-section and Layer Scheme

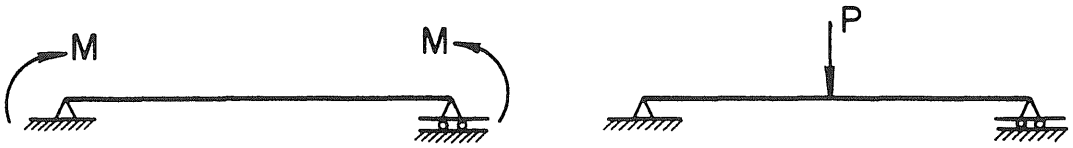

(c) Loading Conditions

(d) One Element Idealization

f_c = 3000 psi	$E_c = 4.0 \times 10^6$ psi
f_d = 3000 psi	$E_d = 4.0 \times 10^6$ psi
f_t = 300 psi	$E_s = 30.0 \times 10^6$ psi
f_y = 40,000 psi	ν = 0.0

(e) Material Properties

FIG. 15 BEAM INFORMATION FOR SIMPLY SUPPORTED THEORETICAL BEAM

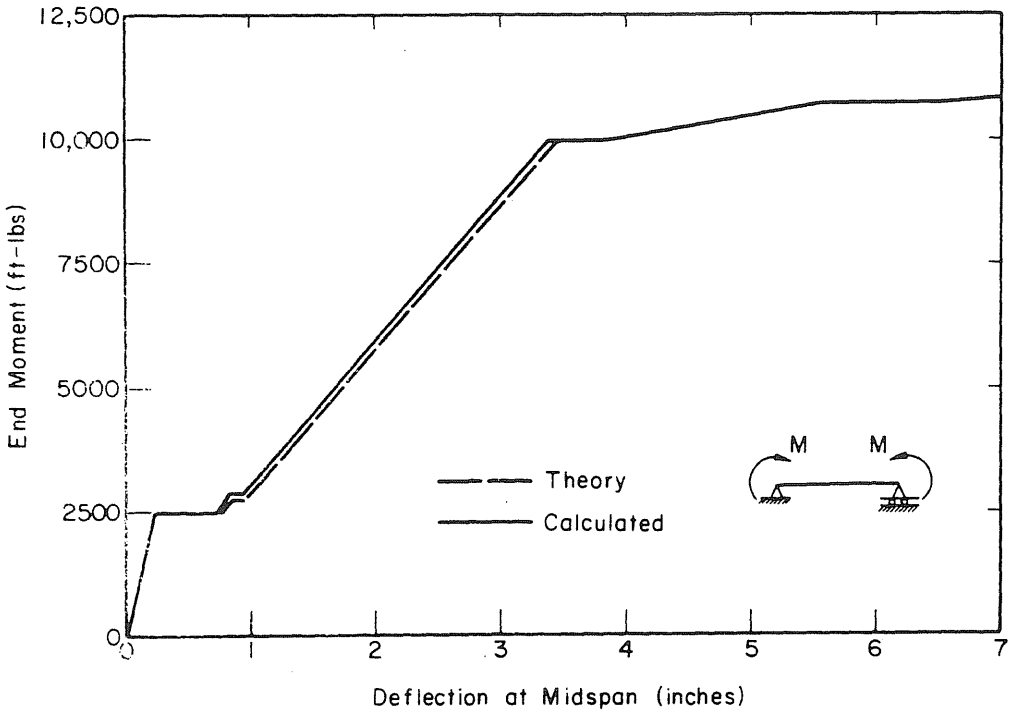

FIG. 16 LOAD-DEFLECTION CURVES FOR SIMPLY SUPPORTED THEORETICAL BEAM WITH EQUAL END MOMENTS

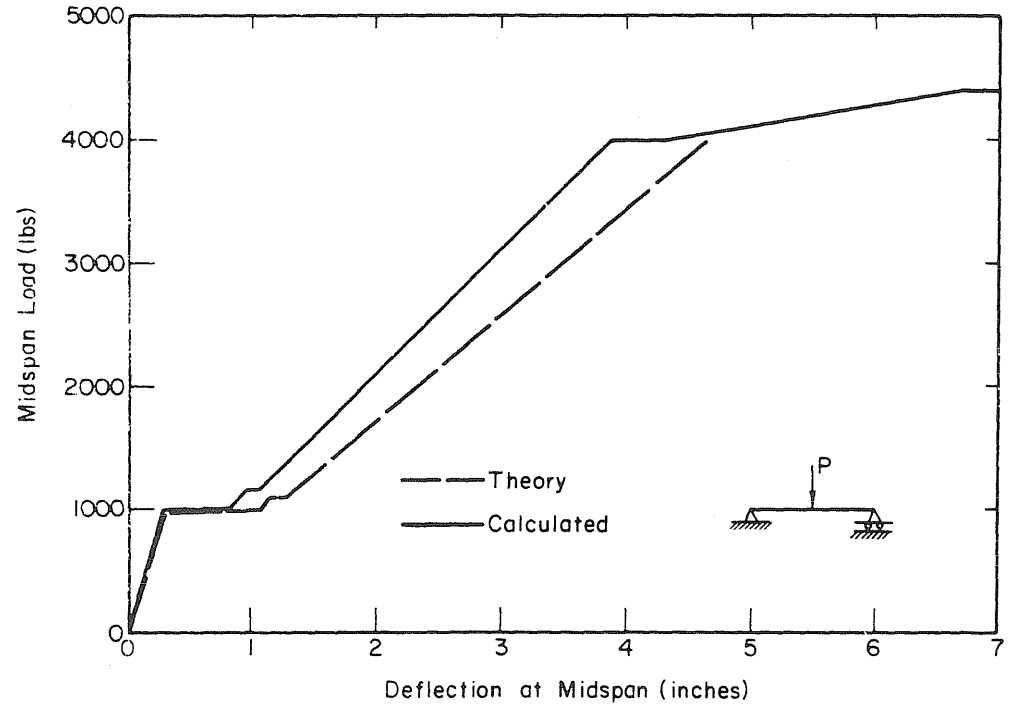

FIG. 17 LOAD-DEFLECTION CURVES FOR SIMPLY SUPPORTED THEORETICAL BEAM WITH CONCENTRATED MIDSPAN LOAD

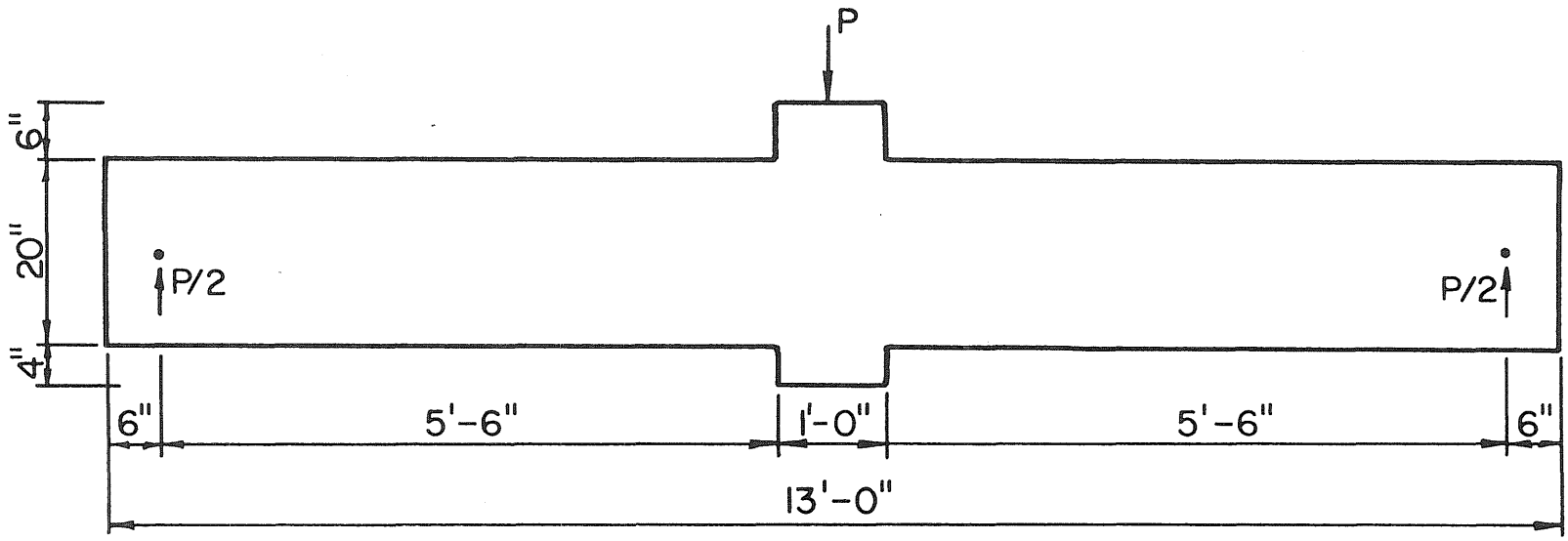

(a) Beam

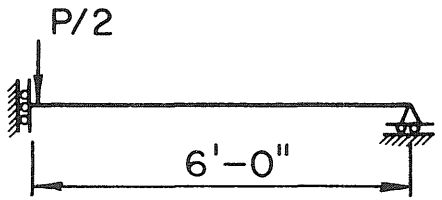

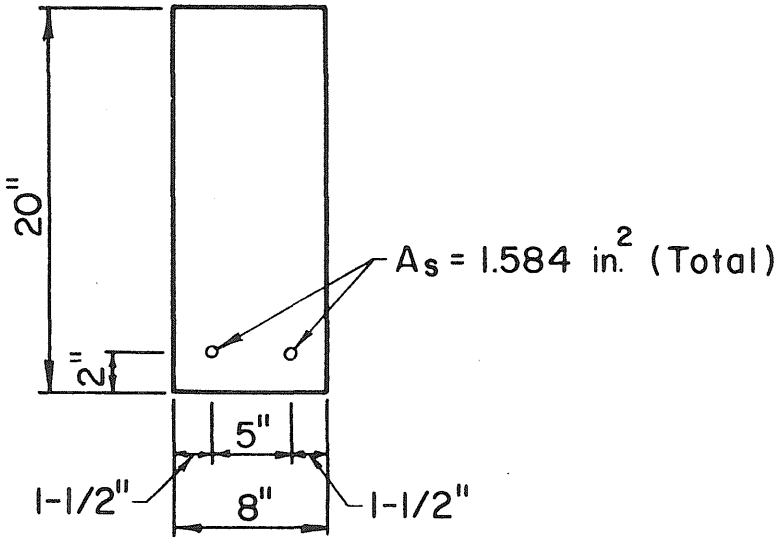

FIG. 18 BEAM INFORMATION FOR BURNS AND SIESS

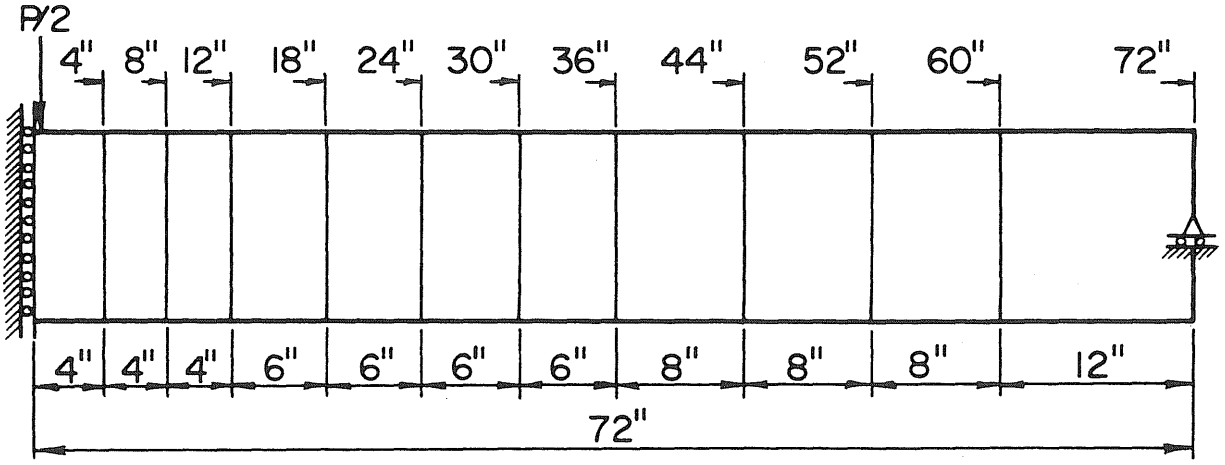

(a) Element Grid

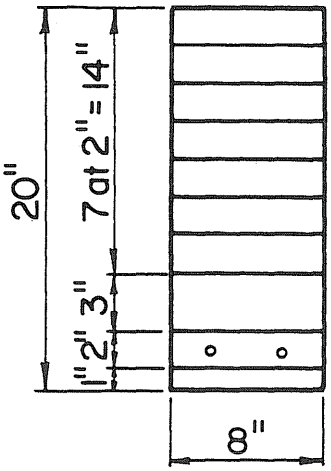

(b) Layer Scheme

Given	Assumed
$f'_c = 4820$ psi	$f_c = f_d = 4820$ psi
$f_t = 546$ psi	$E_c = E_d = 3.8 \times 10^6$ psi
$E_c \approx 3.8 \times 10^6$ psi	$E_s = 30 \times 10^6$
$f_y = 44{,}900$ psi	$\nu = 0.15$

(c) Material Properties

FIG. 19 ELEMENT GRID INFORMATION FOR BURNS AND SIESS' BEAM

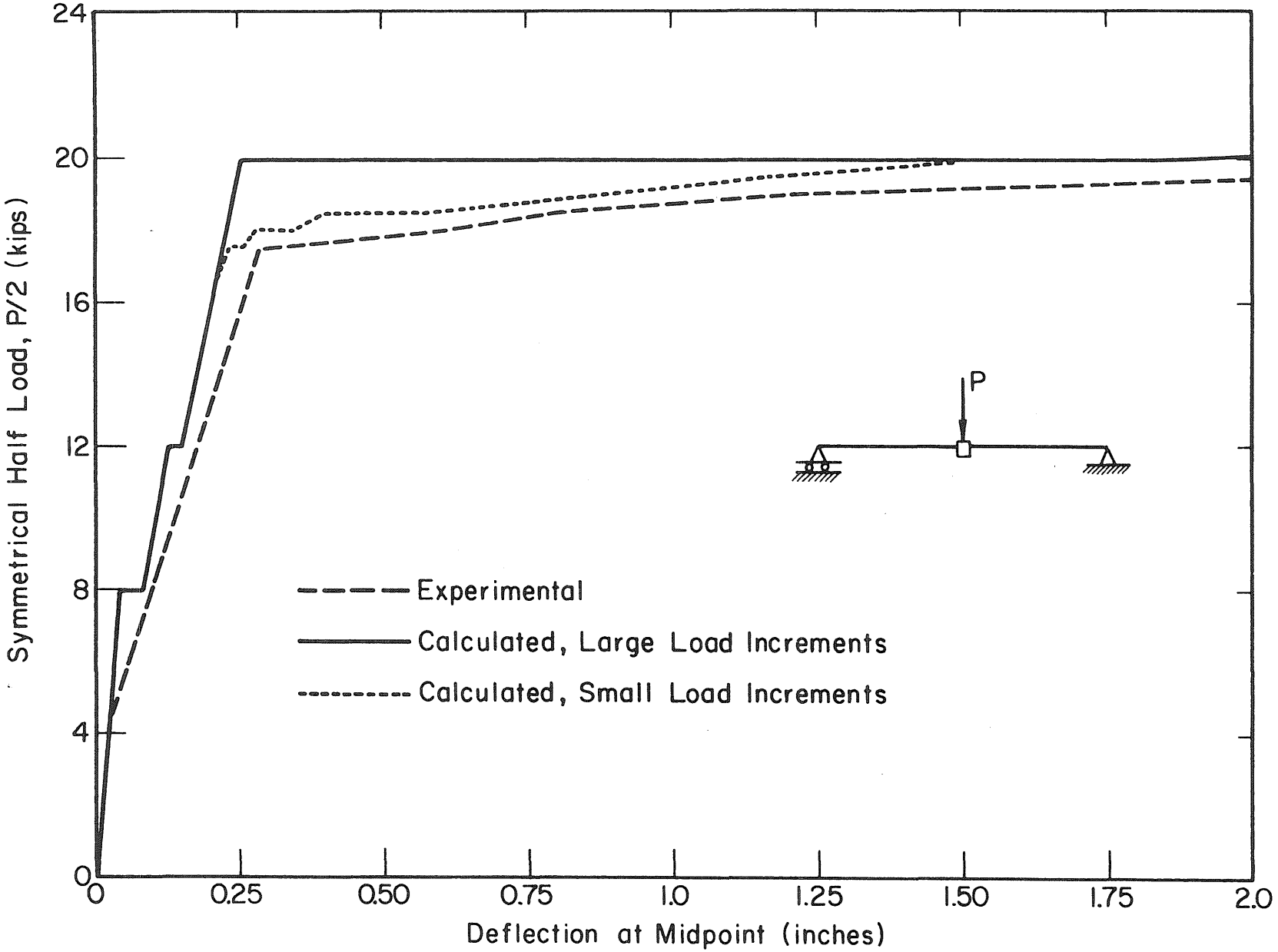

FIG. 20 LOAD-DEFLECTION CURVES FOR BURNS AND SIESS' BEAM

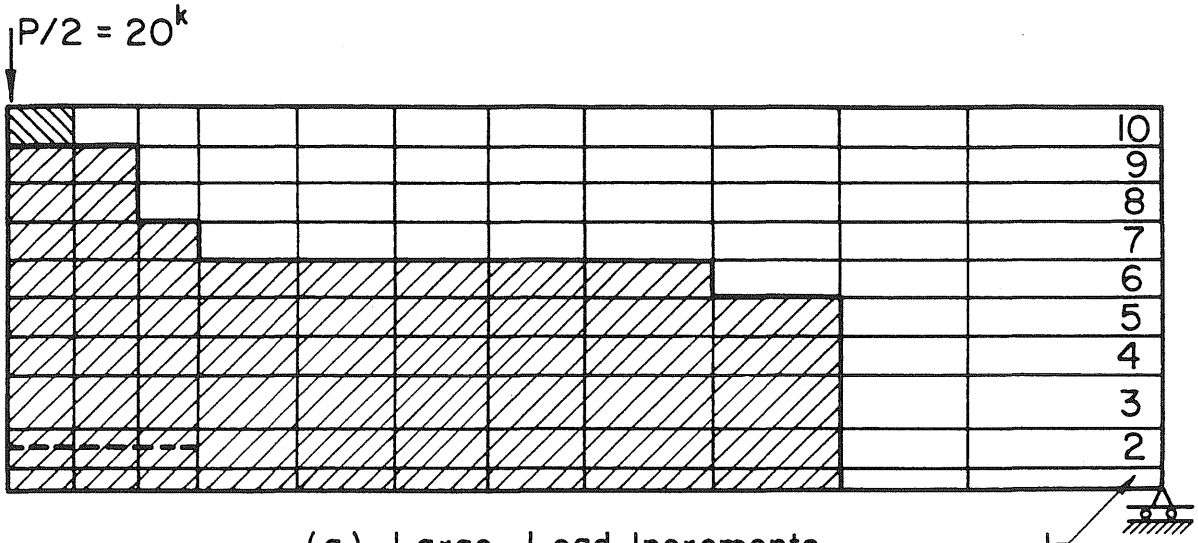

(a) Large Load Increments

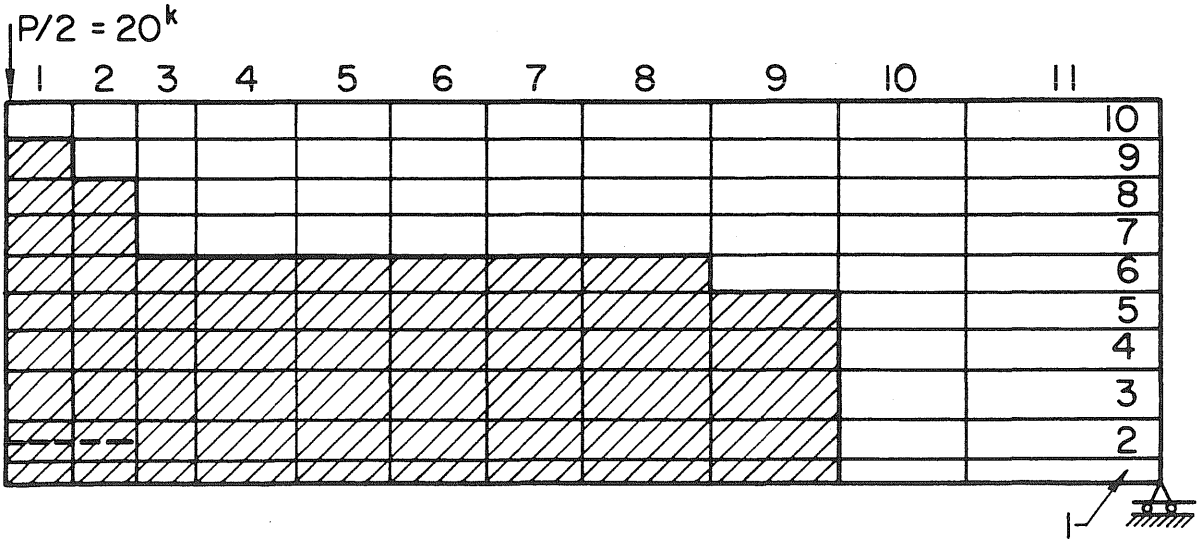

(b) Small Load Increments

=> Cracked Layer

---- => Yielded Reinforcement

=> Plastic Layer

FIG. 21 CRACK CONFIGURATION FOR BURNS AND SIESS' BEAM AT EQUILIBRIUM WITH LOAD OF 20 kips

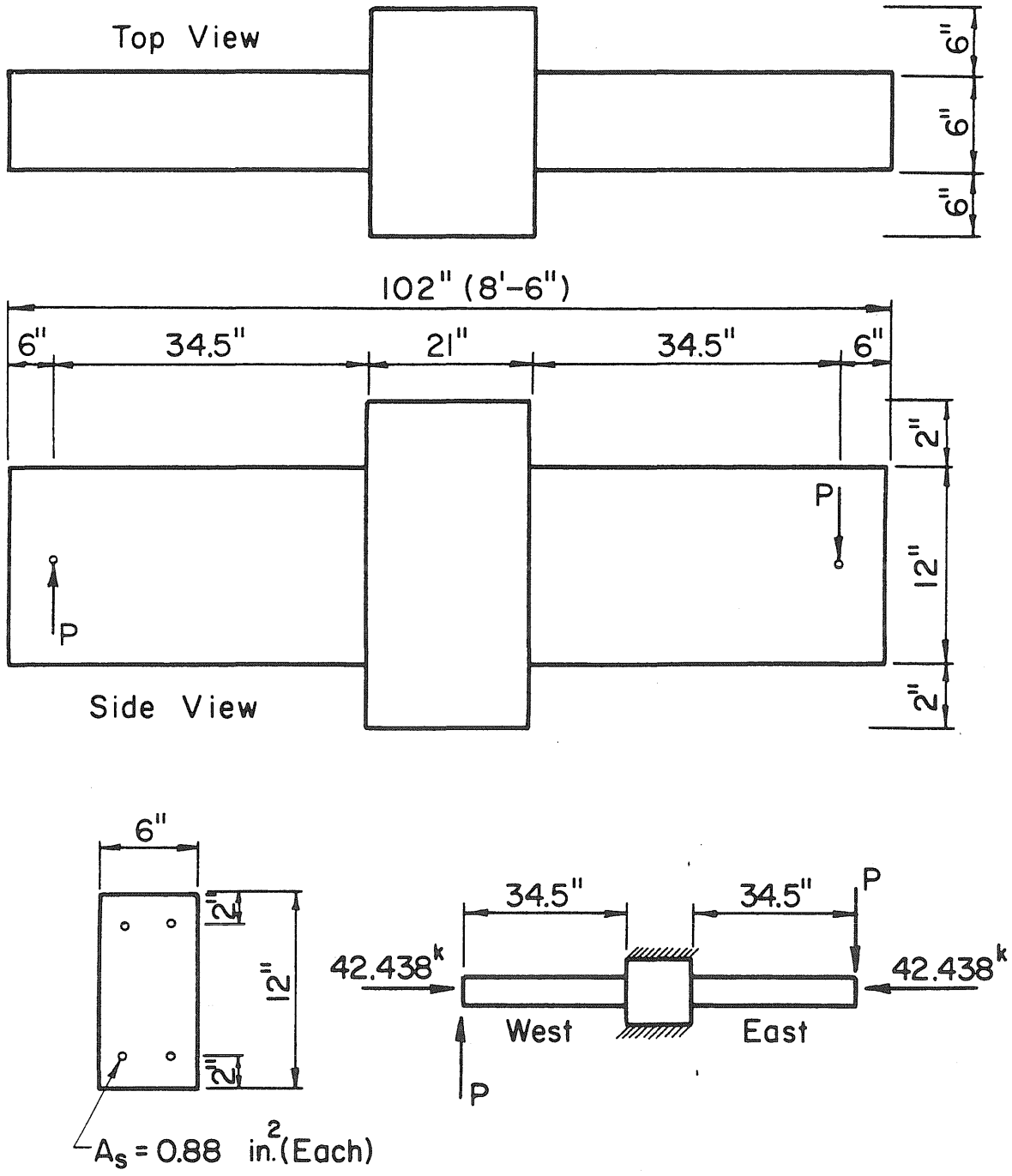

FIG. 22 BEAM INFORMATION FOR WIGHT

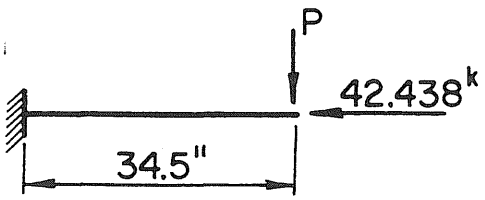

(a) Analytical Idealization

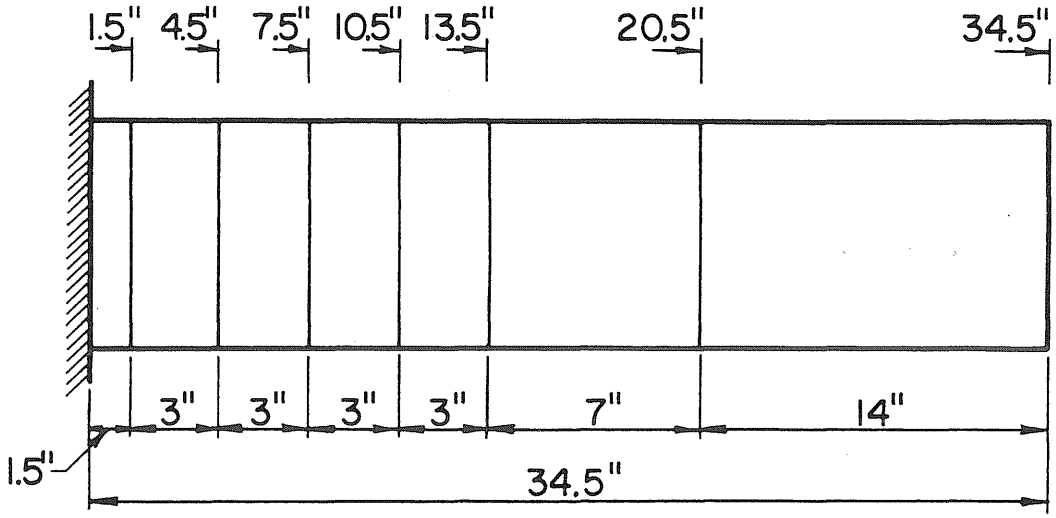

(b) Element Grid

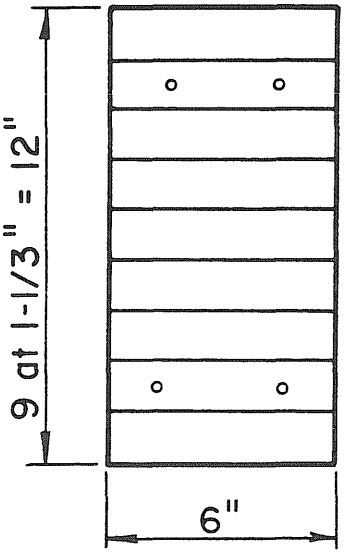

(c) Layer Scheme

Given	Assumed
f'_c = 5000 psi	f_c = 3800 psi
E_c = 3.56 x 10^6 psi	f_d = 5000 psi
f_t = 391 psi	E_c = 3.45 x 10^6 psi
f_y = 72,000 psi	E_d = 0.94 x 10^6 psi
E_s = 29 x 10^6 psi	ν = 0.0
	ϵ_u = 0.0038 in./in.

(d) Material Properties

FIG. 23 ELEMENT GRID FOR WIGHT'S BEAM

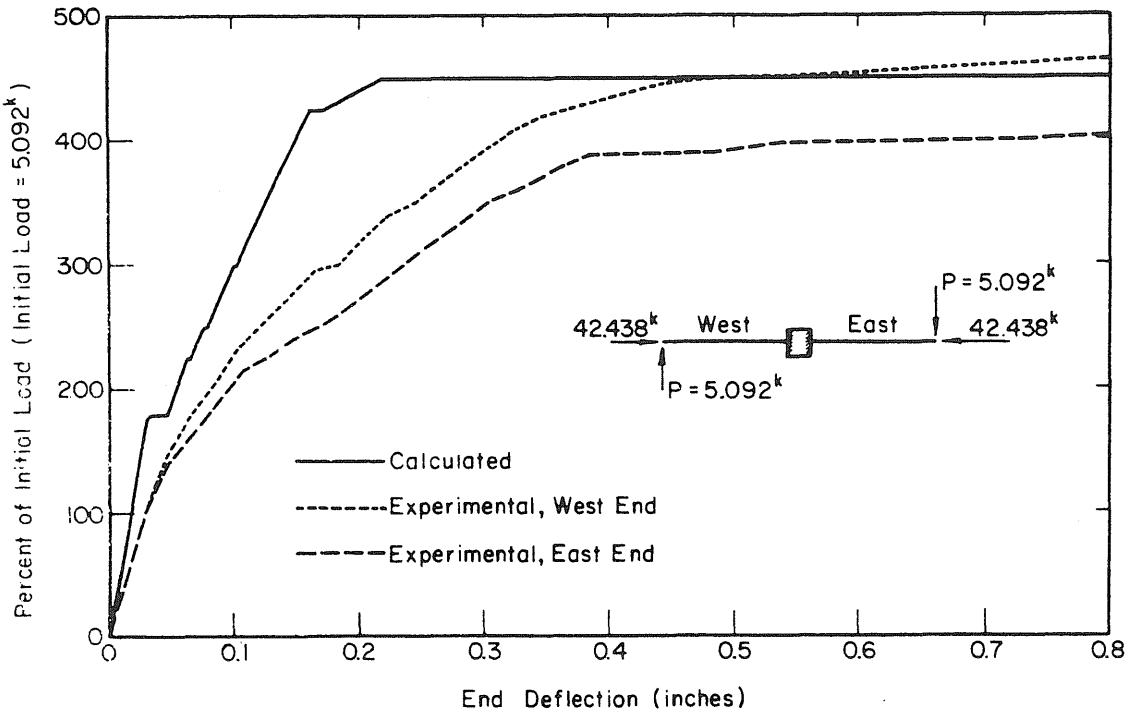

FIG. 24 LOAD-DEFLECTION CURVES FOR WIGHT'S BEAM

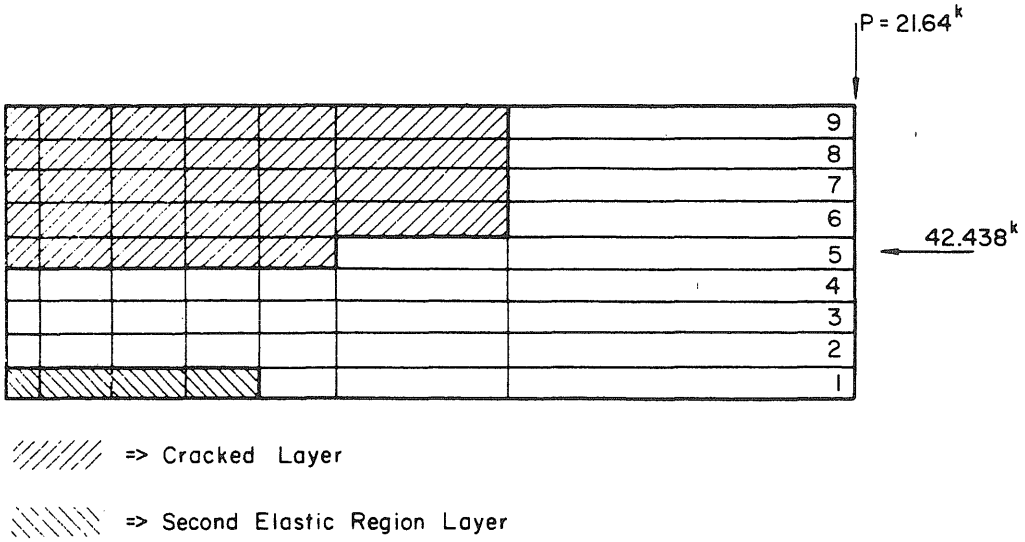

FIG. 25 CRACK CONFIGURATION FOR WIGHT'S BEAM AT EQUILIBRIUM WITH LOAD OF 21.64 kips

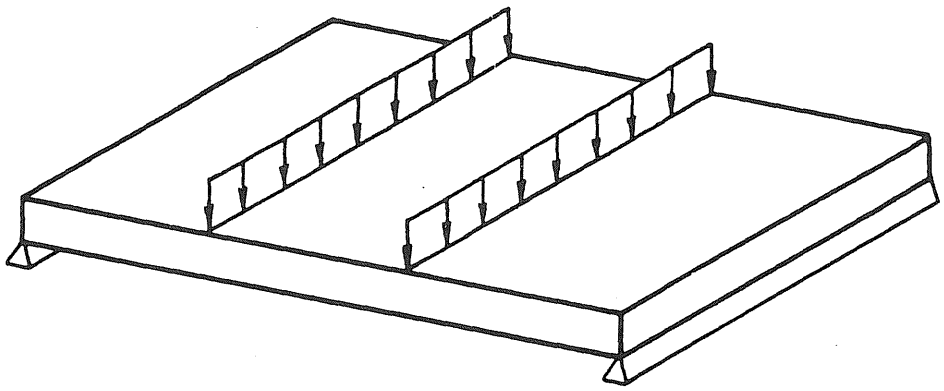

(a) Test Set-up

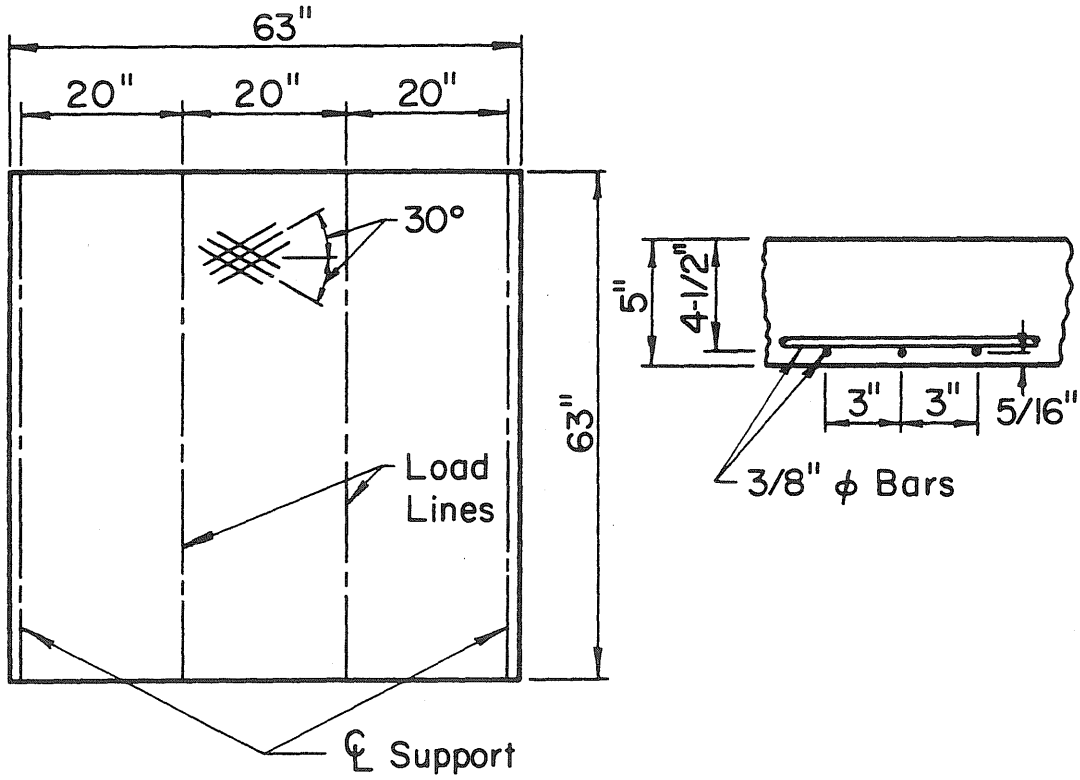

(b) Dimensions of Test Specimens

FIG. 26 HOUBOLT'S RECTANGULAR SPECIMENS

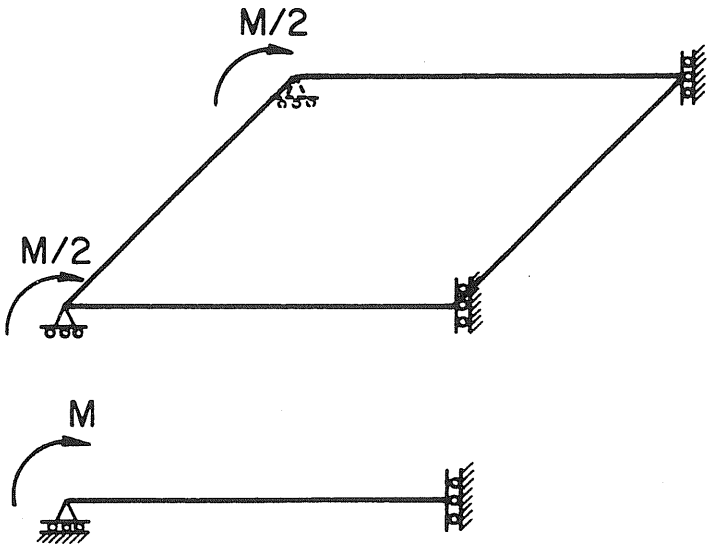

(a) One Element Idealization of Constant Stress Region

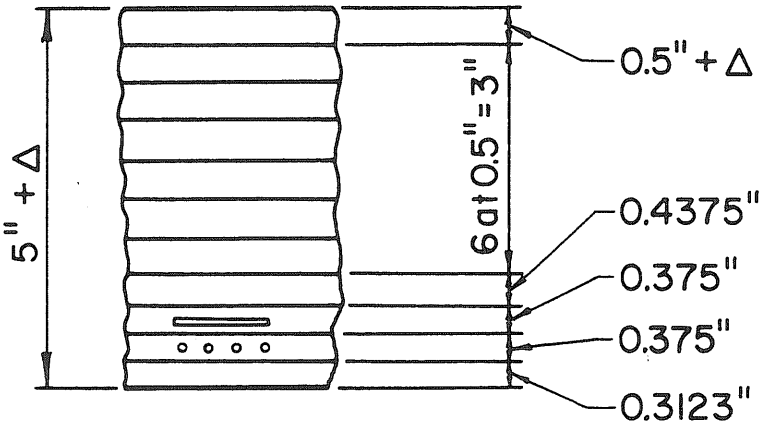

(b) Layer Scheme

FIG. 27 ELEMENT GRID FOR HOUBOLT'S SPECIMENS

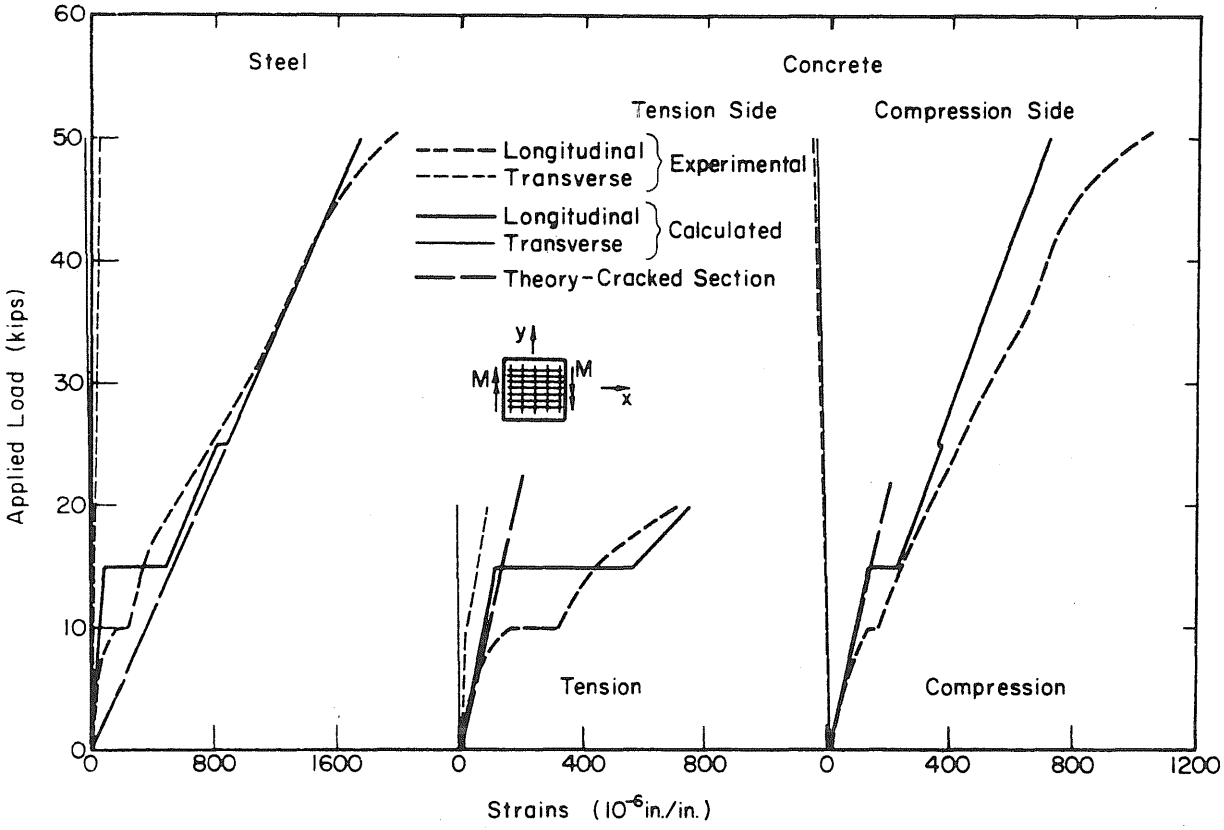

FIG. 28 LOAD STRAIN DIAGRAMS FOR SLAB 03-906

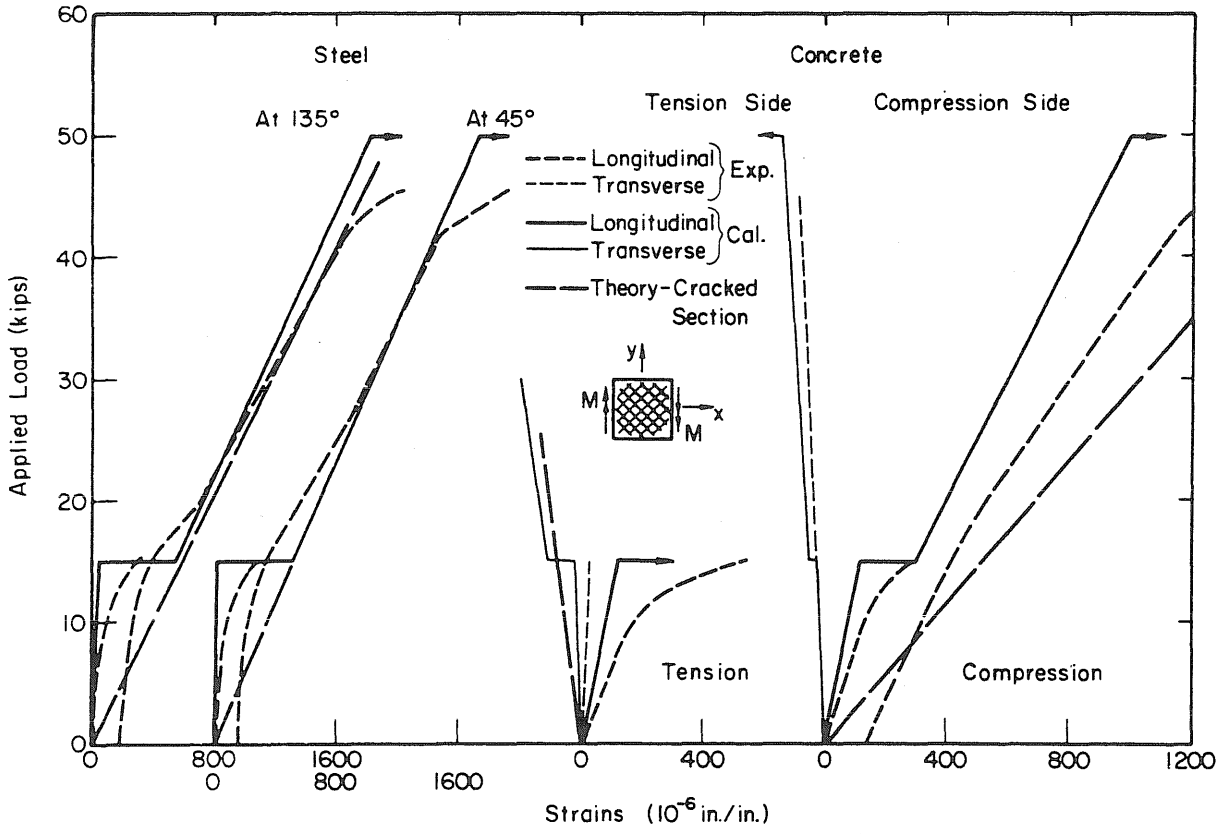

FIG. 29 LOAD STRAIN DIAGRAMS FOR SLAB 453-453

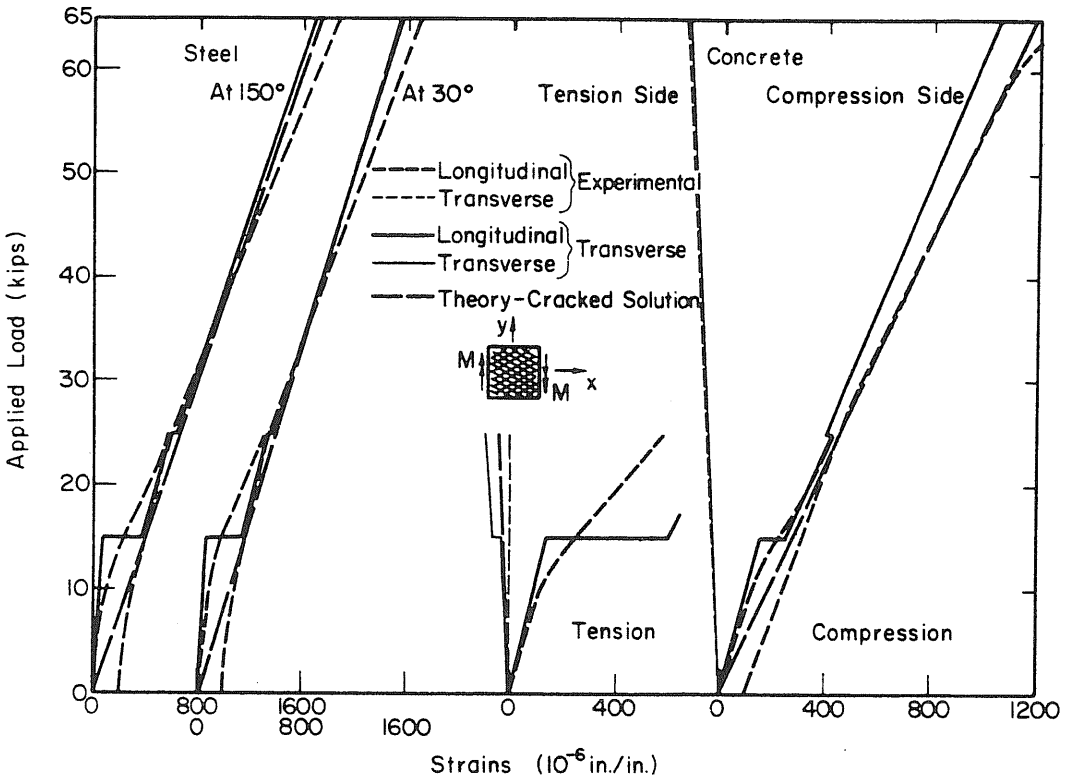

FIG. 30 LOAD STRAIN DIAGRAMS FOR SLAB 303-303

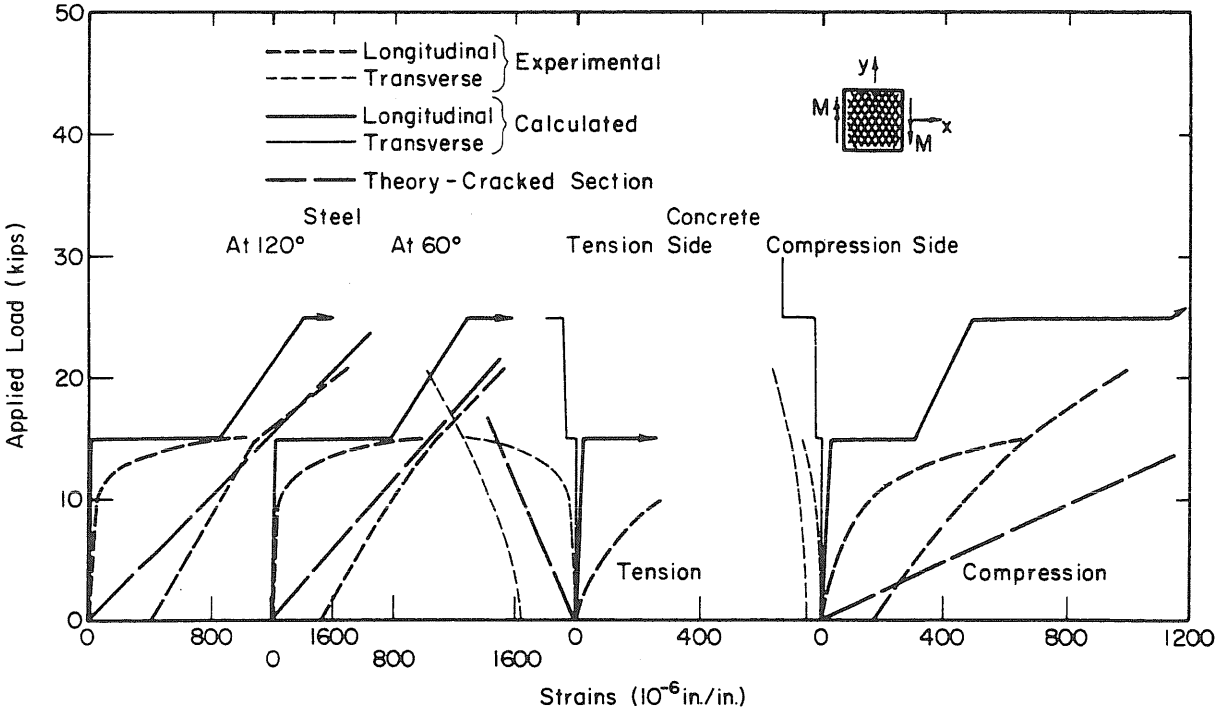

FIG. 31 LOAD STRAIN DIAGRAMS FOR SLAB 603-603

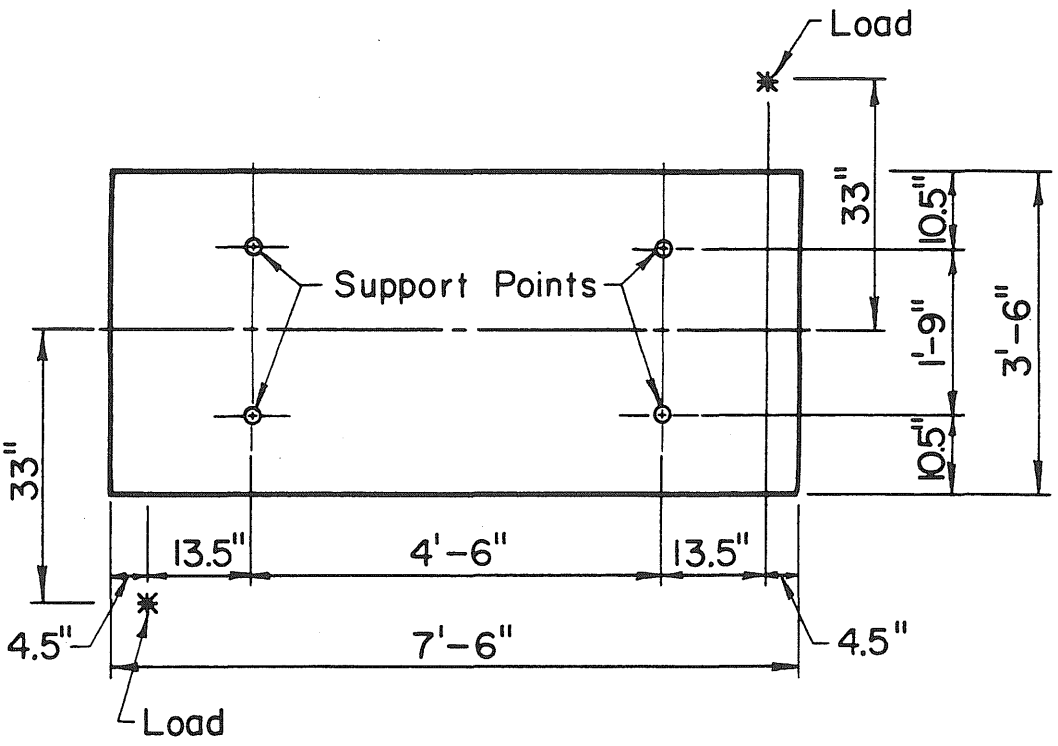

(a) Dimensions of Test Specimens

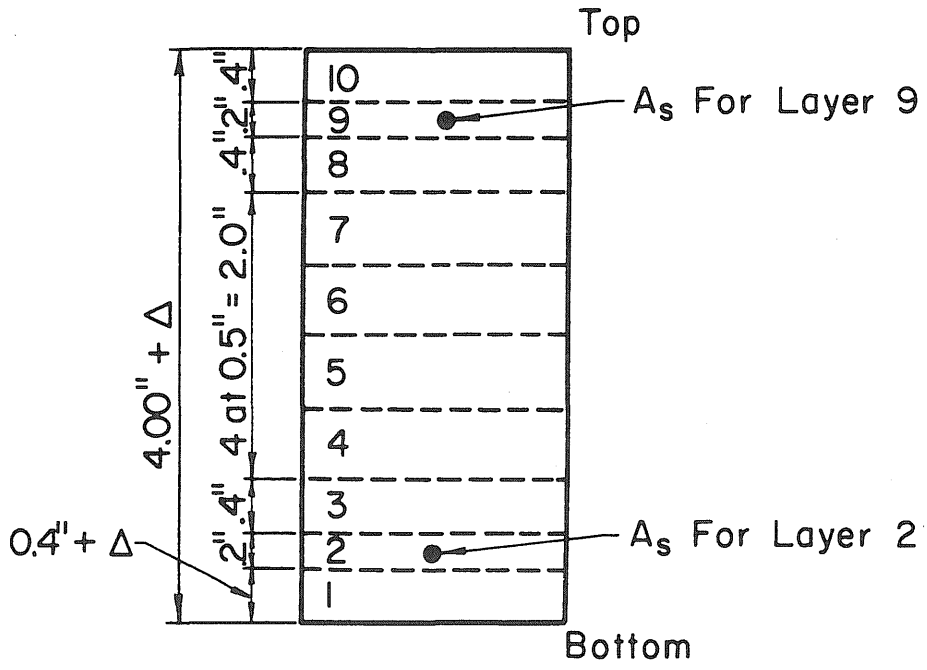

(b) Layer Scheme

FIG. 32 CARDENAS' RECTANGULAR SPECIMENS

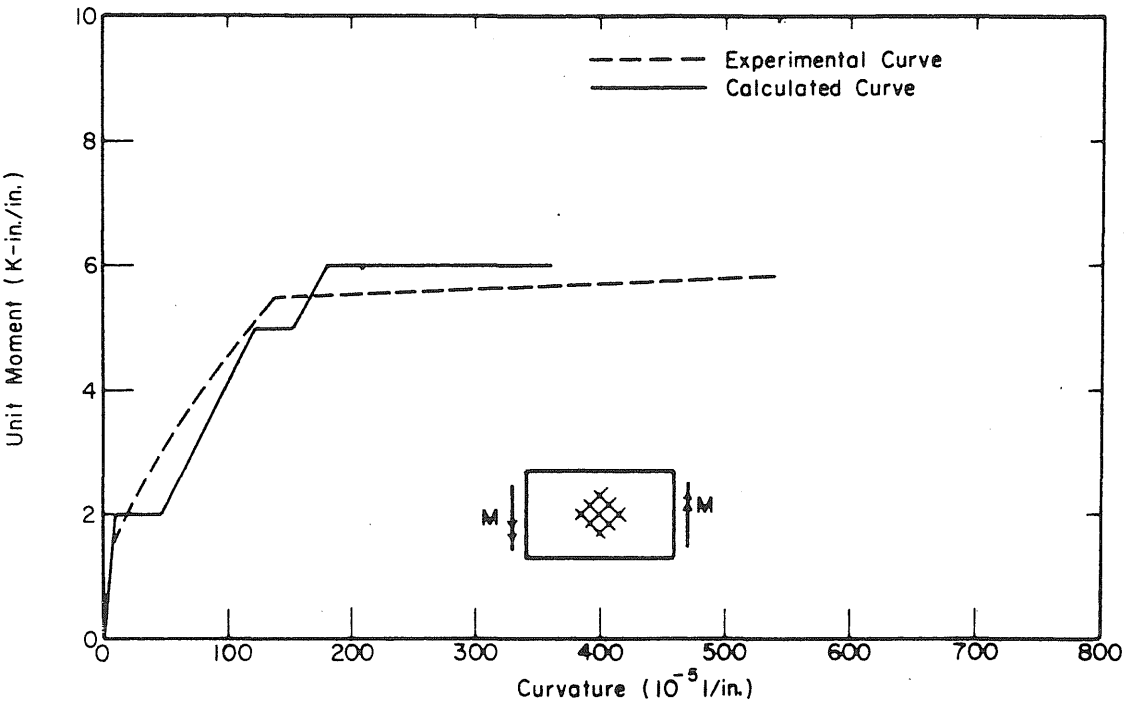

FIG. 33a MOMENT-CURVATURE PLOT, SPECIMEN B7

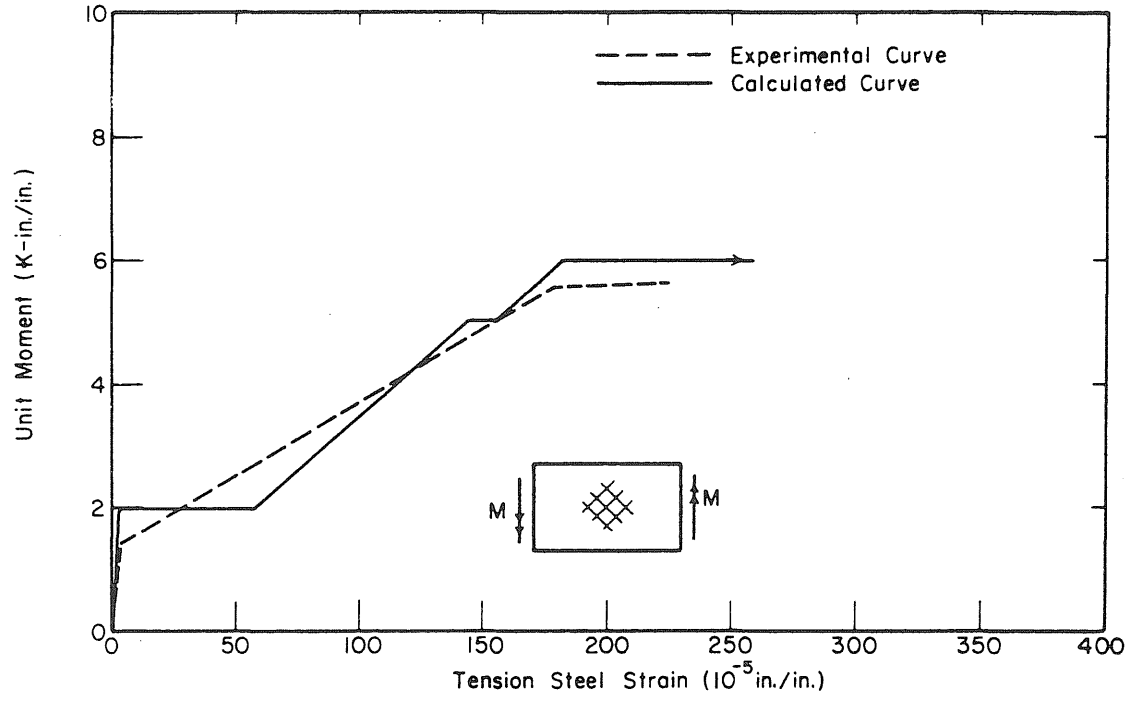

FIG. 33b MOMENT-STEEL STRAIN PLOT, TENSION SIDE OF SPECIMEN B7

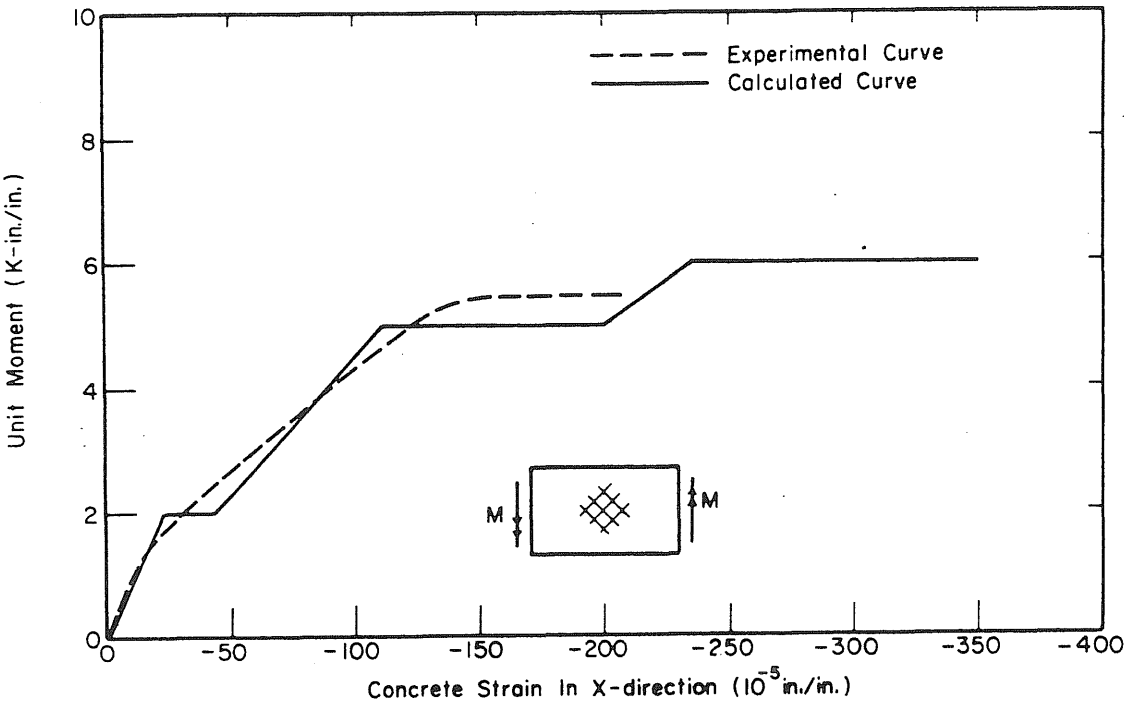

FIG. 33c MOMENT-CONCRETE STRAIN PLOT, COMPRESSIVE SIDE OF SPECIMEN B7, X DIRECTION

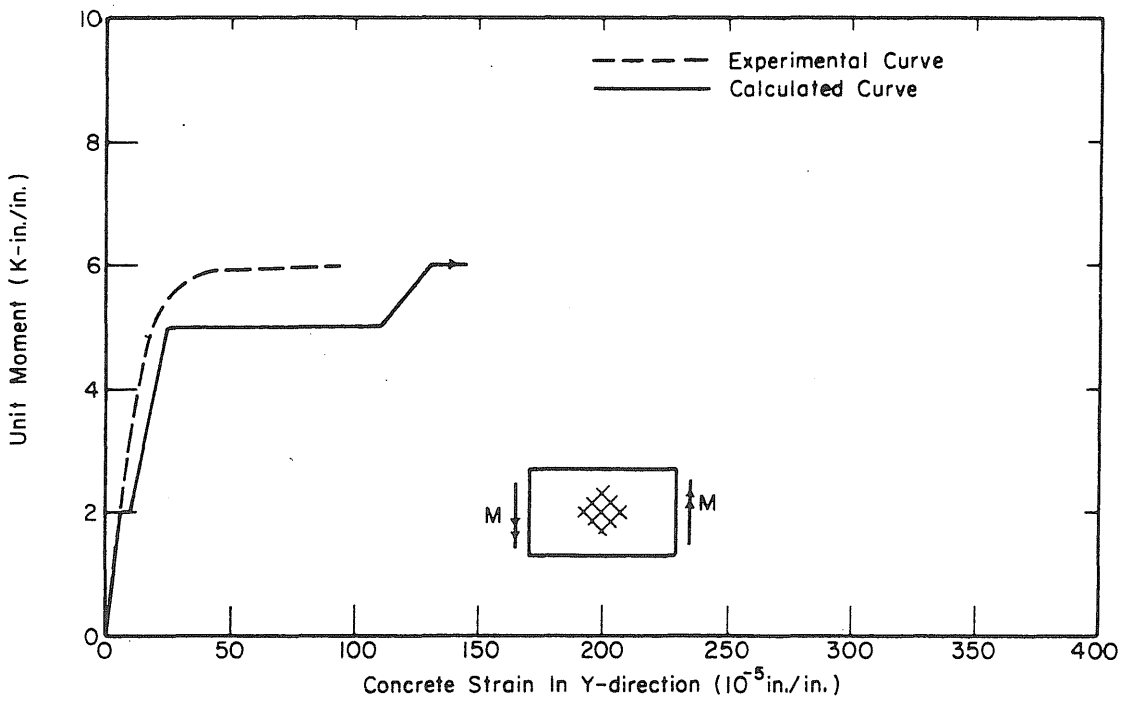

FIG. 33d MOMENT-CONCRETE STRAIN PLOT, COMPRESSIVE SIDE OF SPECIMEN B7, Y DIRECTION

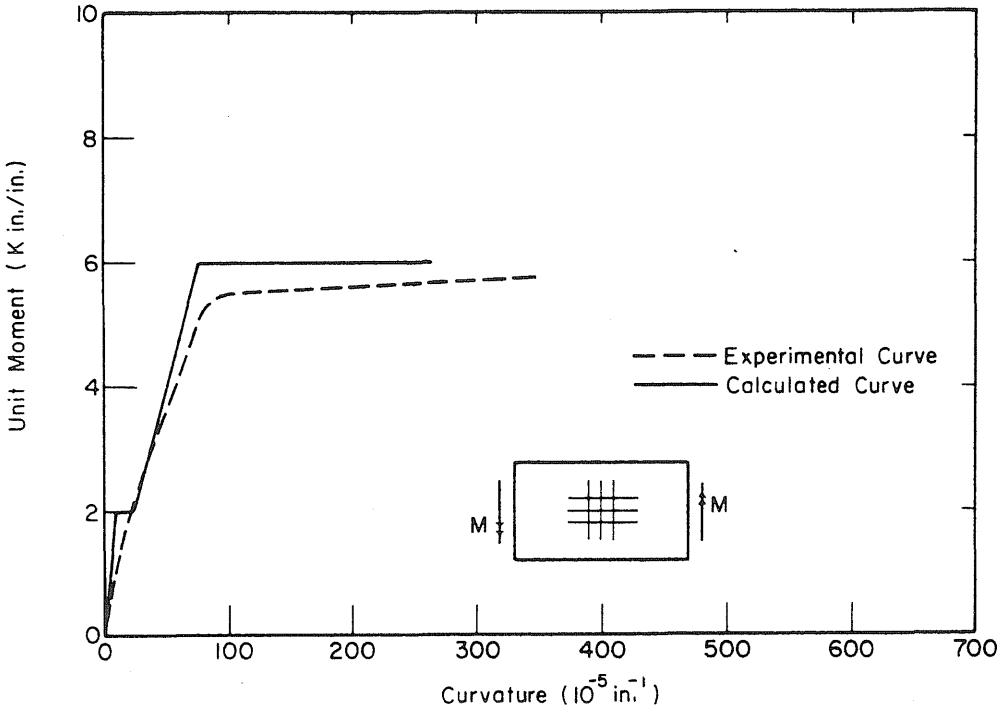

FIG. 34a MOMENT–CURVATURE PLOT, SPECIMEN B10

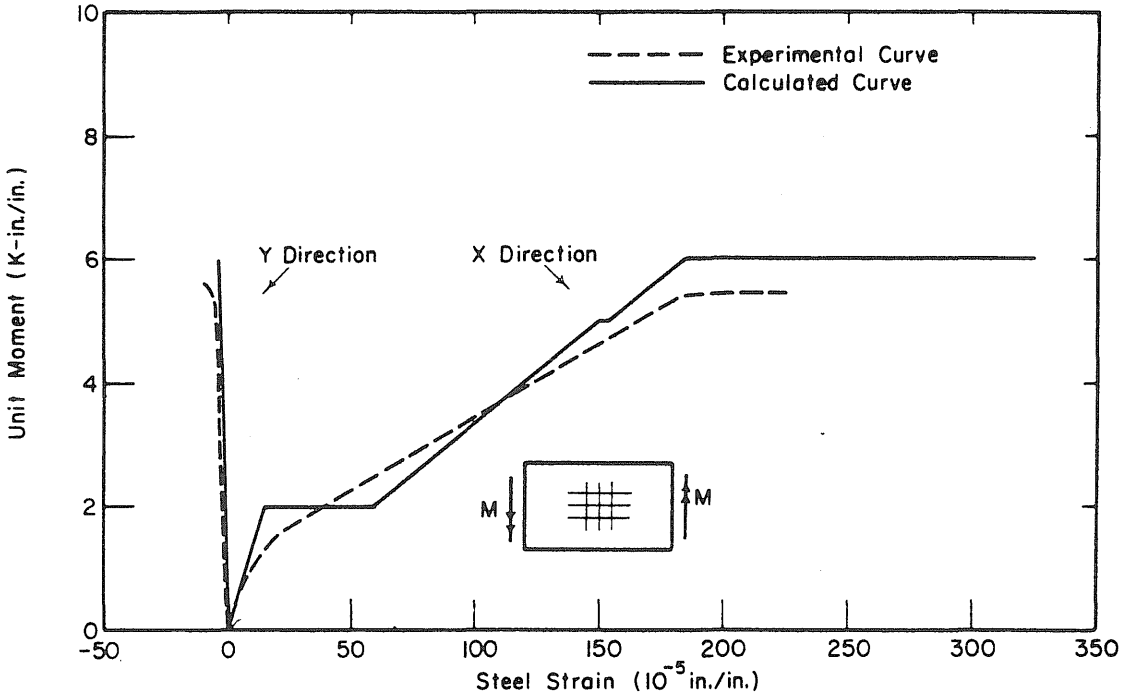

FIG. 34b MOMENT–STEEL STRAIN PLOT, TENSION SIDE OF SPECIMEN B10

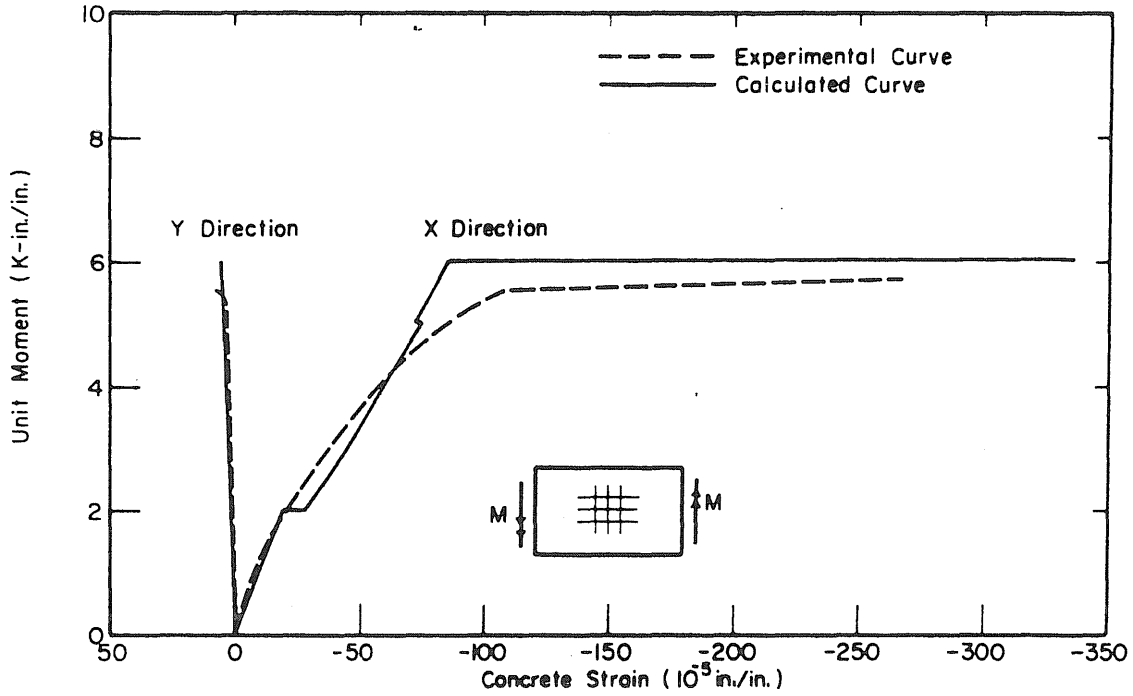

FIG. 34c MOMENT-CONCRETE STRAIN PLOT, COMPRESSION SIDE OF SPECIMEN B10

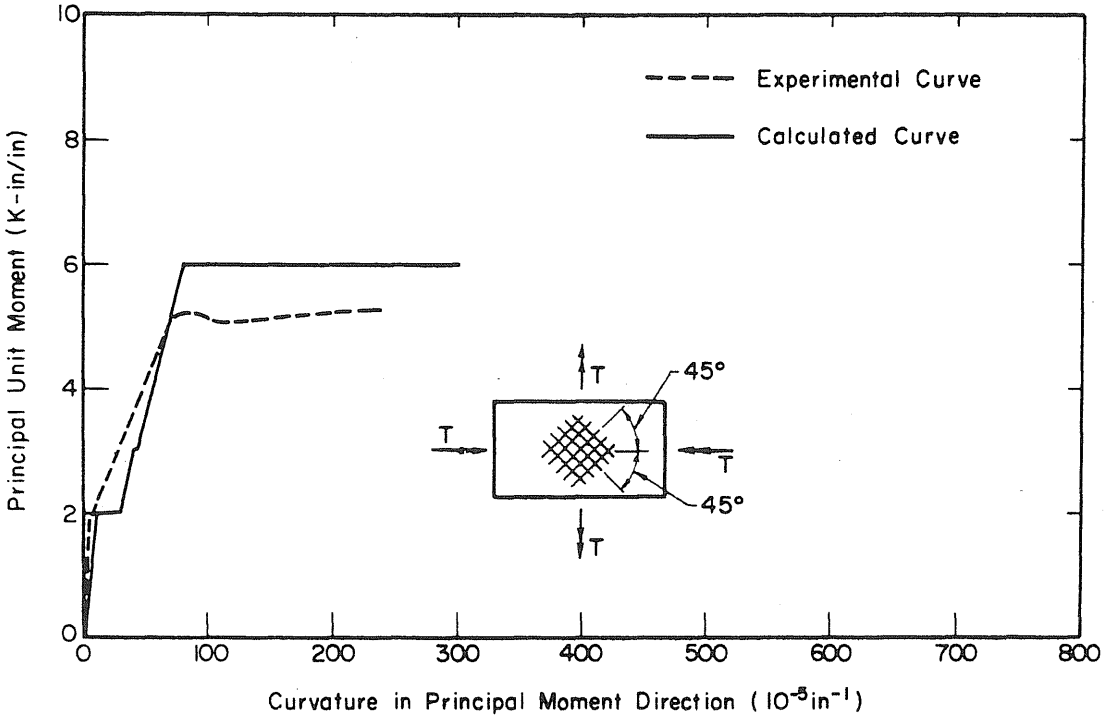

FIG. 35a MOMENT–CURVATURE PLOT, SPECIMEN B15

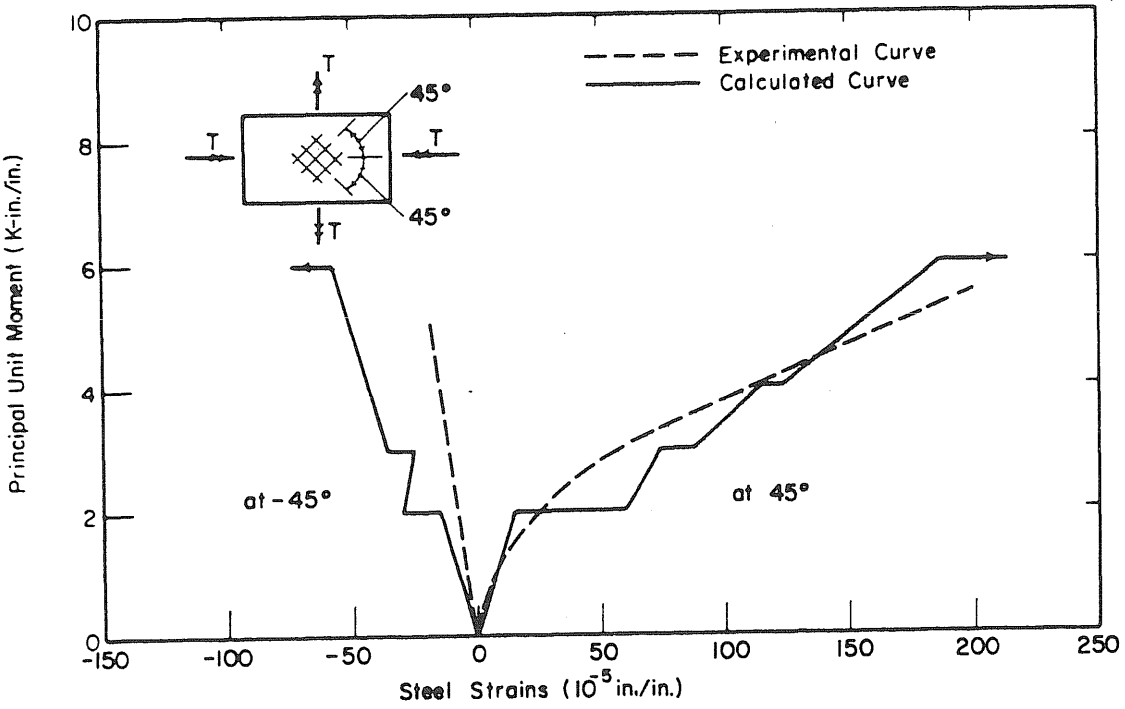

FIG. 35b MOMENT–STEEL STRAIN PLOT, SPECIMEN B15

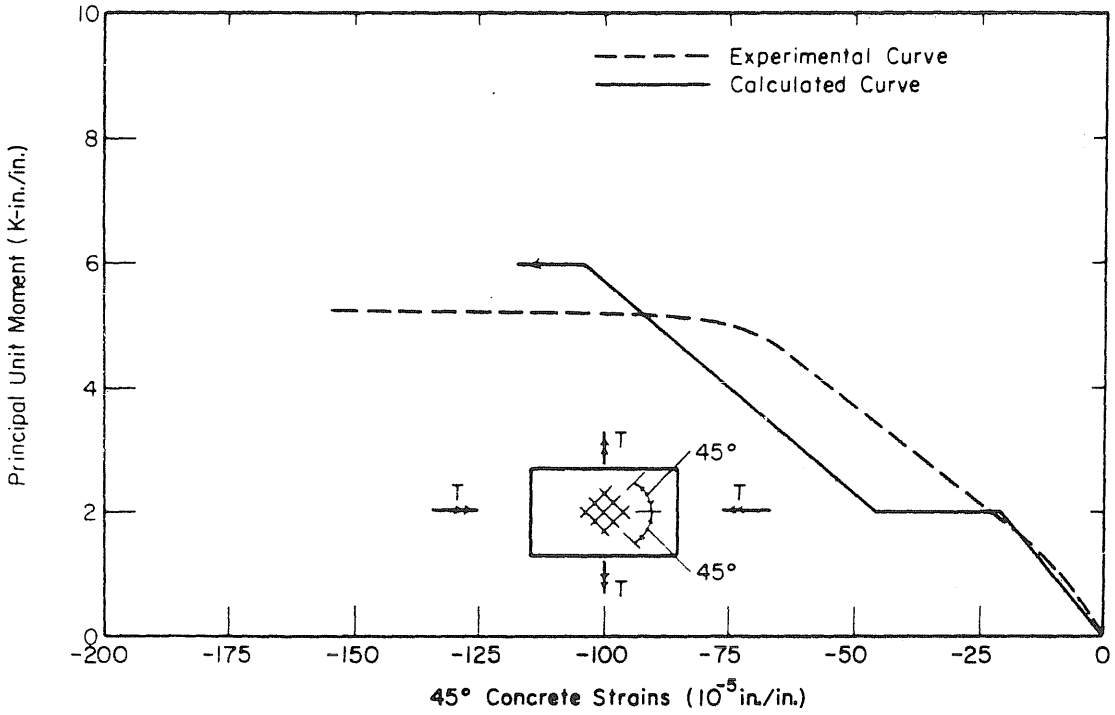

FIG. 35c MOMENT-CONCRETE STRAIN PLOT, BOTTOM SIDE OF SPECIMEN B15

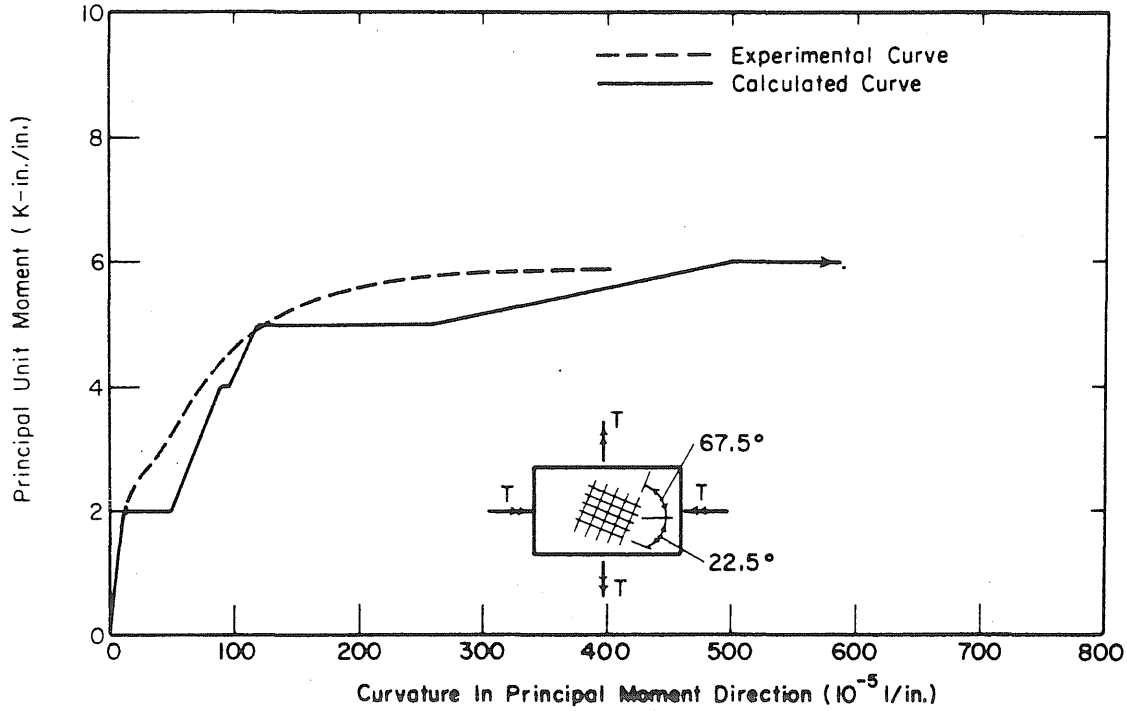

FIG. 36a MOMENT-CURVATURE PLOT, SPECIMEN B17

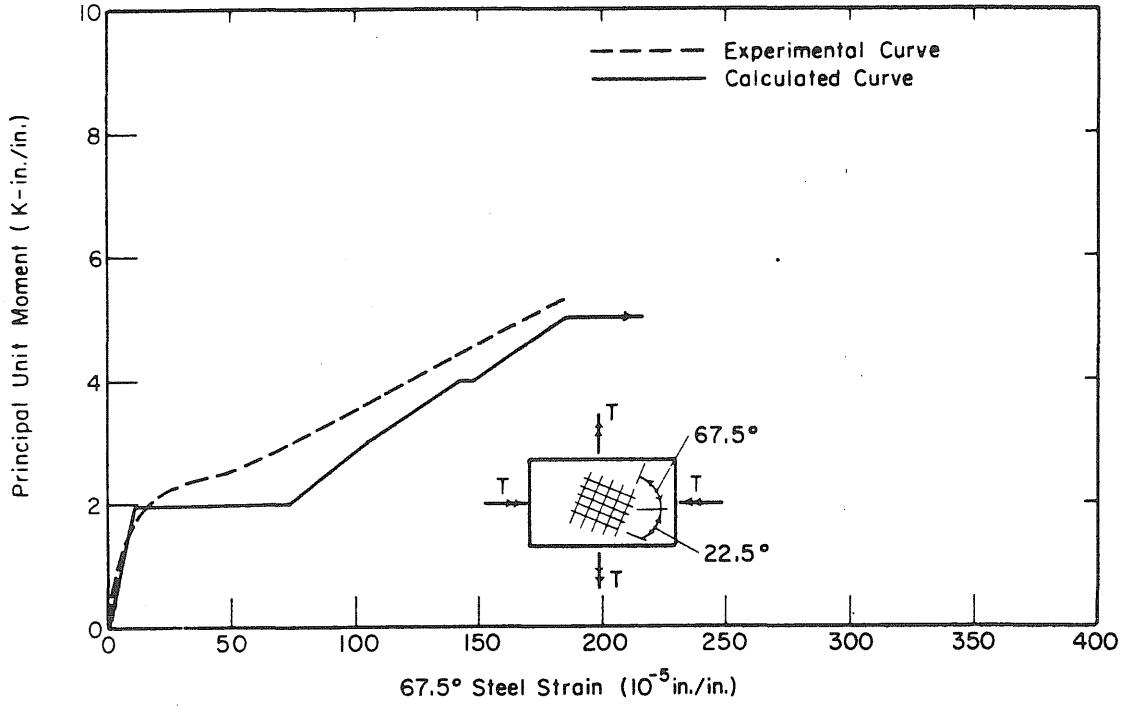

FIG. 36b MOMENT-STEEL STRAIN PLOT, TOP SIDE OF SPECIMEN B17

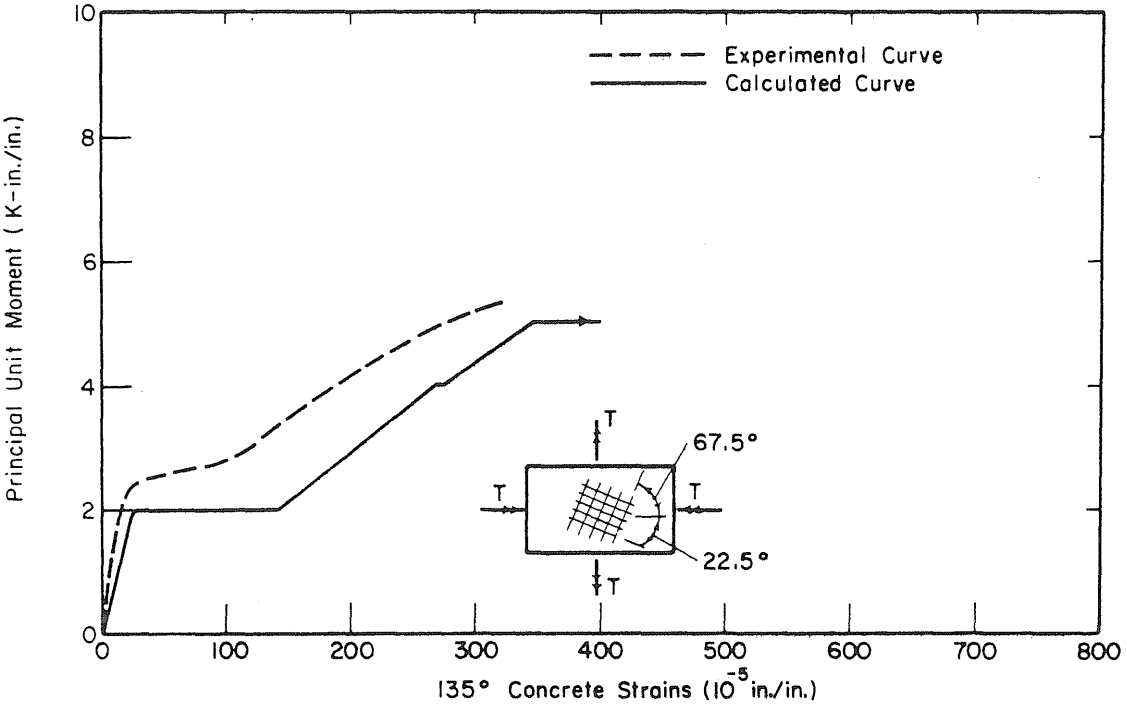

FIG. 36c MOMENT-CONCRETE STRAIN PLOT, BOTTOM SIDE OF SPECIMEN B17

Main Reference Room
Civil Engineering Department
B106 C. E. Building
University of Illinois
Urbana, Illinois 61801

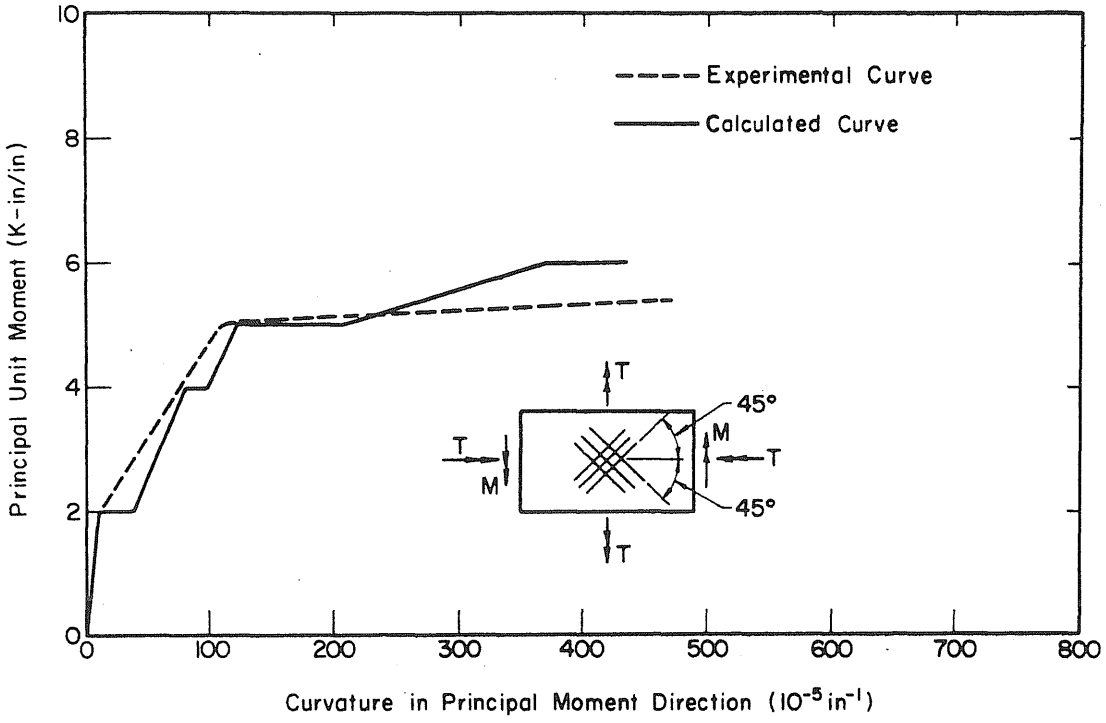

FIG. 37a MOMENT – CURVATURE PLOT, SPECIMEN B27A

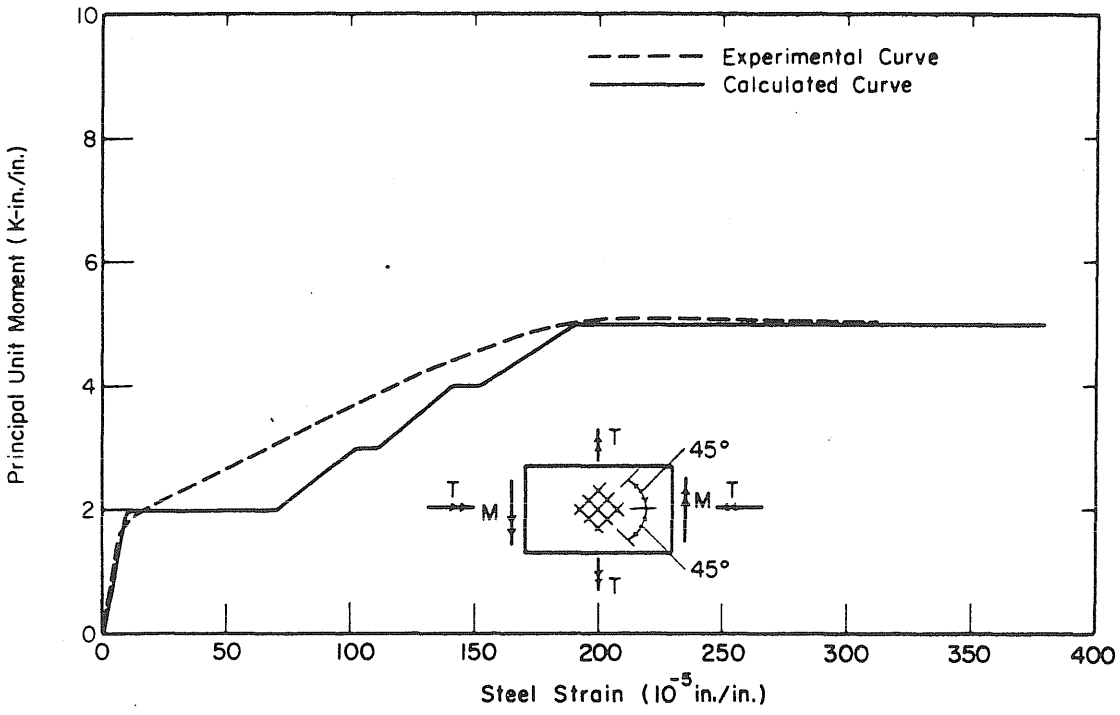

FIG. 37b MOMENT-STEEL STRAIN PLOT, TOP SIDE OF SPECIMEN B27A, 45 DEGREES

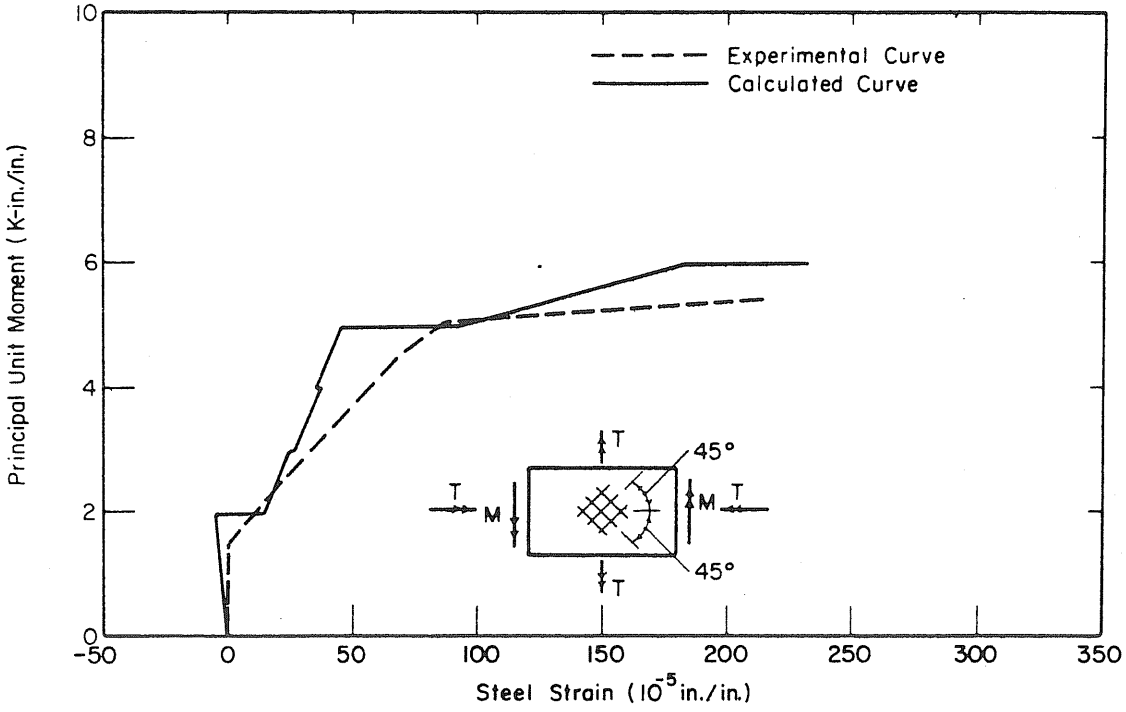

FIG. 37c MOMENT–STEEL STRAIN PLOT, TOP SIDE OF SPECIMEN B27A, 135 DEGREES

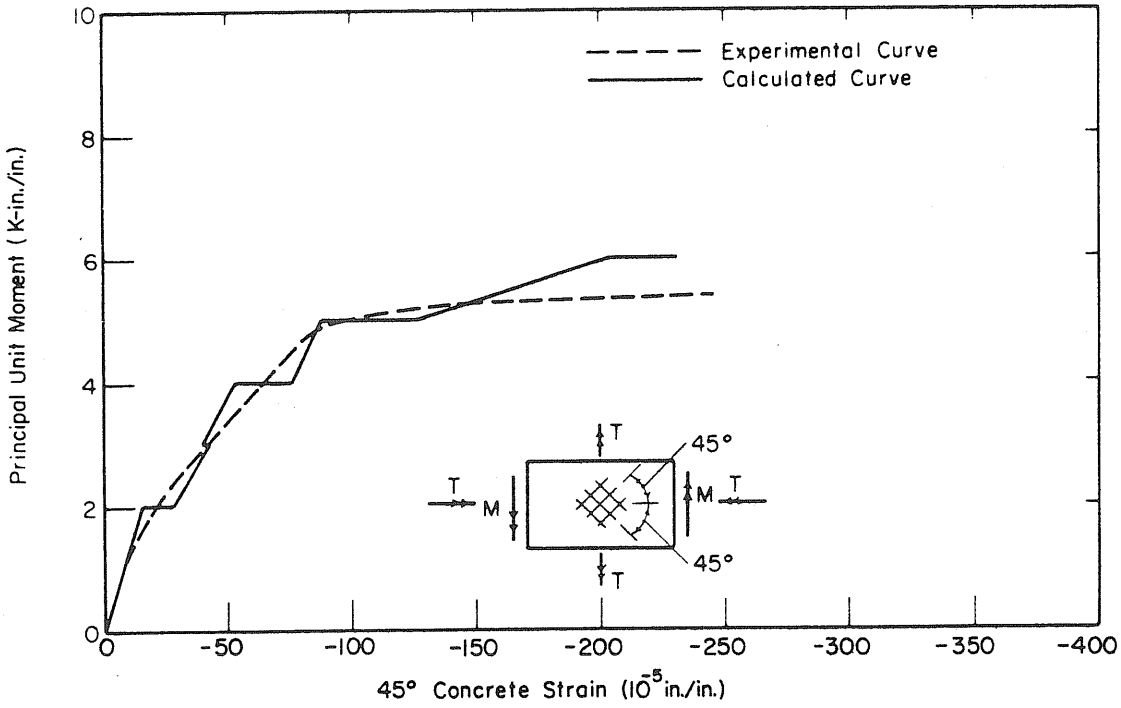

FIG. 37d MOMENT–CONCRETE STRAIN PLOT, BOTTOM SIDE OF SPECIMEN B27A

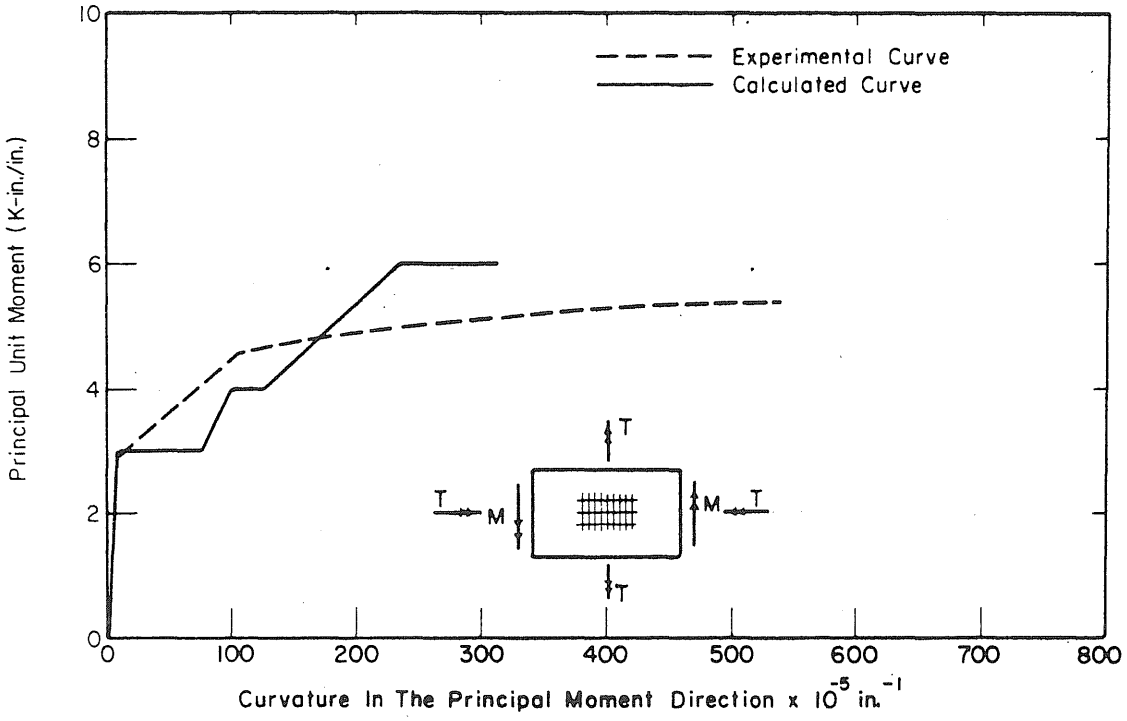

FIG. 38a MOMENT – CURVATURE PLOT, SPECIMEN B39

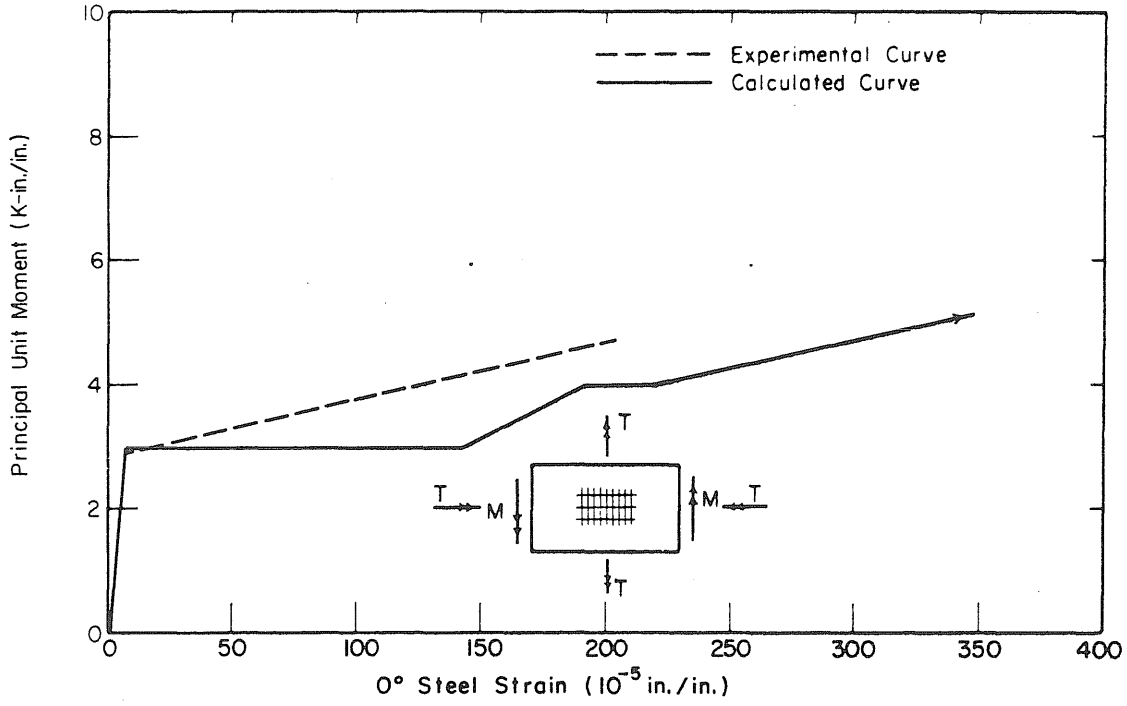

FIG. 38b MOMENT–STEEL STRAIN PLOT, TOP SIDE OF SPECIMEN B39, 0 DEGREES

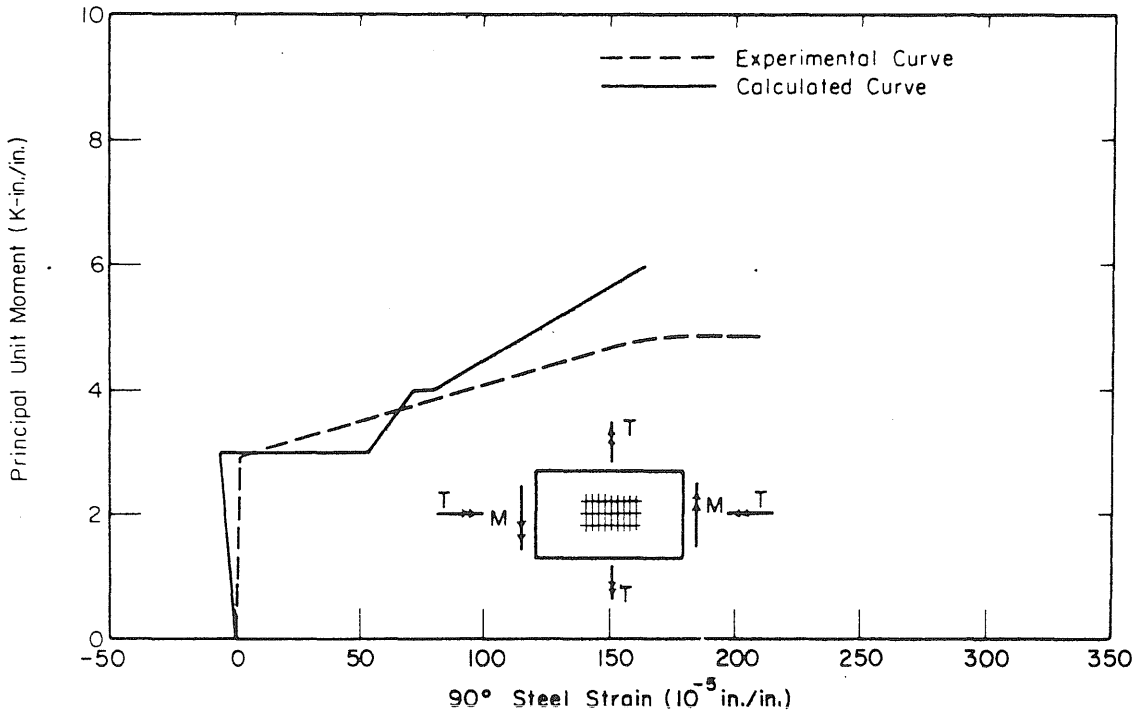

FIG. 38c MOMENT-STEEL STRAIN PLOT, TOP SIDE OF SPECIMEN B39, 90 DEGREES

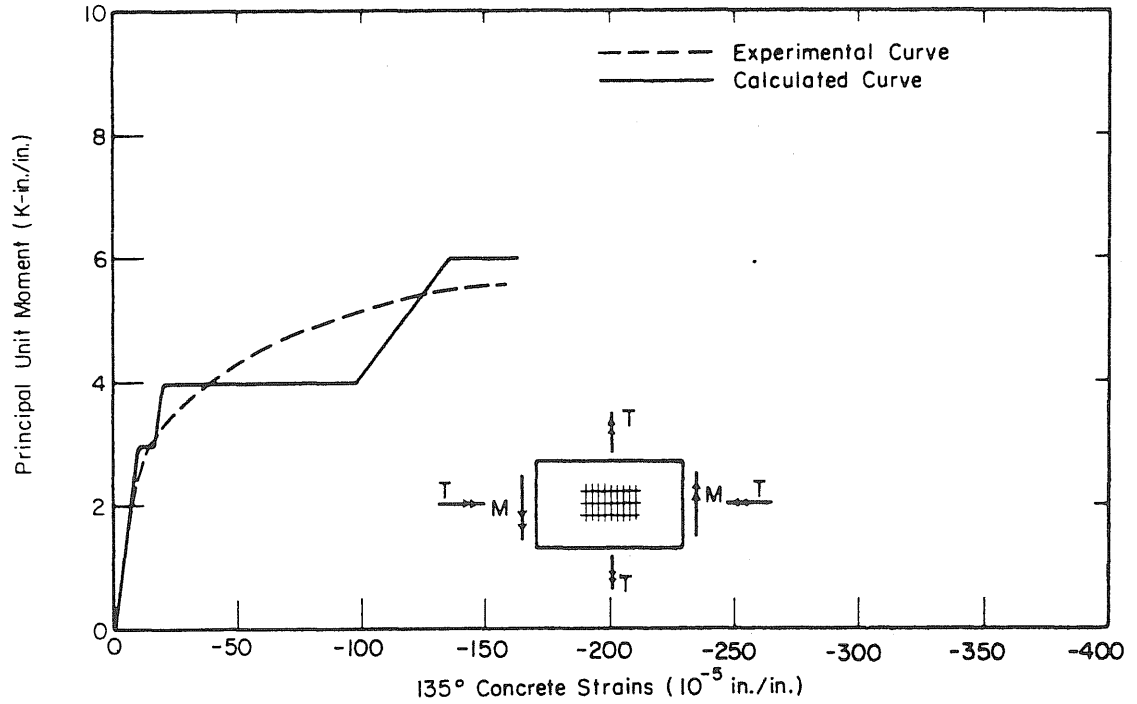

FIG. 38d MOMENT-CONCRETE STRAIN PLOT, BOTTOM SIDE OF SPECIMEN B39

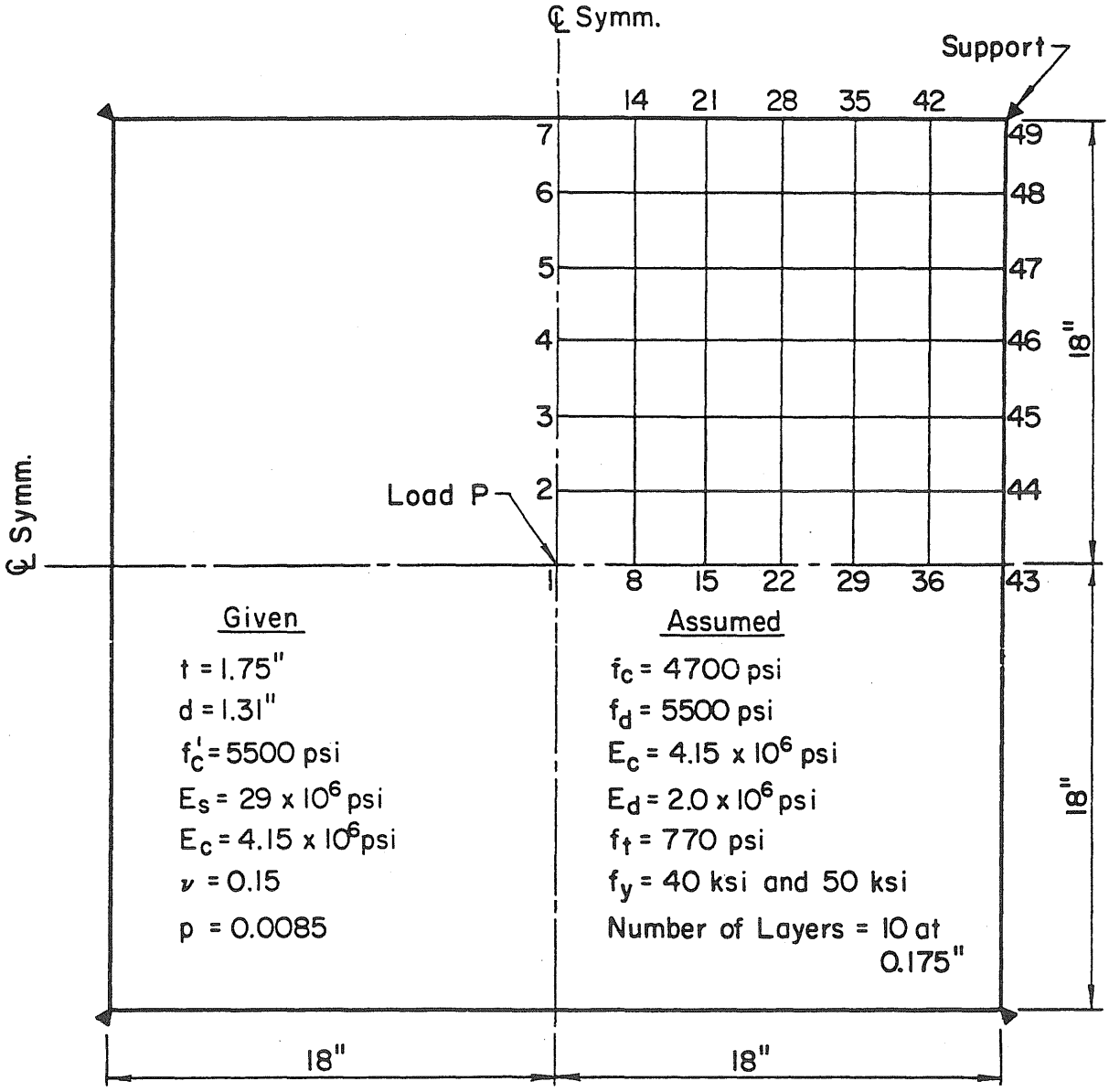

FIG. 39 CORNER SUPPORTED TWO-WAY SLAB OF MCNEICE

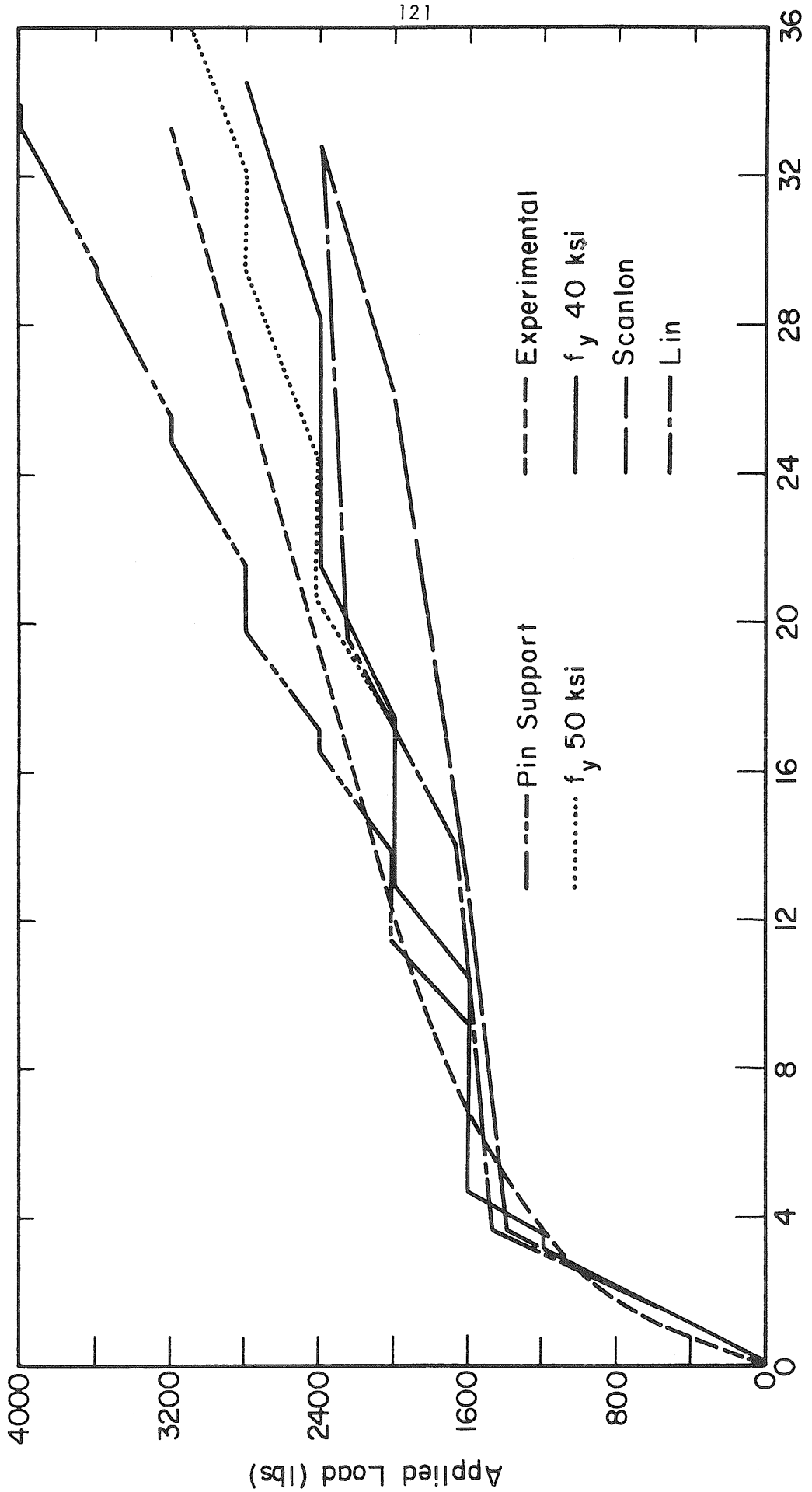

FIG. 40 LOAD-DEFLECTION CURVES AT NODE 2 OF McNEICE'S SLAB

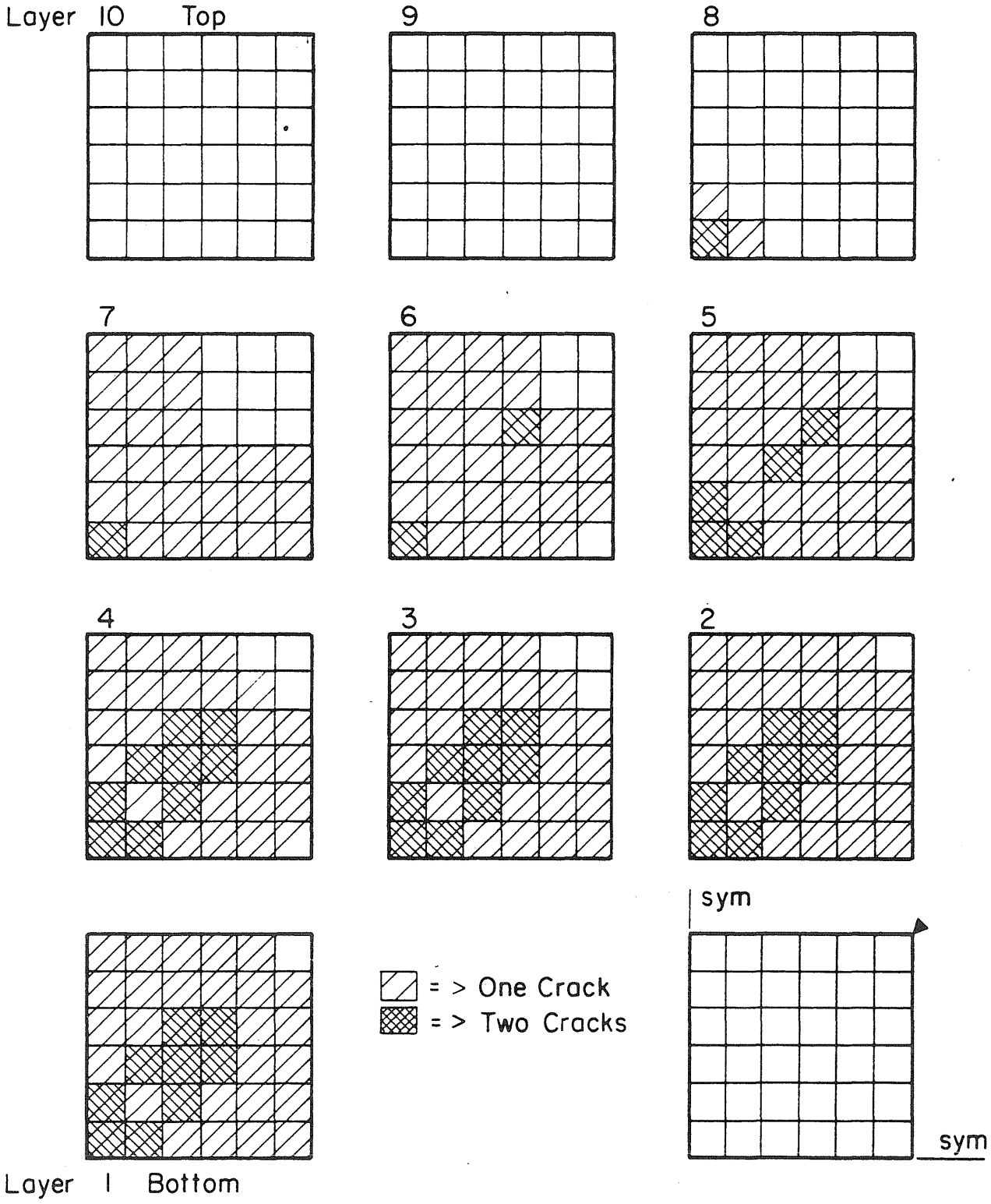

FIG. 41 CRACK CONFIGURATION FOR MCNEICE'S SLAB AT EQUILIBRIUM WITH LOAD OF 2800 POUNDS, ROLLER SUPPORT

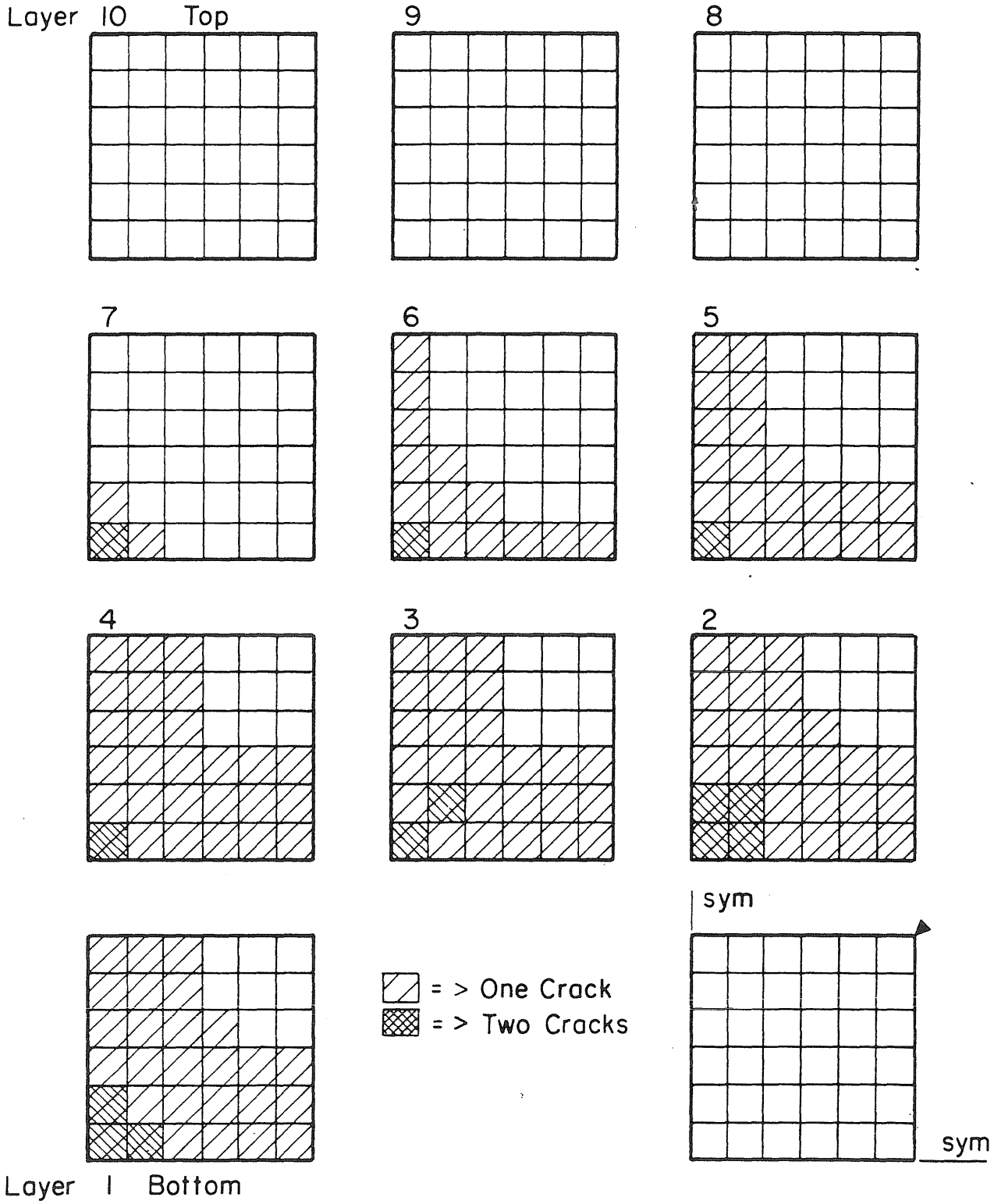

FIG. 42 CRACK CONFIGURATION FOR MCNEICE'S SLAB AT EQUILIBRIUM WITH LOAD OF 2800 POUNDS, PIN SUPPORT

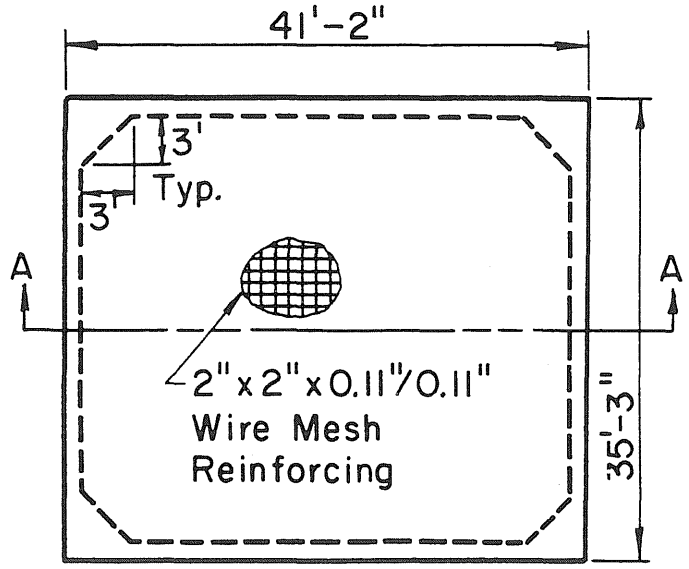

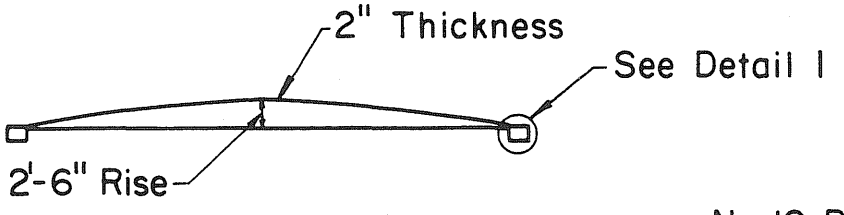

Section A-A

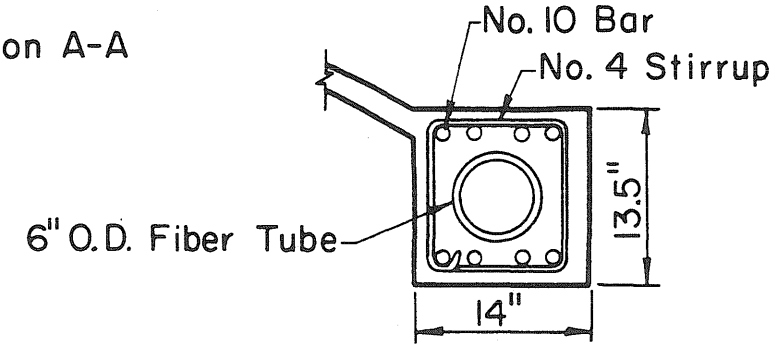

Detail 1

FIG. 43 DIMENSIONS OF SHELL AND EDGE BEAMS

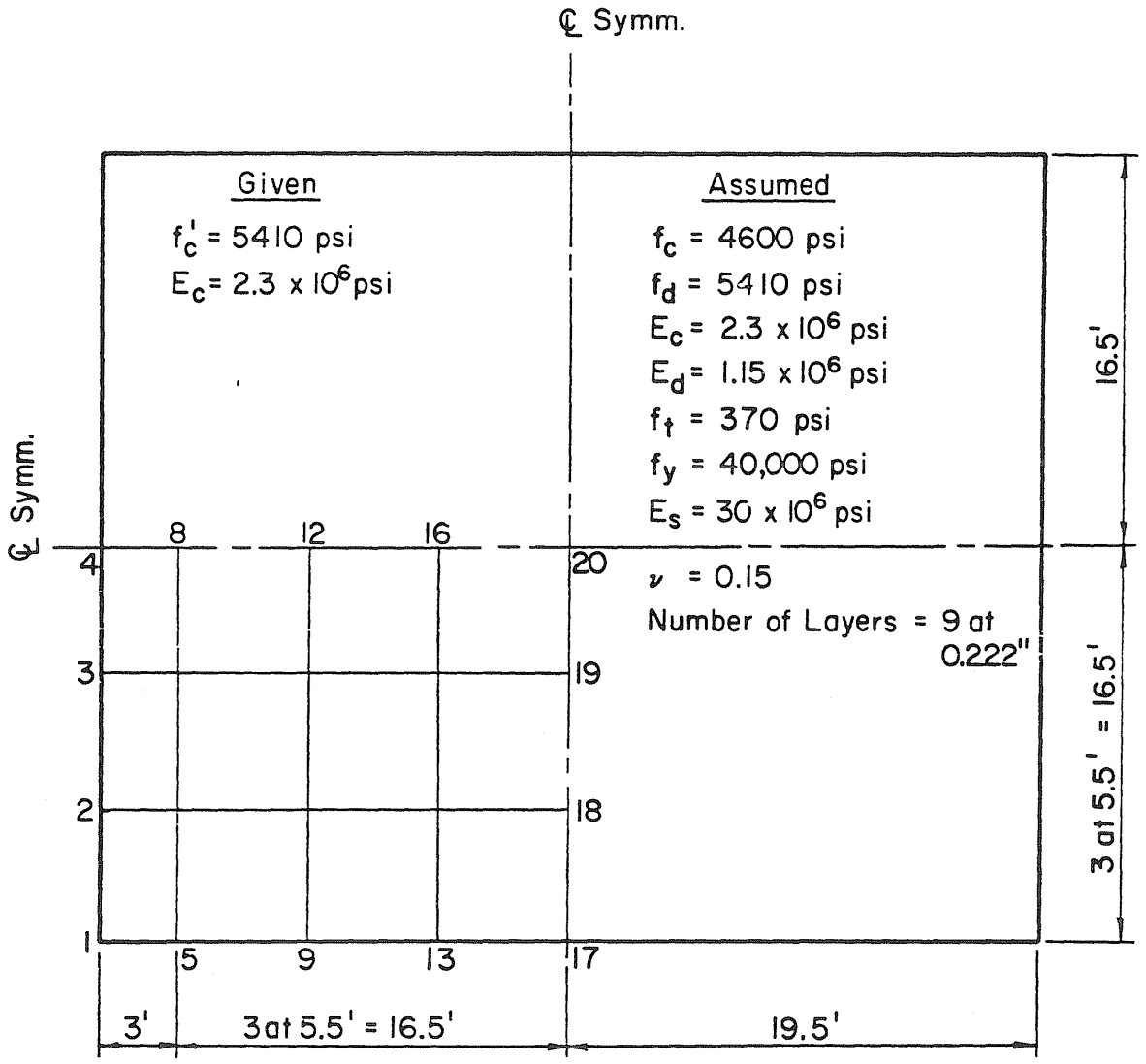

FIG. 44 ELEMENT GRID FOR ODELLO AND ALLGOOD'S SHELL

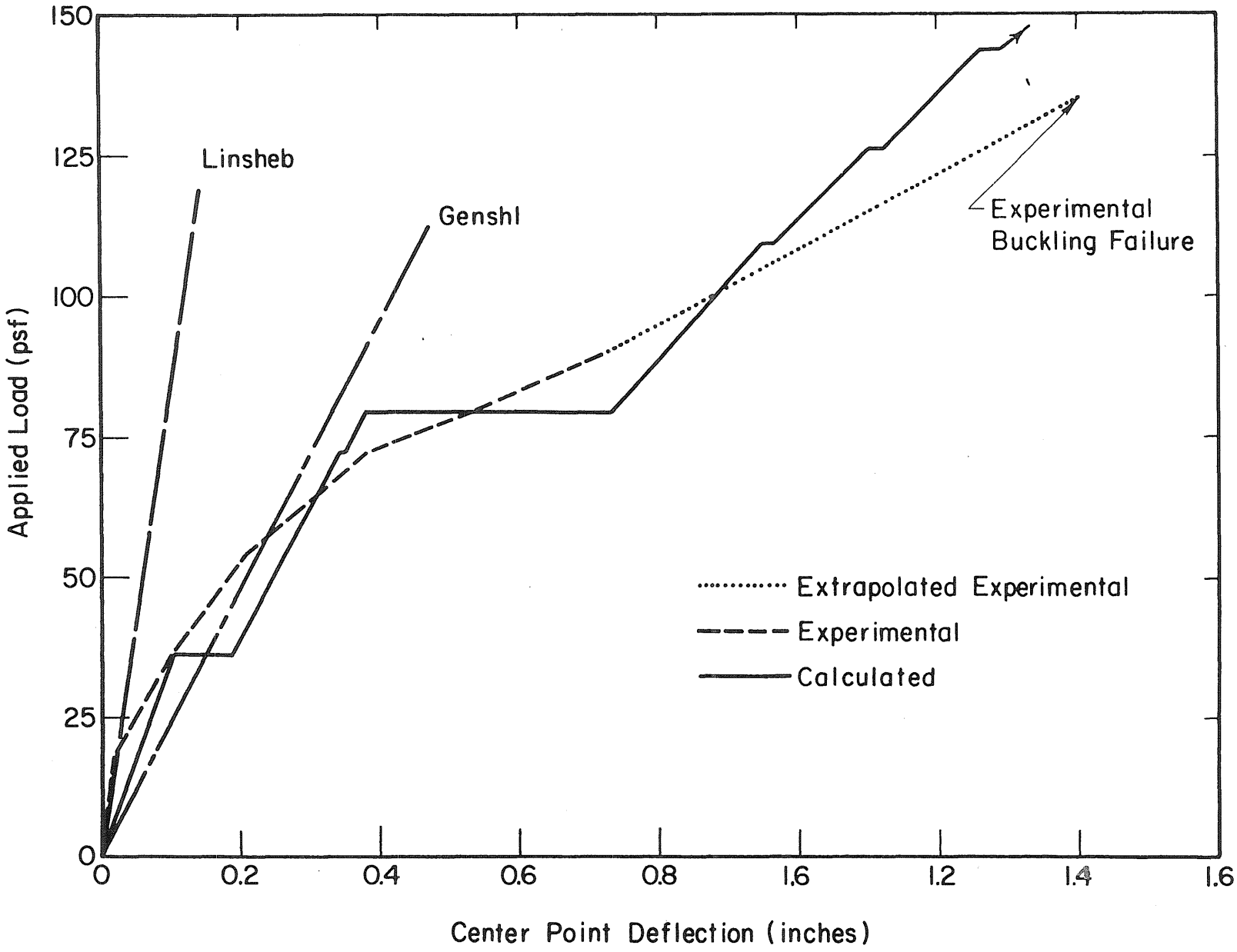

FIG. 45 LOAD-DEFLECTION CURVES FOR CENTER NODE OF SHELL

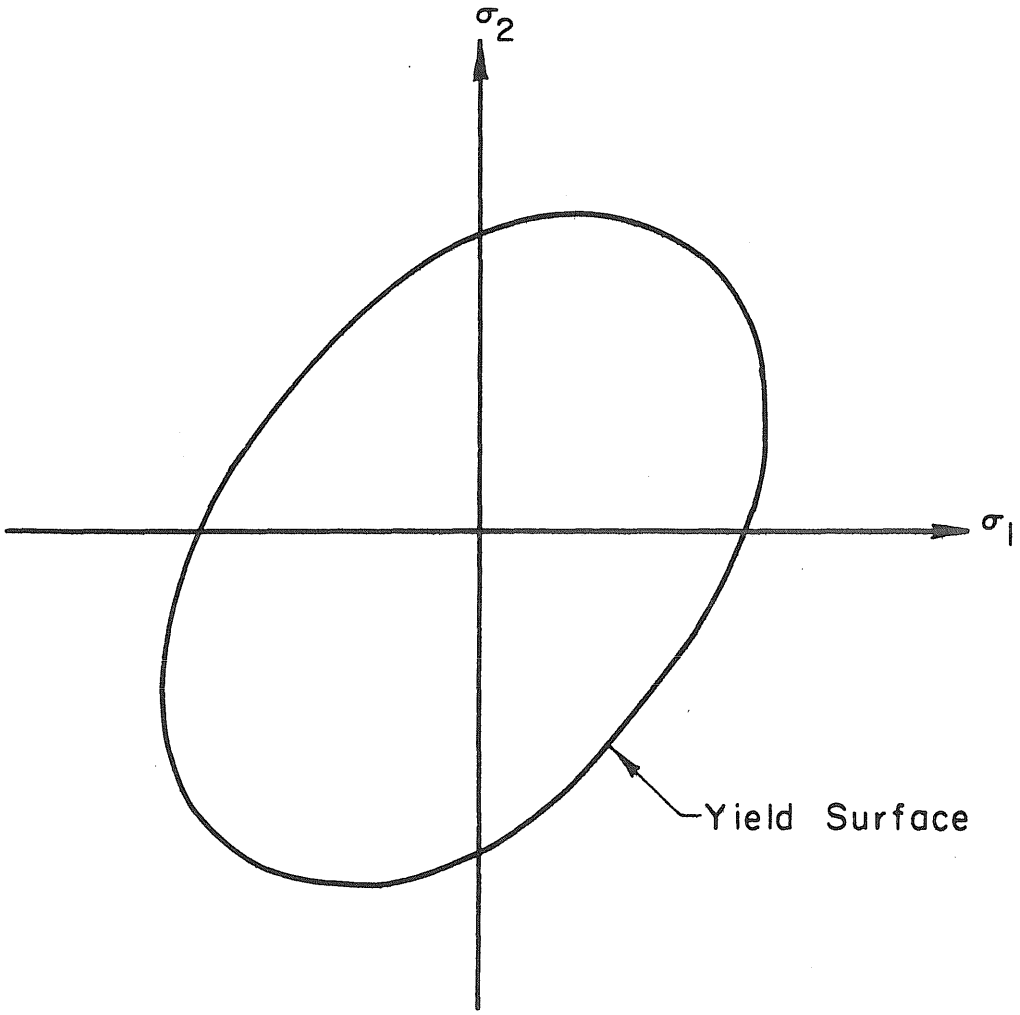

FIG. 46 HYPOTHETICAL YIELD SURFACE

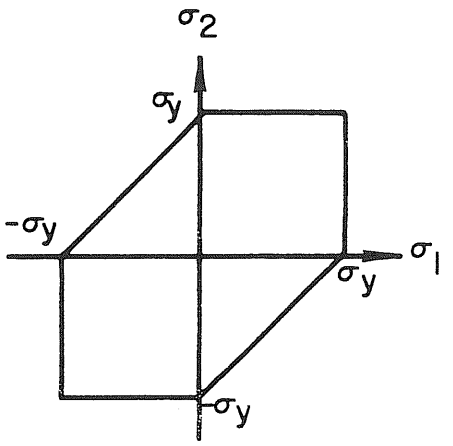

Tresca
(Ductile-Steel)

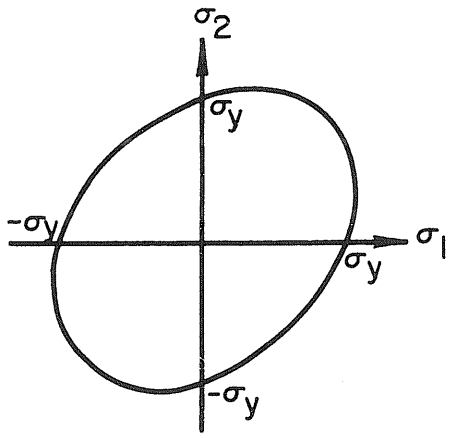

Von Mises
(Ductile-Steel)

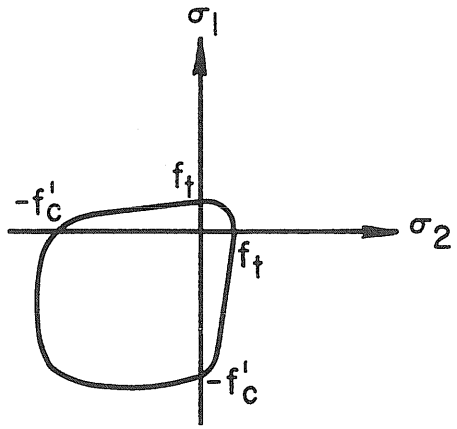

Kupfer, Hilsdorf,
and Rüsch
(Brittle-Concrete)

FIG. 47 SOME COMMON YIELD SURFACES

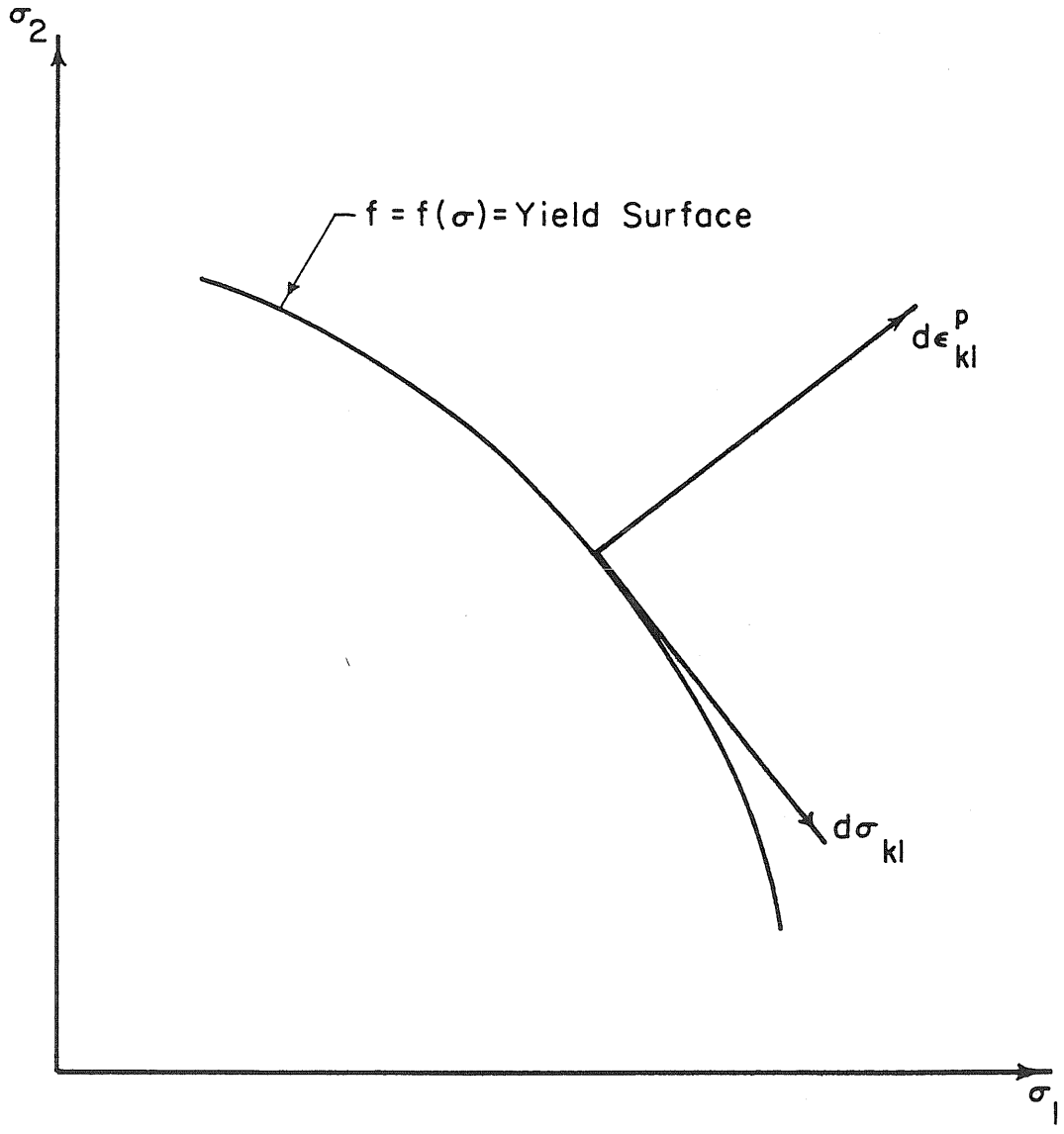

FIG. 48 DIAGRAMMATIC REPRESENTATION OF THE NORMALITY LAW IN PLASTICITY

APPENDIX C

PLASTIC INCREMENTAL STRESS-STRAIN RELATIONS

C.1 General Considerations

The total strain experienced by a plastic body is the sum of the elastic (ε^e) and plastic (ε^p) strains. That is,

$$\varepsilon = \varepsilon^e + \varepsilon^p$$

or in terms of incremental strains,

$$d\varepsilon = d\varepsilon^e + d\varepsilon^p$$

For an elastic material the total stresses and total strains are related by Hooke's Law. When expressed in tensor notation this is

$$\sigma_{ij} = C_{ijkl}\,\varepsilon_{kl} \qquad i, j, k, l = 1, 2, 3 \text{ (sum)}$$

or for incremental values,

$$d\sigma_{ij} = C_{ijkl}\,d\varepsilon_{kl} \qquad i, j, k, l = 1, 2, 3 \text{ (sum)}$$

However, for plastic materials total stresses and total strains cannot be related, but incremental stresses and strains may be related by an expression such as

$$d\sigma_{ij} = A_{ijkl}\,d\varepsilon_{kl} \qquad i, j, k, l = 1, 2, 3 \text{ (sum)}$$

Thus, the desired plastic incremental stress-strain relations are the A_{ijkl}'s.

C.1.1 Yield Surface

The yield surface for an elastic-perfectly plastic material is simplily the extreme locus of all elastic stress configurations. Diagrammatically this is shown in Fig. 46 where all points inside the yield surface represent stable elastic stress states, while all points on the yield surface represent unstable plastic stress states where the material deforms plastically. Stress states outside the yield surface are not possible because the structure would deform plastically to keep the stress state on the yield surface or, if unable to do this, the structure would rupture or collapse. Figure 47 shows some common yield surfaces for the purpose of comparison. Tresca's yield criterion assumes when the maximum shear stress reaches a definite value plastic flow starts. With Von Mises's yield criterion yielding occurs when the stored shear strain energy reaches a critical value.

C.1.2 Flow Rule and Normality Law

The flow rule in plasticity is

$$d\varepsilon^{p}_{kl} = \lambda \frac{\partial f}{\partial \sigma_{kl}}$$

where

$d\varepsilon^{p}_{kl}$ = the plastic strain increment,

λ = a positive constant,

f = an expression representing the yield surface in the form $f = f(\sigma)$.

The normality law in plasticity is,

$$d\varepsilon^{p}_{kl}\ d\sigma_{kl} = 0$$

This implies that the direction of the strain increment vector is orthogonal to the stress increment vector. Diagrammatically this is represented in Fig. 48. Note that the strain increment is normal to the yield surface and the stress increment is tangent to the yield surface.

C.1.3 Hooke's Generalized Law

In terms of double subscript tensor notation for the stress, σ_{ij}, and strain, ε_{ij}, components, Hooke's generalized law has the following form relative to axes X_1, X_2, X_3

$$\sigma_{ij} = C_{ijkl}\ \varepsilon_{kl} \qquad i, j, k, l = 1, 2, 3 \text{ (sum)}$$

For an elastic isotropic material, Hooke's law becomes in matrix form

$$\begin{Bmatrix} \sigma_{11} \\ \sigma_{22} \\ \sigma_{33} \\ \sigma_{12} \\ \sigma_{13} \\ \sigma_{23} \end{Bmatrix} = \begin{bmatrix} C_{1111} & C_{1122} & C_{1133} & 0 & 0 & 0 \\ C_{2211} & C_{2222} & C_{2233} & 0 & 0 & 0 \\ C_{3311} & C_{3322} & C_{3333} & 0 & 0 & 0 \\ 0 & 0 & 0 & C_{1212} & 0 & 0 \\ 0 & 0 & 0 & 0 & C_{1313} & 0 \\ 0 & 0 & 0 & 0 & 0 & C_{2323} \end{bmatrix} \begin{Bmatrix} \varepsilon_{11} \\ \varepsilon_{22} \\ \varepsilon_{33} \\ 2\varepsilon_{12} \\ 2\varepsilon_{13} \\ 2\varepsilon_{23} \end{Bmatrix} \tag{C.1}$$

where

$$2\varepsilon_{ij} = \gamma_{ij} \qquad i \neq j;\ i, j, k, l = 1, 2, 3$$

If the material is linearly elastic also, Eq. C.1 reduces to

$$\begin{Bmatrix} \sigma_{11} \\ \sigma_{22} \\ \sigma_{33} \\ \sigma_{12} \\ \sigma_{13} \\ \sigma_{23} \end{Bmatrix} = \frac{E}{(1+\nu)(1-2\nu)} \begin{bmatrix} 1-\nu & \nu & \nu & 0 & 0 & 0 \\ \nu & 1-\nu & \nu & 0 & 0 & 0 \\ \nu & \nu & 1-\nu & 0 & 0 & 0 \\ 0 & 0 & 0 & 1-2\nu & 0 & 0 \\ 0 & 0 & 0 & 0 & 1-2\nu & 0 \\ 0 & 0 & 0 & 0 & 0 & 1-2\nu \end{bmatrix} \begin{Bmatrix} \varepsilon_{11} \\ \varepsilon_{22} \\ \varepsilon_{33} \\ 2\varepsilon_{12} \\ 2\varepsilon_{13} \\ 2\varepsilon_{23} \end{Bmatrix} \tag{C.2}$$

Expressing Eq. C.2 in index notation

$$\sigma_{ij} = \frac{E}{(1+\nu)(1-2\nu)} \left[\frac{1}{2}(1-2\nu)\delta_{ik}\,\delta_{jl} + \frac{1}{2}(1-2\nu)\,\delta_{il}\,\delta_{jk} + \nu\,\delta_{ij}\,\delta_{kl}\right] \varepsilon_{kl} \qquad i, j, k, l = 1, 2, 3 \text{ (sum)} \tag{C.3}$$

where δ_{ij} is the Kronecker delta. Introducing

$$G = \frac{E}{2(1+\nu)}$$

Eq. C.3 becomes

$$\sigma_{ij} = G\left[\delta_{ik}\,\delta_{jl} + \delta_{il}\,\delta_{jk} + \frac{2\nu}{1-2\nu}\,\delta_{ij}\,\delta_{kl}\right] \varepsilon_{kl}$$

$$i, j, k, l = 1, 2, 3 \text{ (sum)}$$

Therefore,

$$C_{ijkl} = G\left[\delta_{ik}\,\delta_{jl} + \delta_{il}\,\delta_{jk} + \frac{2\nu}{1-2\nu}\,\delta_{ij}\,\delta_{kl}\right]$$

$$i, j, k, l = 1, 2, 3 \text{ (sum)} \tag{C.4}$$

Note that, the $\delta_{ik}\,\delta_{jl}$ terms are only the main diagonal terms and would be sufficient alone except indexing causes

$$\sigma_{ij} = C_{ijij}\,\varepsilon_{ij} + C_{ijji}\,\varepsilon_{ji} \qquad i \neq j;\ i, j = 1, 2, 3$$

Knowing that

$$\varepsilon_{ij} = \varepsilon_{ji}$$

and because of the isotropity of the material that

$$C_{ijij} = C_{ijji}$$

then

$$\sigma_{ij} = 2C_{ijij}\,\varepsilon_{ij}$$

This is the reason for the $\delta_{il}\,\delta_{jk}$ term, for it picks up the ε_{ji} terms and adds them to the ε_{ij} terms.

C.2 Derivation for Incremental Stress-Strain Relations

C.2.1 Three-Dimensional Relations

Let the total strain be represented as the sum of the elastic and plastic parts

$$\varepsilon = \varepsilon^e + \varepsilon^p$$

or in terms of incremental values

$$d\varepsilon = d\varepsilon^e + d\varepsilon^p \qquad (C.5)$$

For elastic material from Hooke's law

$$\sigma_{ij} = C_{ijkl}\,\varepsilon_{kl}$$

or in terms of incremental values

$$d\sigma_{ij} = C_{ijkl}\, d\varepsilon^{e}_{kl} \tag{C.6}$$

Now, substitution of Eq. C.5 in Eq. C.6 yields

$$d\sigma_{ij} = C_{ijkl}\, (d\varepsilon_{kl} - d\varepsilon^{p}_{kl}) \tag{C.7}$$

The flow rule states

$$d\varepsilon^{p}_{kl} = \lambda \frac{\partial f}{\partial \sigma_{kl}} \tag{C.8}$$

which when substituted in Eq. C.7 yields

$$d\sigma_{ij} = C_{ijkl}\, (d\varepsilon_{kl} - \lambda \frac{\partial f}{\partial \sigma_{kl}}) \tag{C.9}$$

Recalling the normality law

$$d\varepsilon^{p}_{ij}\, d\sigma_{ij} = 0$$

or using Eq. C.8

$$\lambda \frac{\partial f}{\partial \sigma_{ij}} \quad (d\sigma_{ij}) = 0 \tag{C.10}$$

Premultiplying Eq. C.9 by $\lambda \frac{\partial f}{\partial \sigma_{ij}}$ yields

$$\lambda \frac{\partial f}{\partial \sigma_{ij}}\, d\sigma_{ij} = C_{ijkl}\, \lambda \frac{\partial f}{\partial \sigma_{ij}}\, (d\varepsilon_{kl} - \lambda \frac{\partial f}{\partial \sigma_{kl}}) \tag{C.11}$$

Using Eq. C.10, Eq. C.11 becomes

$$C_{ijkl} \frac{\partial f}{\partial \sigma_{ij}}\, d\varepsilon_{kl} - C_{ijkl}\, \lambda \frac{\partial f}{\partial \sigma_{ij}} \frac{\partial f}{\partial \sigma_{kl}} = 0$$

Changing the indexes in the second term to pqrs

$$C_{ijkl} \frac{\partial f}{\partial \sigma_{ij}}\, d\varepsilon_{kl} - C_{pqrs}\, \lambda \frac{\partial f}{\partial \sigma_{pq}} \frac{\partial f}{\partial \sigma_{rs}} = 0$$

and solving for λ yields

$$\lambda = \frac{C_{ijkl} \frac{\partial f}{\partial \sigma_{ij}} d\varepsilon_{kl}}{C_{pqrs} \frac{\partial f}{\partial \sigma_{pq}} \frac{\partial f}{\partial \sigma_{rs}}}$$

Substituting for λ in Eq. C.9 yields

$$d\sigma_{ij} = C_{ijkl} \left[d\varepsilon_{kl} - \frac{C_{ijkl} \frac{\partial f}{\partial \sigma_{ij}} d\varepsilon_{kl}}{C_{pqrs} \frac{\partial f}{\partial \sigma_{pq}} \frac{\partial f}{\partial \sigma_{rs}}} \frac{\partial f}{\partial \sigma_{kl}} \right]$$

and changing some more indexes,

$$d\sigma_{ij} = \left[C_{ijkl} - \frac{C_{ijrs} \frac{\partial f}{\partial \sigma_{rs}} C_{pqkl} \frac{\partial f}{\partial \sigma_{pq}}}{C_{pqrs} \frac{\partial f}{\partial \sigma_{pq}} \frac{\partial f}{\partial \sigma_{rs}}} \right] d\varepsilon_{kl}$$

$$i, j, k, l, p, q, r, s = 1, 2, 3 \text{ (sum)}$$

Thus the desired three-dimensional plastic incremental stress-strain relations are

$$A_{ijkl} = C_{ijkl} - \frac{C_{ijrs} \frac{\partial f}{\partial \sigma_{rs}} C_{pqkl} \frac{\partial f}{\partial \sigma_{pq}}}{C_{pqrs} \frac{\partial f}{\partial \sigma_{pq}} \cdot \frac{\partial f}{\partial \sigma_{rs}}}$$

$$i, j, k, l, p, q, r, s = 1, 2, 3 \text{ (sum)}$$

C.2.2 Reduction to Two-Dimensional Relations

The three-dimensional relations are

$$d\sigma_{ij} = A_{ijkl} \, d\varepsilon_{kl}$$

The two-dimensional relations for plane stress may be obtained by specifying

$$\sigma_{33} = \sigma_{13} = \sigma_{23} = 0$$

This is

$$\sigma_{33} = A_{33kl}\,\varepsilon_{kl} = 0$$

$$\sigma_{13} = A_{13kl}\,\varepsilon_{kl} = 0 \qquad k, l = 1, 2, 3 \text{ (sum)}$$

$$\sigma_{23} = A_{23kl}\,\varepsilon_{kl} = 0$$

which implies, respectively,

$$A_{33pq}\,\varepsilon_{pq} + A_{3333}\,\varepsilon_{33} = 0 \qquad p, q = 1, 2 \text{ (sum)}$$

$$\varepsilon_{13} = 0$$

$$\varepsilon_{23} = 0$$

Thus, also

$$\varepsilon_{33} = -\frac{A_{33pq}\,\varepsilon_{pq}}{A_{3333}}$$

Then, it follows that

$$B_{pqrs} = A_{pqrs} - \frac{A_{pq33}\,A_{33rs}}{A_{3333}} \qquad p, q, r, s = 1, 2 \text{ (sum)}$$

are the desired two-dimensional plastic incremental stress-strain relations. These relations are of the form

$$\sigma_{pq} = B_{pqrs}\,\varepsilon_{rs} \qquad p, q, r, s = 1, 2 \text{ (sum)}$$

Expanding the expression for σ_{11} yields

$$\sigma_{11} = B_{1111}\,\varepsilon_{11} + B_{1122}\,\varepsilon_{22} + B_{1112}\,\varepsilon_{12} + B_{1121}\,\varepsilon_{21}$$

Due to the symmetrical way the A_{ijkl}'s were obtained and reduced, then the B_{pqrs}'s are symmetric. Thus

$$B_{1112} = B_{1121}$$

Also, the strain tensor is symmetrical, hence

$$\varepsilon_{12} = \varepsilon_{21}$$

Then σ_{11} may be expressed as,

$$\sigma_{11} = B_{1111}\,\varepsilon_{11} + B_{1122}\,\varepsilon_{22} + 2B_{1112}\,\varepsilon_{12}$$

or

$$\sigma_{11} = B_{1111}\,\varepsilon_{11} + B_{1122}\,\varepsilon_{22} + B_{1112}\,\gamma_{12}$$

where

$$2\varepsilon_{12} = \gamma_{12}$$

Since this procedure could be repeated for σ_{22} and σ_{12}, then the B_{pqrs}'s are exactly the C_{ij}'s where

$$\begin{Bmatrix} \sigma_x \\ \sigma_y \\ \tau_{xy} \end{Bmatrix} = [C]_{3x3} \begin{Bmatrix} \varepsilon_x \\ \varepsilon_y \\ \gamma_{xy} \end{Bmatrix}$$

where x corresponds to 1, y to 2, and xy to 12. Thus, the B_{pqrs}'s are directly compatible with the strain vector, $\{\varepsilon\}$.

C.2.3 Evaluation of the Three-Dimensional Relations

The yield criterion proposed by Kupfer, Hilsdorf, and Rüsch is of the form

$$\tau_{oct} + bp - a = f(\sigma_{ij}) - a = o$$

where

$$\tau_{oct} = \left(\frac{1}{3}\sigma_{ij}\,\sigma_{ij} - p^2\right)^{1/2} \qquad i, j = 1, 2, 3 \text{ (sum)}$$

and

$$p = \frac{1}{3}\sigma_{kk} \qquad k = 1, 2, 3 \text{ (sum)}$$

Thus

$$\frac{\partial f}{\partial \sigma_{ij}} = \sigma_{ij} + (b\tau - p)\delta_{ij} \qquad i, j = 1, 2, 3$$

where

$$\tau = \tau_{oct}$$

From before, Eq. C.4,

$$C_{ijkl} = G\left[\delta_{ik}\,\delta_{jk} + \delta_{il}\,\delta_{jk} + \frac{2\nu}{1 - 2\nu}\,\delta_{ij}\,\delta_{kl}\right]$$

$$i, j, k, l = 1, 2, 3 \text{ (sum)}$$

Then evaluating the terms in Eq. C.12 by performing the indicated summations, yields,

$$C_{abcd}\frac{\partial f}{\partial \sigma_{cd}} = \frac{2G}{3\tau}\left[\sigma_{ab} - p\delta_{ab} + b\tau\left(\frac{1 + \nu}{1 - 2\nu}\right)\delta_{ab}\right]$$

and

$$C_{pqrs}\frac{\partial f}{\partial \sigma_{pq}}\frac{\partial f}{\partial \sigma_{rs}} = \frac{2G}{3}\left[1 + b^2\,\frac{1 + \nu}{1 - 2\nu}\right]$$

Thus, the three-dimensional relations are

$$A_{ijkl} = G\left[\delta_{ik}\,\delta_{jl} + \delta_{il}\,\delta_{jk} + \frac{2\nu}{1-2\nu}\,\delta_{ij}\,\delta_{kl} - \frac{2}{3\tau^2}\,\frac{\left[\sigma_{ij} + p\delta_{ij} + b\tau\left(\frac{1+\nu}{1-2\nu}\right)\delta_{ij}\right]\left[\sigma_{kl} - p\delta_{kl} + b\tau\left(\frac{1+\nu}{1-2\nu}\right)\delta_{kl}\right]}{1 + b^2\left(\frac{1+\nu}{1-2\nu}\right)}\right]$$

$$i, j, k, l = 1, 2, 3$$